PEARL Inc.
Web: http://www.pearl-hifi.com 86008, 2106 33 Ave. SW, Calgary, AB; CAN T2T 1Z6
E-mail: custserv@pearl-hifi.com Ph: +.1.403.244.4434 Fx: +.1.403.245.4456
Perkins Electro-Acoustic Research Lab, Inc. ❦ Engineering and Intuition Serving the Soul of Music

Please note that the links in the PEARL logotype above are "live" and can be used to direct your web browser to our site or to open an e-mail message window addressed to ourselves.

To view our item listings on eBay, click here.

To see the feedback we have left for our customers, click here.

Sec. 107. - Limitations on exclusive rights: Fair Use

Notwithstanding the provisions of sections 106 and 106A, the fair use of a copyrighted work, including such use by reproduction in copies or phono records or by any other means specified by that section, for purposes such as criticism, comment, news reporting, teaching (including multiple copies for classroom use), scholarship, or research, is not an infringement of copyright. In determining whether the use made of a work in any particular case is a fair use the factors to be considered shall include:

1 - the purpose and character of the use, including whether such use is of a commercial nature or is for nonprofit educational purposes;

2 - the nature of the copyrighted work;

3 - the amount and substantiality of the portion used in relation to the copyrighted work as a whole; and

4 - the effect of the use upon the potential market for or value of the copyrighted work.

The fact that a work is unpublished shall not itself bar a finding of fair use if such finding is made upon consideration of all the above factors

Technical Review

No.1 – 1994

Digital Filter Techniques vs. FFT Techniques for Damping Measurements

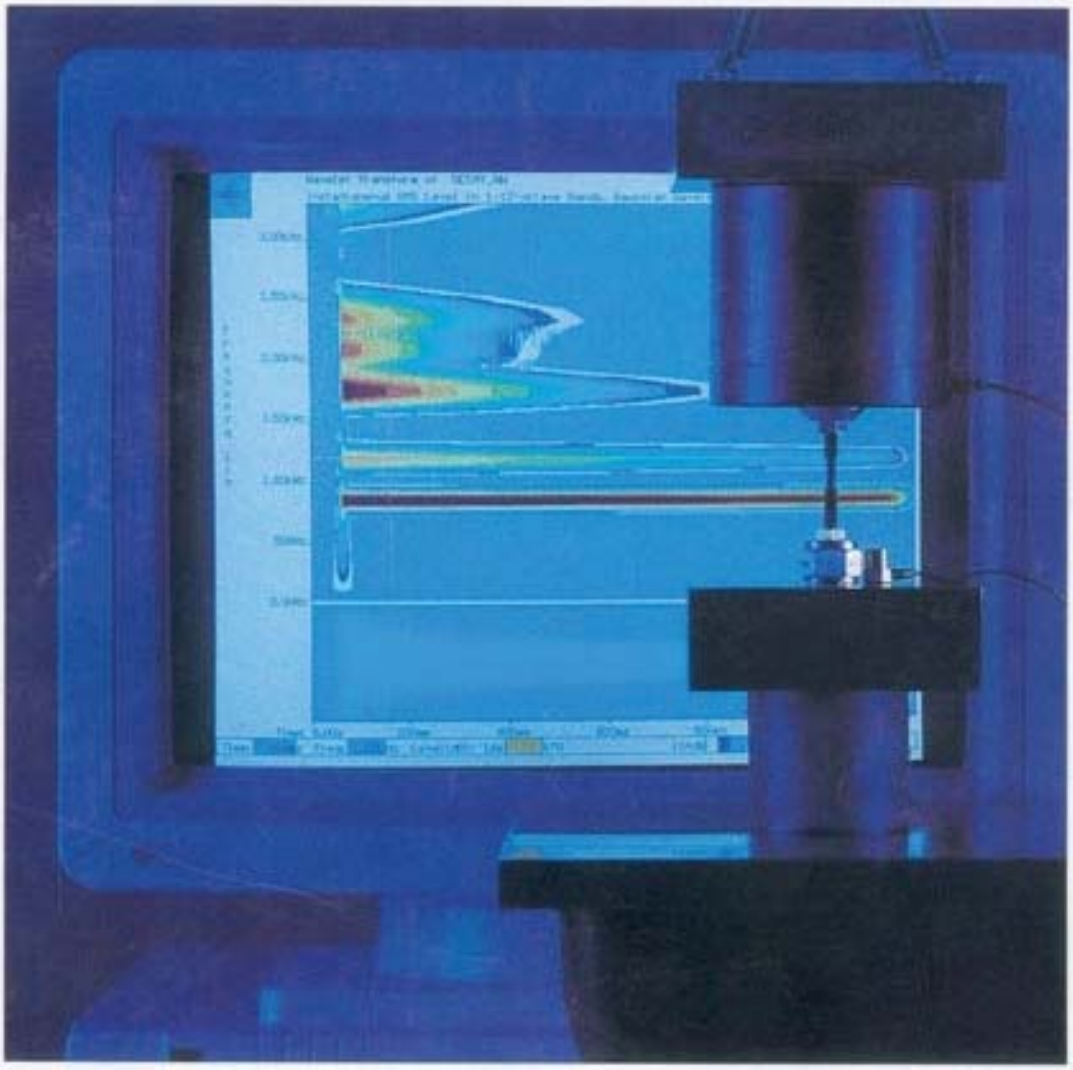

Brüel & Kjær

Previously issued numbers of Brüel & Kjær Technical Review

(Continued on cover page 3)

Technical Review

No. 1 -1994

Contents

Editor: K. Zaveri Photographer: Peder Dalmo
Layout: Judith Sarup Printed by Nærum Offset

Digital Filter Techniques vs. FFT Techniques for Damping Measurements (Damping Part I)

by Svend Gade & Henrik Herlufsen

Abstract

In this article several methods for measurements of damping are summarized with respect to their advantages and disadvantages. Especially the use of Digital Filters (DF) and Fast Fourier Transform (FFT) are compared. In general FFT analysis is best suited for heavily damped structures although with proper memory and postprocessing facilities, lightly damped structures may also be covered, while it is advantageous to use DF analysis when dealing with lightly damped structures only. The use of Time-frequency analysis techniques such as the Wavelet Transform and the Short-time Fourier Transform is also demonstrated.

Resume

Cet article décrit succintement les avantages et les inconvénients respectifs de plusieurs méthodes utilisées pour les mesures d'amortissement. Y sont spécialement comparées la méthode par filtrage numérique (DF) et la méthode par Transformée de Fourier rapide (FFT). Si l'analyse FFT convient généralement mieux pour les structures fortement amorties, bien que, avec mémoire et posttraitement appropriés, elle puisse également s'appliquer pour les structures légèrement amorties, l'analyse DF est, elle, particulièrement adéquate lorsque seules les structures légèrement amorties sont à mesurer. L'utilisation de techniques d'analyse en fréquence dans le domaine temporel, telles que la Transformée d'ondelettes et la Transformée de Fourier courte durée y est égaleemnt traitée.

Zusammenfassung

Dieser Artikel stellt die Vor- mid Nachteile für mehrere Methoden der Dämpfungsmessung einander gegenüber. Insbesondere werden die Digitalfilter-Technik (DF) und die Fast Fourier Transformation (FFT) miteinander verglichen. Im allgemeinen eignet sich die FFT-Analyse am besten für stark gedämpfte Strukturen, wobei mit geeigneten Speicher- und Nachbearbeitungsfunktionen auch die Analyse schwach gedämpfter Strukturen möglich ist. DF-Analyse ist vorteilhaft, wenn ausschließlich schwach gedämpfte Strukturen zu untersuchen sind. Die Anwendung von Zeit/Frequenz-Analysetechniken wie Wavelet-Transformation und Kurzzeit-Fourier-Transformation wird ebenfalls diskutiert.

Nomenclature

a	wavelet scaling factor
b	time parameter
c	viscous damping coefficient
c_c	critical damping coefficient
dB	decibels, ten times the logarithm to a (power) ratio
e	base of natural logarithm, 2,72...
f	frequency [Hz]
f_o	undamped natural frequency [Hz]
fd	modal damping frequency [Hz]
g	grammes, time weighting function
m	milli, 10^{-3}
min	minutes
s	seconds
sec	seconds
A,A_o,A_{ref}	constants, amplitudes
B&K	Brüel&Kjær
C_o	constant, initial value
D	decay rate [dB/s]
DF	digital filters
DFT	discrete fourier transform
E	total energy [J]
FFT	Fast Fourier Transform
FRF	Frequency response function
$H_1(f)$	estimator of frequency response function

$H_2(f)$	estimator of frequency response function
Hz	hertz [s^{-1}]
IRF	Impulse response function
J	joules
MDOF	Multiple Degree of Freedom
P	input power [W]
Q	quality factor, gain factor
s	time signal
S	Frequency Spectrum
SDOF	Single Degree of Freedom
SMS	Structural Measurement System
STAS	Structural Testing and Analysis System
STFT	Short-time Fourier Transform
T	FFT record length
T_A	averaging time
T_{60}	reverberation time [s]
W	watts
W_s	Wigner-Ville distribution
WVD	Wigner-Ville distribution
WT	Wavelet Transform
^	estimated value
δ	the logarithm decrement
ζ	fraction of critical damping, damping ratio
ζ_ω	damping ratio of exponential weighting function
η	loss factor
π	pi 3.14.....
ψ	Wavelet
σ	decay constant [s^{-1}]
σ	modal damping frequency [Rad/s]
τ	time constant [s], time shift
τ_s	time constant of structure [s]
τ_d	time constant of exponential detector [s]
τ_w	time constant (length) of exponential weighting function [s]
ω	angular frequency [Rad/s]
ω_d	damped natural frequency [Rad/s]
ω_o	undamped natural frequency [Rad/s]
Δf	3 dB bandwidth [Hz]
ΔF	FFT line spacing [Hz]
$\Delta\omega$	3 dB bandwidth [Rad/s]

%	per cent, 10^{-2}
$\langle\rangle$	inner products
*	complex conjugate

Introduction

One of the modal parameters is the damping. Without any doubt this quantity is very important to know for the design and analysis of vibrating structures. For example the predicted response due to a simulated input requires an accurate knowledge of the damping properties. The damping of combined and complex structures is often dominated by losses at joints etc. and thus is very difficult to model and predict analytically. In general, the damping of materials and structures must be determined experimentally i.e. measured.

Many different methods exist for the measurement of damping. These can roughly be divided into three groups namely

1) Vibration decay measurements
2) Bandwidth determination of measured modal resonances
3) Steady-state measurements of input and stored energy

This article will not deal with steady-state technique which is based on the energy balance in structures that are vibrationally excited (see Ref.[1]). In the steady-state techniques the input power flow, P *is* estimated from the time-averaged product of force and velocity at the driving point, and the total stored energy, E is determined as twice the kinetic energy, which is estimated by integrating the product of mass density and squared velocity over the structure. Then the loss factor, η is determined from the relation $\eta = P/\omega E$. Using this method damping can in theory be estimated even in frequency bands without resonance frequencies.

In this paper the use of *Digital Filter* (DF) techniques and *Discrete Fourier Transform* (DFT/FFT) techniques are compared. A DF analyzer gives a real-time constant percentage bandwidth analysis i.e. 1/1 octaves, 1/3 octaves, 1/12 octaves and 1/24 octaves which are respectively 70%, 23%, 6% and 3% analysis, while an DFT/FFT analyzer gives a blockwise constant bandwidth (narrow band) analysis. The use of Time-frequency analysis techniques such as the Wavelet transform and the Short-time Fourier Transform is also demonstrated.

There exist of course several other methods than those described in this paper. For example in Ref.[11] it is shown how to measure damping via probability functions.

Damping Descriptors

There exist several damping descriptors, e.g. loss factor, quality factor, reverberation time etc. The interrelation between some of these descriptors are summarized in Table 1. The explanation why there exists so many damping descriptors is mainly due to historical reasons and the different fields of applications. For modal damping based on frequency response functions it is quite natural to measure the 3dB bandwidth $\Delta\omega$, Δf while for free decay measurements one will normally measure decay rate, D, time constants, τ or reverberation time, T_{60}. In room acoustics the reverberation time (i.e. the time it takes the signal level to decrease 60 dB after the signal source has been switched off) is exclusively used due to specifications as found in international standards, while in mechanics the decay rate, D is preferred (Ref. [8]). The logarithmic decrement, δ is very seldom used nowadays. This descriptor is defined as the logarithm of the amplitude ratio of successive maxima, normally observed using an oscilloscope and provided that only one resonance is present.

In modal analysis the decay constant, σ (or modal damping frequency in [Rad/s]) is often used since $-\sigma$ indicates the real part of the pole location of transfer functions in the Laplace plane. On decay curves the decay constant, σ corresponds to the number of -8.7dBs the curve decays per second (i.e. the number of time constants, τ, per second).

For material testing damping is often expressed as a relative thus dimensionless quantity such as loss factor, η, fraction of critical damping, ζ or quality factor, Q.

The original definition of loss factor for non-resonant materials is taken as the ratio between the quadrature and coincident part of the complex modulus, which is relating stress and strain in a material. The loss factor indicates what fraction of the vibratory mechanical energy that is lost (i.e., converted into heat) in one cycle of vibration (see for example, Refs. [6] and [7]).

The quality (or gain) factor is often used in the field of electronics to describe the properties of resonators and filters.

The fraction of critical damping which only differs from the loss factor by a factor of 2 is used in the field of modal analysis and expresses the ratio between the modal damping frequency σ and the undamped natural frequency ω_o, i.e. the unsigned ratio between the real part and the distance from the origin of the pole location of transfer functions in the complex Laplace plane. It can be shown that using a viscously damped single degree of freedom model consisting of a mass, a spring and a viscous dashpot, c that the fraction of critical damping (often also called the damping ratio) equals the ratio between the actual damping, c and damping there would have been, c_c if the system was

Natural Frequency $\omega_0 = 2\pi f_o$ (= ω_d for lightly damped resonances)											
Unknown / Known	$\Delta\omega$=	Δf =	f_d =	η =	ζ =	Q =	σ =	τ =	T_{60}=	D =	δ =
3dB Bandwidth $\Delta\omega$ [Rad/s]	$\Delta\omega$	$\frac{\Delta\omega}{2\pi}$	$\frac{\Delta\omega}{4\pi}$	$\frac{\Delta\omega}{\omega_o}$	$\frac{\Delta\omega}{2\omega_o}$	$\frac{\omega_o}{\Delta\omega}$	$\frac{\Delta\omega}{2}$	$\frac{2}{\Delta\omega}$	$\frac{13.8}{\Delta\omega}$	$4.34\Delta\omega$	$\frac{\pi\Delta\omega}{\omega_o}$
3dB Bandwidth Δf [Hz]	$2\pi\Delta f$	Δf	$\frac{\Delta f}{2}$	$\frac{\Delta f}{f_o}$	$\frac{\Delta f}{2f_o}$	$\frac{f_o}{\Delta f}$	$\pi\Delta f$	$\frac{1}{\pi\Delta f}$	$\frac{6.9}{\pi\Delta f}$	$27.3\Delta f$	$\frac{\pi\Delta f}{f_o}$
Damping frequency f_d [Hz}	$4\pi f_d$	$2f_d$	f_d	$\frac{2f_d}{f_o}$	$\frac{f_d}{f_o}$	$\frac{f_o}{2f_d}$	$2\pi f_d$	$\frac{1}{2\pi f_d}$	$\frac{1.1}{f_d}$	$54.6f_d$	$\frac{2\pi f_d}{f_o}$
Loss Factor η	$\eta\omega_o$	ηf_o	$\frac{\eta f_o}{2}$	η	$\frac{\eta}{2}$	$\frac{1}{\eta}$	$\eta\pi f_o$	$\frac{1}{\pi f_o\eta}$	$\frac{2.2}{\eta f_o}$	$4.34\omega_o\eta$	$\eta\pi$
Fraction of critical damping ζ	$2\zeta\omega_o$	$2\zeta f_o$	$2\zeta f_o$	2ζ	ζ	$\frac{1}{2\zeta}$	$2\pi f_o\zeta$	$\frac{1}{2\pi f_o\zeta}$	$\frac{1.1}{\zeta f_o}$	$8.69\omega_o\zeta$	$2\pi\zeta$
Quality factor Q	$\frac{\omega_o}{Q}$	$\frac{f_o}{Q}$	$\frac{f_o}{2Q}$	$\frac{1}{Q}$	$\frac{1}{2Q}$	Q	$\frac{\omega_o}{2Q}$	$\frac{2Q}{\omega_o}$	$\frac{22Q}{f_o}$	$\frac{4.34\omega_o}{Q}$	$\frac{\pi}{Q}$
Decay constant σ [s^{-1}]	2σ	$\frac{\sigma}{\pi}$	$\frac{\sigma}{2\pi}$	$\frac{2\sigma}{\omega_o}$	$\frac{\sigma}{\omega_o}$	$\frac{\omega_o}{2\sigma}$	σ	$\frac{1}{\sigma}$	$\frac{6.9}{\sigma}$	8.69σ	$\frac{\sigma}{f_o}$
Time constant τ [s]	$\frac{2}{\tau}$	$\frac{1}{\pi\tau}$	$\frac{1}{2\pi\tau}$	$\frac{1}{\pi f_o\tau}$	$\frac{1}{2\pi f_o\tau}$	$\pi f_o\tau$	$\frac{1}{\tau}$	τ	6.9τ	$\frac{8.69}{\tau}$	$\frac{1}{f_o\tau}$
Reverberation time T_{60} [s]	$\frac{13.8}{T_{60}}$	$\frac{2.2}{T_{60}}$	$\frac{1.1}{f_oT_{60}}$	$\frac{2.2}{f_oT_{60}}$	$\frac{1.1}{f_oT_{60}}$	$\frac{f_oT_0}{2.2}$	$\frac{6.9}{T_{60}}$	$\frac{T_{60}}{6.9}$	T_{60}	$\frac{60}{T_{60}}$	$\frac{6.9}{f_oT_{60}}$
Decay rate D [dB/s]	$\frac{D}{4.34}$	$\frac{D}{27.3}$	$\frac{D}{54.6}$	$\frac{D}{4.34\omega_o}$	$\frac{D}{8.69\omega_o}$	$\frac{4.34\omega_o}{D}$	$\frac{D}{8.69}$	$\frac{8.69}{D}$	$\frac{60}{D}$	D	$\frac{D}{8.69f_o}$
The logarithmic decrement δ	$\frac{\delta\omega_o}{\pi}$	$\frac{\delta f_o}{\pi}$	$\frac{\delta f_o}{2\pi}$	$\frac{\delta}{\pi}$	$\frac{\delta}{2\pi}$	$\frac{\pi}{\delta}$	δf_o	$\frac{1}{\delta f_o}$	$\frac{6.9}{\delta f_o}$	$8.69f_o\delta$	δ

Table 1. Interrelations between measures of damping

critically damped. A critically damped system will as free vibrations show an exponentially decaying vibration without free oscillations.

In this article measurement of the *fraction of critical damping* is used exclusively for the comparison of the different methods.

Measurement Conditions and Equipment Used

The damping measurements were performed on a freely suspended and thus extremely lightly damped aluminium plate with the dimensions of 30cm x 25cm x 2cm. The structure was for some measurements excited by an impact hammer Brüel&Kjær Type 8202 (see Fig. 1) with a built-in Brüel&Kjær Force Transducer Type 8200. The steel tip was used to ensure proper excitation in the frequency range of interest which was from 500 Hz to 3kHz, a range that includes the first five modal frequencies.

In other situations the structure was excited via a nylon stinger by a small Brüel&Kjær Vibration Exciter Type 4810 (see Fig.1) using either a Random or a Pseudo Random signal. The input force was also in these cases measured using a Brüel&Kjær Force Transducer Type 8200.

The output vibration signal was measured using a small lightweight (~2.4g) Brüel&Kjær Accelerometer Type 4375. The force and vibration signals were analyzed using either the Brüel&Kjær Multichannel Analysis System Type 3550 (DFT/FFT) or the Brüel&Kjær Dual Channel Real-time Frequency Analyzer Type 2133 (DF). All results were plotted on a Brüel&Kjær Graphics Plotter Type 2319. Post-processing of data was in some cases carried out using the SMS modal software STAS SE (Brüel&Kjær Type number WT9100), the Brüel&Kjær 3D-plot of spectra software Type WT9321 and the Brüel&Kjær Non-stationary Signal Analysis Software Type WT9362.

Using the digital filter analyzer the damping was estimated by the Schroeder method, also called "Integrated Impulse Response Method" (Ref.[9]).

Experimental Results using Digital Filter Analysis

The damping is here estimated from the decay of the free vibration response due to an impact excitation. The plate structure was excited by an impact hammer in a comer point ensuring excitation of the first five modes of interest. The acceleration was measured in another comer ensuring that the response from the modes of interest were all included in the measured

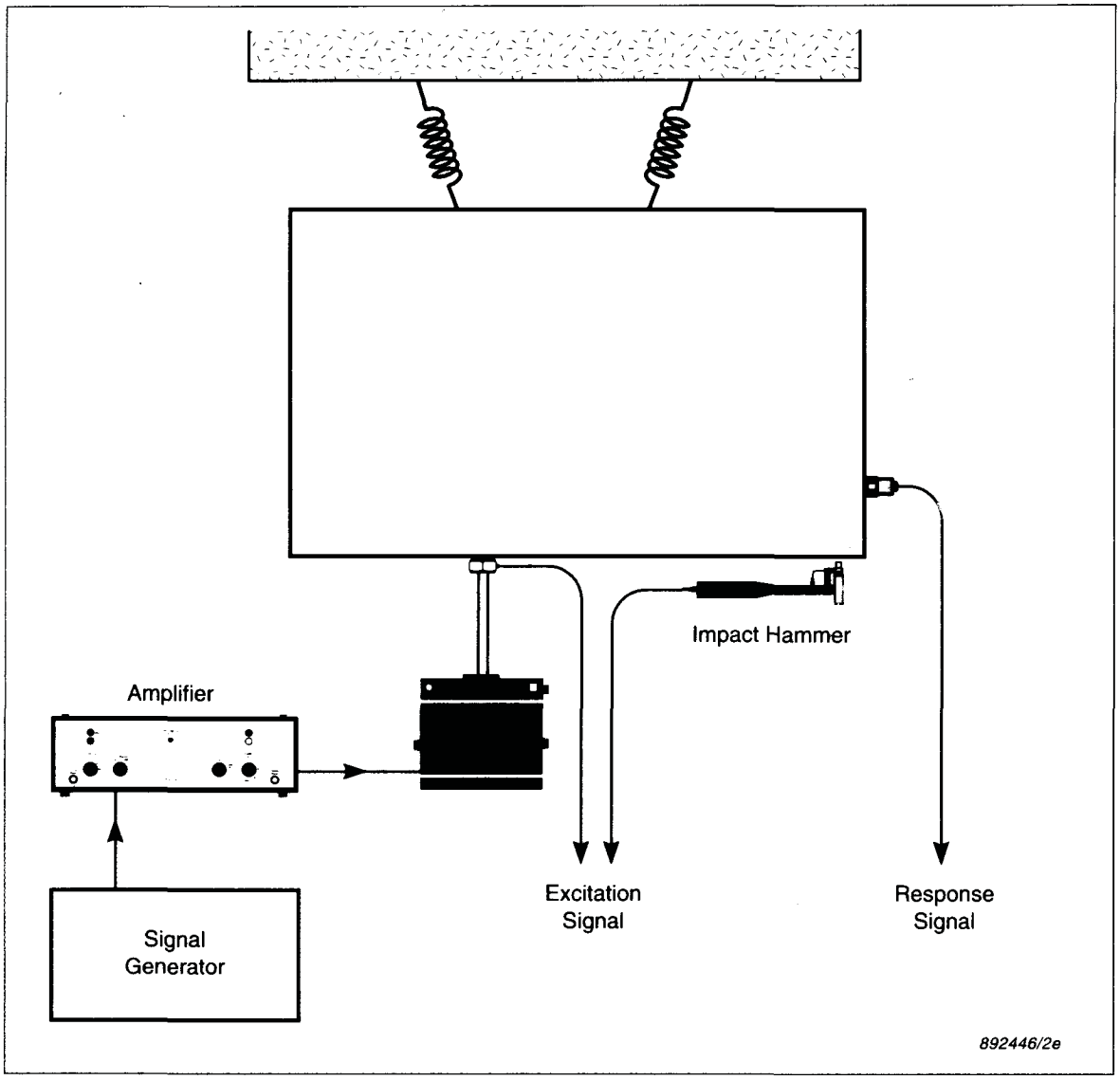

Fig. 1. Measurement configuration/setup shown without the frequency analyzers

response signal. 1/12 octave bandwidth was selected in order to have the resonance frequencies separated in different analysis bands. This makes estimation of the damping for each mode of vibration possible. Exponential averaging, T_A of 1/32 sec was used which means that a reverberation time T_{60} $>14 \cdot T_A$ = 14/32 sec = 0.44 sec could be estimated with sufficient accuracy (see Ref. [3]). The Brüel&Kjær Real-time Frequency Analyzer Type 2133 can store spectra at specified time intervals in a multi-spectrum. In this experiment 200 spectra of the response signal were stored with an interval of 25 msec between

spectra. Fig. 2 shows the measurement setup in the analyzer and the slice of the multispectrum at 866 Hz i.e. the 1/12 octave band at 866 Hz, containing the 1st resonance, as a function of time. The amplitude is presented on a logarithmic dB scale which means that the exponential decay

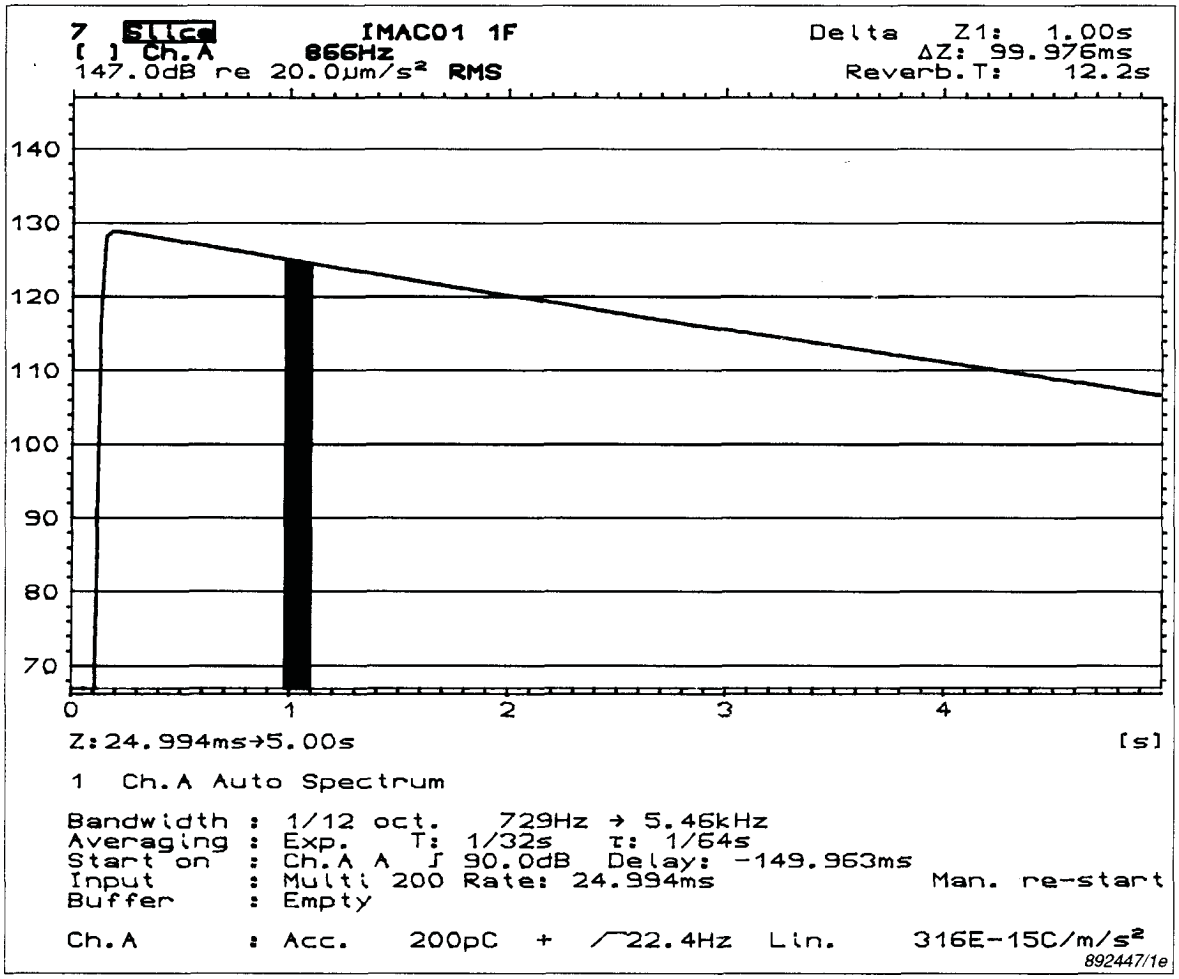

Fig. 2. Measurement setup for the analysis and decay of the 1st resonance in the 1/12 octave band at 866 Hz

$$A(t) = A_o e^{-\sigma t} \tag{1}$$

will appear as

$$10\log [A(t)/A_{ref}]^2 = 10\log [A_o/A_{ref}]^2 - \sigma \cdot t \cdot 10\log e^2$$

$$= C_o - 8.69 \cdot t \cdot \sigma$$

$$= C_o - 8.69 \cdot t/\tau \quad (2)$$

i.e. as a straight line with a slope of -8.69dB · σ = 8.69dB/T, where σ is the decay constant and τ the time constant of the resonance. C_o is the maximum level of the response and depends upon the amplitude and the spectral shape of the impact as well as the position of the excitation and response measurement. The reverberation time, $T_{60} = 6.9\tau$, calculated from the slope of the slice in the highlighted part of the graph, defined by a delta cursor, is given in the upper right comer of the plot.

Fig. 3 shows a 3D plot of vibration decays in the 1/12 octave bands. The five modes of interest are clearly seen in the plot in the 866 Hz, 1220 Hz, 1730 Hz, 2050 Hz and 2300 Hz 1/12 octave bands. Due to the non-ideal amplitude characteristic of the filters (6 pole filters) energy has leaked into the neighbouring frequency bands. The initial broadband excitation is seen as well.

The slices of the 2nd and the 3rd resonance in the 1220Hz and 1730Hz band are shown in Fig. 4. The decays have here been backwards integrated, see Ref. [9], in order to obtain smooth decays and well defined initial levels for automatic reverberation time calculations. The reverberation time for all the bands were estimated from the backwards integrated decays in an evaluation range from 5dB to 25 dB below the initial level, except for the 866 Hz band where the evaluation range was set between 5dB and 15 dB below the initial level. This was due to the long reverberation time for the 1st resonance. The reverberation time spectrum is given in Fig. 5 a. and in tabular form in the left column of Fig. 6.

The reverberation time is then converted (see Table 1) to the fraction of critical damping ζ by

$$\zeta = 1.1/f_o \cdot T_{60} \quad (3)$$

where f_o is undamped natural frequency of the resonance. For the calculations the centre frequency of the 1/12 octave bands are used for f_o, which

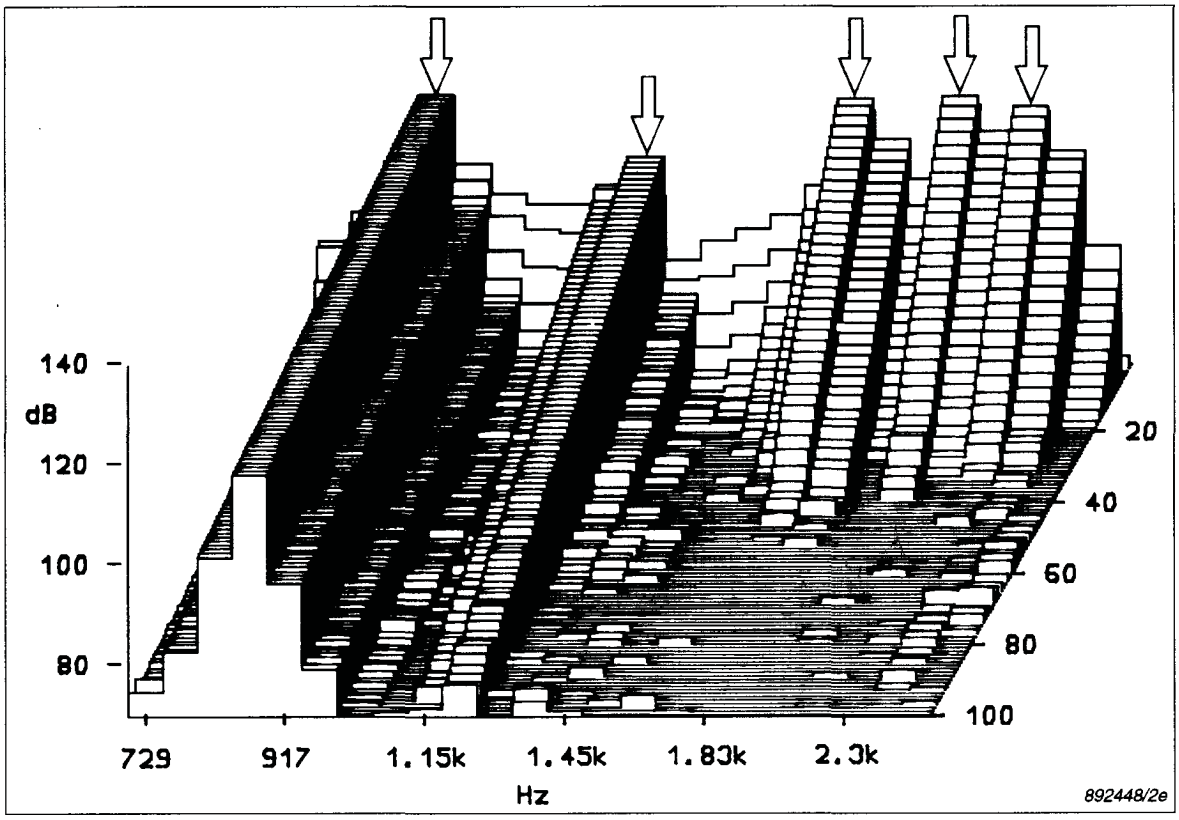

Fig. 3. 3D plot of the first 100 spectra of the multispectrum showing the vibration decay in 1/12 octave bands. The 5 bands containing the resonances are indicated by arrows

imposes an uncertainty of maximum 3% on the results. The spectrum of the percentage of critical damping ($\zeta\% = 100 \cdot \zeta$) called C_r. Damping is shown in Fig.5b and in tabular form in the right column of Fig. 6. The values for the percentage of critical damping are inserted in Table 2.

A reverberation time and thus a damping value has been calculated in some of the bands not containing a resonance. This is due to the leakage effect caused by the non-ideal filtershape in the analysis as mentioned earlier. For those bands where a T_{60}, and thus ζ, could not be calculated, a warning line is indicated below the frequency axis in the spectrum and an empty space is left in the table.

One advantage of this method is that it is extremely fast. After one hammer impact the damping values are automatically calculated in the analyzer without any operator interference. Also this method has practically no limitations in dealing with very lightly damped systems.

For single resonance damping measurements the basic requirement is however that the resonances are separated in different bands. Otherwise the cal-

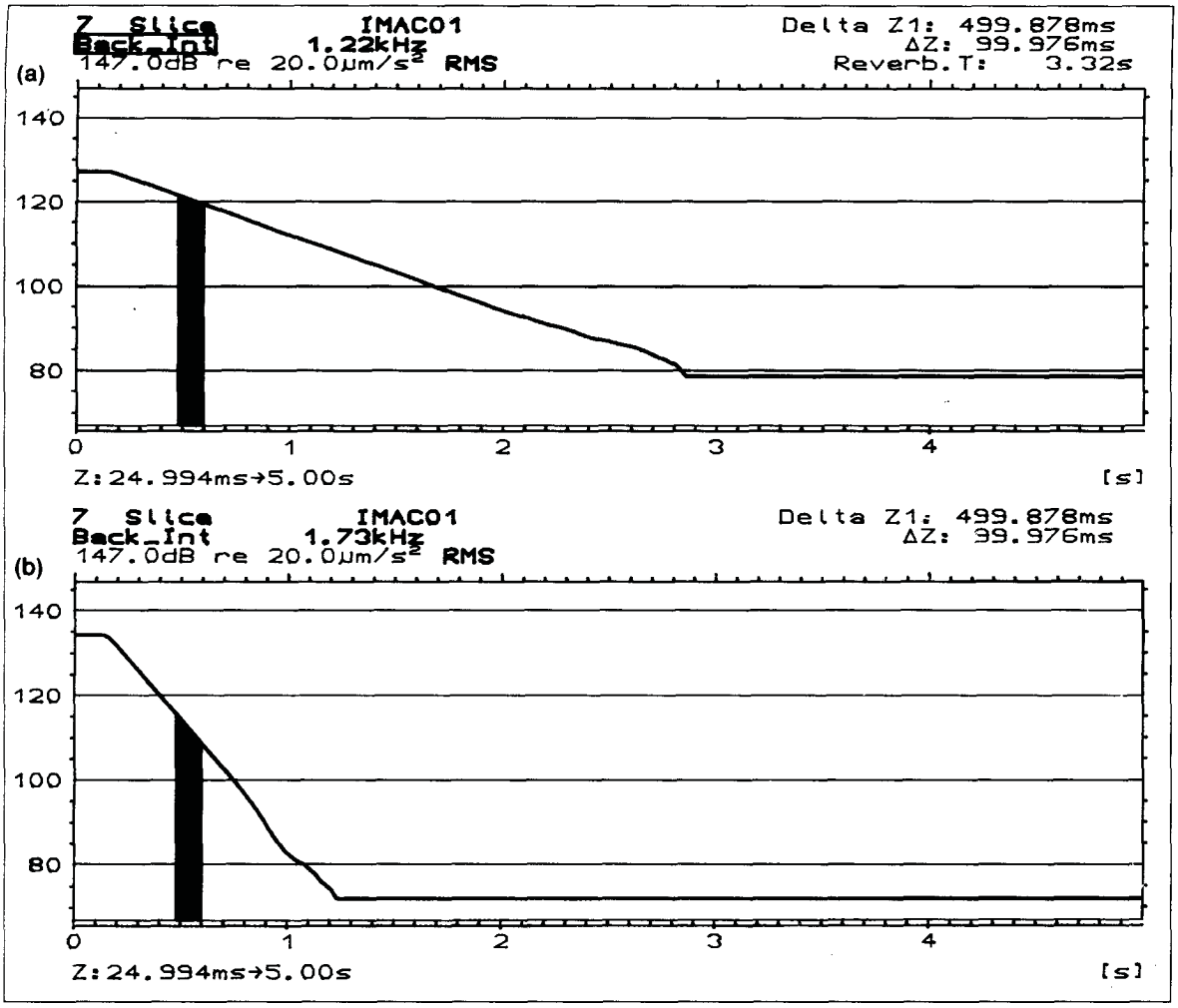

Fig. 4. Decay curves for the 2nd and the 3rd resonance in the 1/12 octave bands at 1220 Hz and 1730Hz. The decays have been backwards integrated in order to give smooth decays and well defined initial levels (used for reverberation time calculations)

culated damping values will depend upon how the test is performed (excitation point and response point) and how the reverberation time is calculated. In situations with high modal density i.e. many mode within each band this method will give an average damping value of the modes. This will normally require averaging of the decay curves over several measurement and excitation points. This multipoint technique is extremely useful and very often required in acoustical applications.

The upper limit of damping values which can be handled by this method will depend upon the bandwidth and the integration time in the detector. This is discussed in the following section.

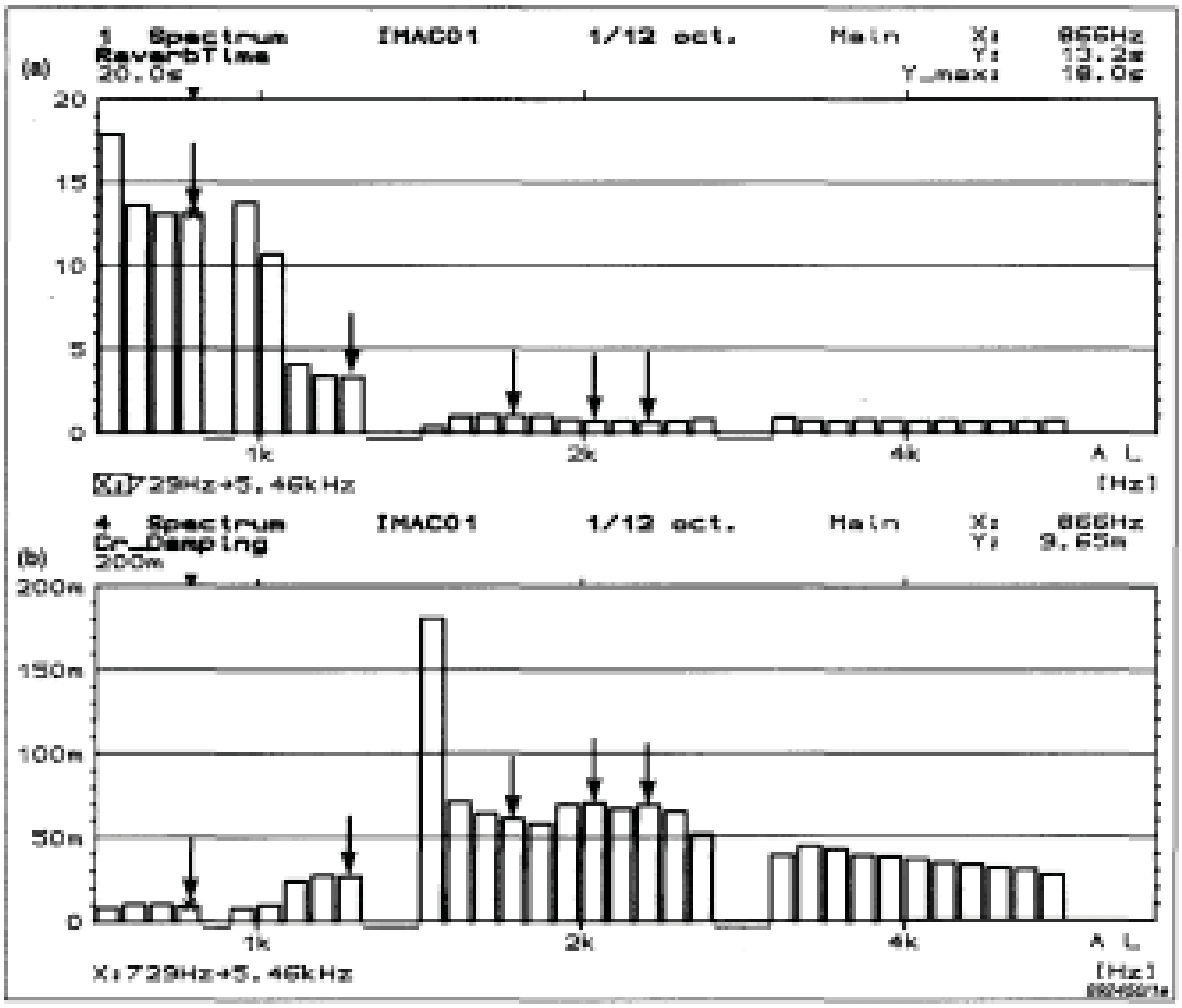

Fig. 5. Spectrum of the a) calculated reverberation time and b) calculated fraction of critical damping (in percent ζ%). The 5 bands containing the resonances are indicated by arrows

Time Reversed Decay Measurements

Using "classical" analysis techniques, i.e. filtering in 1/3 or 1/1 octave bands, limitation exists due to "ringing" in bandpass filters and smoothing caused by the detector.

According to Ref.[3] reliable decay curves are obtained only if the fraction of critical damping is less than 0.017 (1.7%) for 1/3 octave analysis. For 1/1 octave and 1/12 octave analysis the limits are 3 times higher and 4 times lower respectively.

However, in Ref. [4] it has been demonstrated that reversing the time signal to the filters leads to much less distortion on the decay curve and reliable

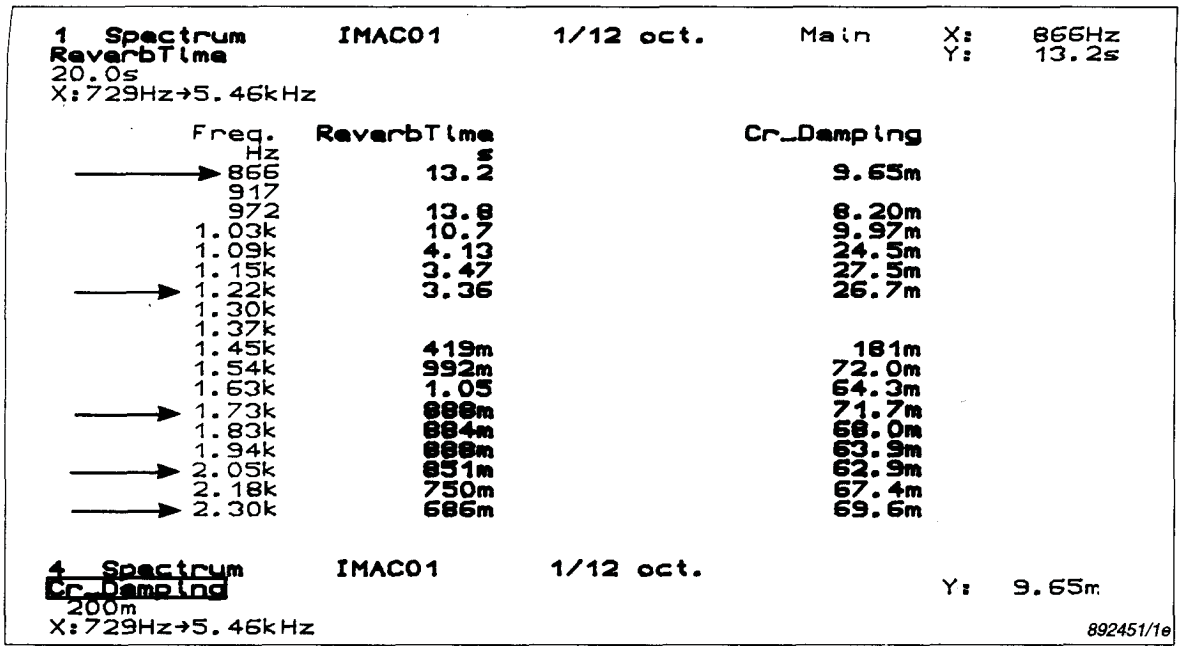

Fig. 6. Table of the reverberation time spectrum and the fraction of critical damping (in percent ζ %) spectrum. The 5 bands containing the resonances are indicated by arrows

damping measurements on four times more damped systems can be performed. Thus for 1/3 octave analysis the fraction of critical damping should be less than 0.07 (7%).

When measuring on highly damped structures (short decay curves) it is important to choose the averaging time of the detector short enough to avoid influence on the decay curve. On the other hand we should also choose an averaging time as long as possible in order to minimize statistical errors. Using a device with exponential averaging (time constant, τ_d corresponding to an averaging time, $T_{AV} = 2\tau_d$) the averaging time should obey

$$\tau_s > 2\tau_d \tag{4}$$

where τ_s is the time constant of the system under test. The factor of 2 is due to the fact that the averaging is performed on the squared output of the filters. Thus τ_s is the time taken for the signal amplitude to decay 8.68 dB while τ_d is the time it takes for the averaging device to decay 4.34 dB.

In Ref. [3] the factor for the inequality (4) is chosen as four

$$\tau_s > 4\tau_d, \tag{5}$$

to be on the safe side.

	Fraction of critical damping				
	ζ_1% (860 Hz)	ζ_2% (1198 Hz)	ζ_3% (1756Hz)	ζ_4% (2091 Hz)	ζ_5% (2341 Hz)
Free decay DF 1/12 octave	0.0097	0.0267	0.0717	0.0629	0.0696
Free decay FFT $\Delta f = 8Hz$	0.0103	0.0261	0.0738	0.0625	0.0696
Curvefit Baseband Impact*	0.273	0.215	0.193	0.178	0.161
Curvfit Baseband Impact Corrected	0.0093	0.0250	0.0643	0.0688	0.0640
Curvefit Baseband Random*	0.029	0.108	0.177	0.130	0.144
Curvefit Zoom Random	0.011	0.029	0.066	0.071	0.063
IRF decay Baseband Pseudo Random	0.0134	0.0286	0.0633	0.0662	0.0633
Curvefit Baseband Pseudo Random	0.013	0.029	0.063	0.066	0.063
IRF decay Zoom Pseudo Random	0.0121	0.0275	0.0703	0.0672	0.0657

*Table 2. Damping values, fraction of critical damping in percent ζ %, from the different test methods. Those values in the rows indicated with an * are heavily biased as expected*

However since the response of the detector is much faster when the signal increases instead of decreasing it will be of great advantage to use time reversed analysis. According to Ref.[4] the requirements (5) can be replaced by

$$2\tau_s > \tau_d \tag{6}$$

Thus it is possible to measure eight times higher damping factors without the need for decreasing the averaging time by a factor of eight.

Experimental Results Using FFT Techniques

The damping was here measured using the following methods:

a) Free vibration decay
b) Curve fit of frequency response functions measured using impact excitation
c) as b) but using random excitation with a shaker
d) Decay of impulse response function calculated from weighted frequency response function using pseudo random excitation with a shaker. These results were compared with results of curve fit of the frequency response function.

In all the measurements the Brüel&Kjær Multichannel Analysis System Type 3550 was used.

a) Free Vibration Decay

The free vibration decay technique used here was similar to the technique just described using digital filtering.

A frequency resolution of ΔF = 8Hz was selected on the analyzer which means that the time record $T = 1/\Delta F$ =125 ms was sufficiently short to follow the decay of the signal. Averaging was set to exponential of 1 which means that the autospectrum is the magnitude of the instantaneous spectrum (i.e. no averaging). The FFT was performed with Hanning weighting on the time signal. 400 frequency lines from 0 Hz to $400 \cdot \Delta F$ = 3200 Hz were transferred to the multibuffer every 25ms. A 3D plot of the autospectra in the multibuffer is shown in Fig.7. The decay of the 5 resonances is clearly seen. The initial broadband response due to the impact is also seen.

The resonances appeared in the frequency lines at 864 Hz, 1220 Hz, 1760hz, 2096 Hz and 2352 Hz. The slices along these frequencies are shown in Fig. 8 and from the slope of these the decay rate, and thus the fraction of critical damping can be determined via a User-definable Auxiliary Information (see Table 1). The results are inserted in Table 2.

As expected the results agree very well with the results from the test using DF. As for the free decay method using DF there is practically no lower limit for the damping values which this method can handle. The requirement is that only one resonance resides in each analysis bandwidth (i.e. only one resonance per three analysis lines when Hanning weighting is used). The upper limit for the damping values to be estimated by this method comes from the storage rate of spectra (typically in the order of 20 to 100 spectra per second) which depends on the transform size and the speed of FFT calculations.

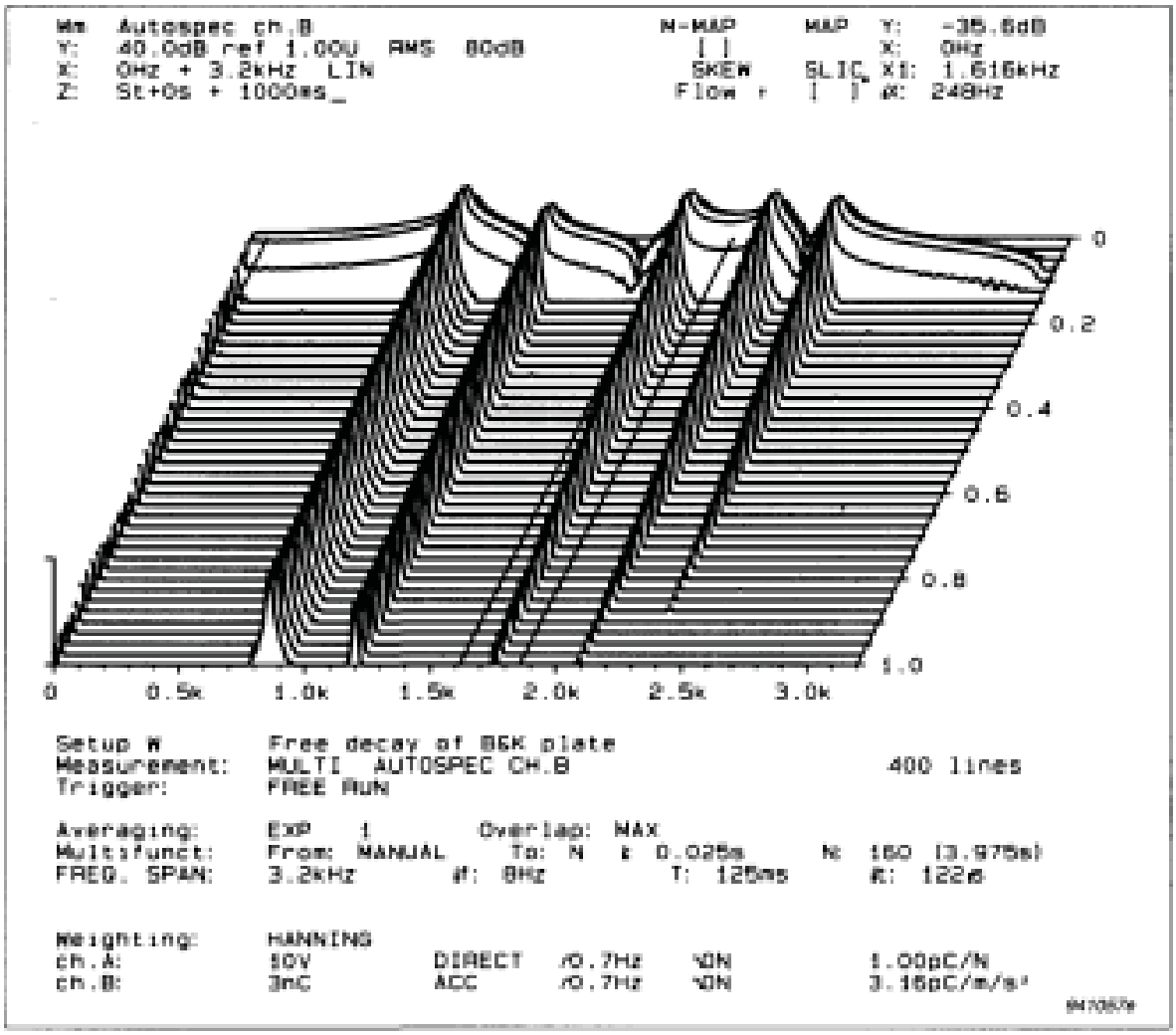

Fig. 7. 3D map of FFT spectra of free vibration decay. Interval between spectra is 25 msec and 400 frequency lines cover the span from 0 Hz to 3200Hz with a resolution of Δf= 8Hz. Only the first second of the 4 sec recording is shown

If the decay is too fast (i.e. the damping is too high) another possibility is to record the response signal in a time buffer sufficiently long to contain the whole signal (or most of it). For the Multichannel Analysis System Type 3550 a (64 K sample buffer) Time Capture and a (700 K sample to disk) Time History modes are available. The advantages of recording into a buffer is that any (high) overlap between the spectra in the 3-D plot is obtainable, thus giving us a good time resolution. See Fig. 9.

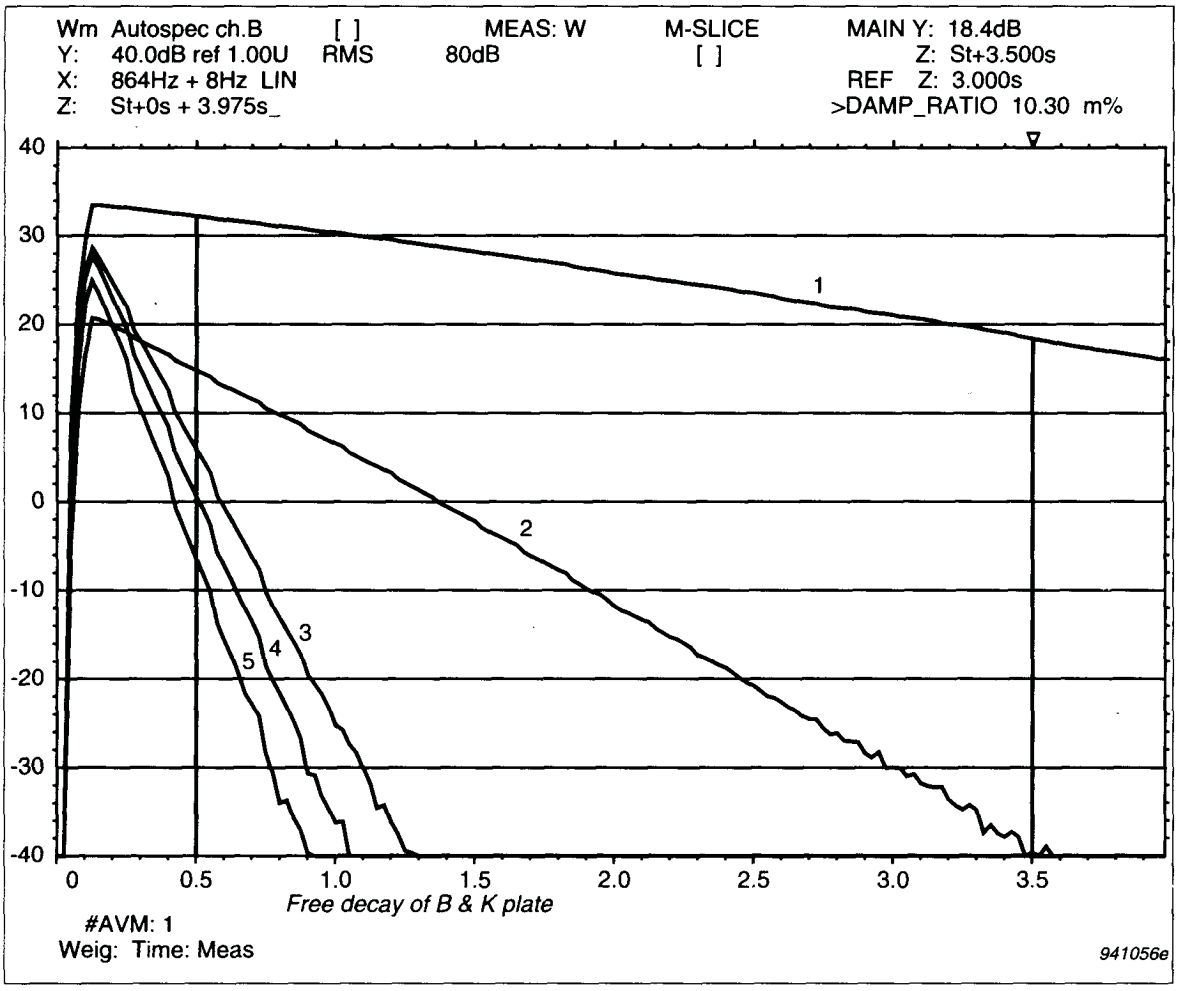

Fig. 8. Plot of the slices at the resonances giving the decay of vibrations. The frequency lines containing the resonance are 1) 864Hz, 2) 1200Hz, 3) 1756Hz, 4) 2096Hz, and 5) 2340Hz

b) Curve Fit of FRFs measured using Impact Excitation

Instead of only measuring the acceleration response the impact force is also measured here and from the two signals the frequency response function (acceleration/force i.e. accelerance) is estimated using dual channel FFT calculation. Fig. 10 shows measurement setup and an estimated accelerance function. A frequency range of 3.2kHz with a line spacing of ΔF = 4 Hz was selected giving a record length of T= 250msec. Since the response signal is much longer than 250msec an exponential weighting function with a time constant of 50msec (given as length in the setup) is applied to the response signal in channel B. The force impulse is measured in channel A with a tran-

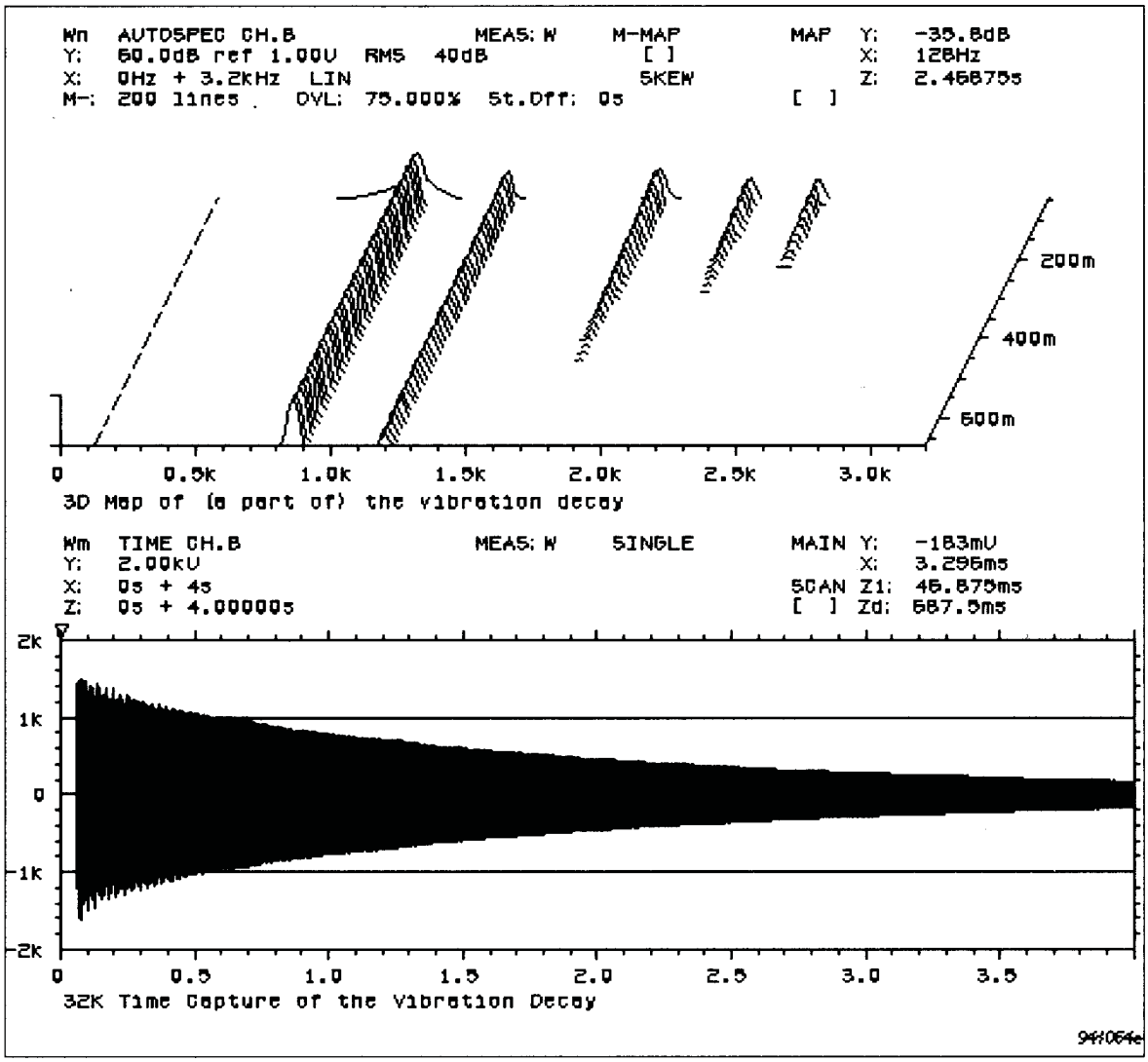

Fig. 9. Time Capture Recording of 32K samples corresponding to 4 sec recording using 3,2 kHz range. The scan cursor has been applied to produce a 200 line 3D map with 75% overlap of the data. A map of the first 625ms is shown

sient weighting function. The response signal is in Fig. 11 shown with and without multiplication of the exponential weighting. Notice that the signal is attenuated more than a factor of 100 at the end of the record with the exponential weighting ensuring a well denned influence of leakage in the analysis (to be corrected for later).

The frequency response function is transferred to the modal analysis software (SMS STAS SE) where curve fitting of the individual resonances is performed. SDOF polynomial curvefitting is used and the resulting damping values (percentage of critical damping) are given in Table 2.

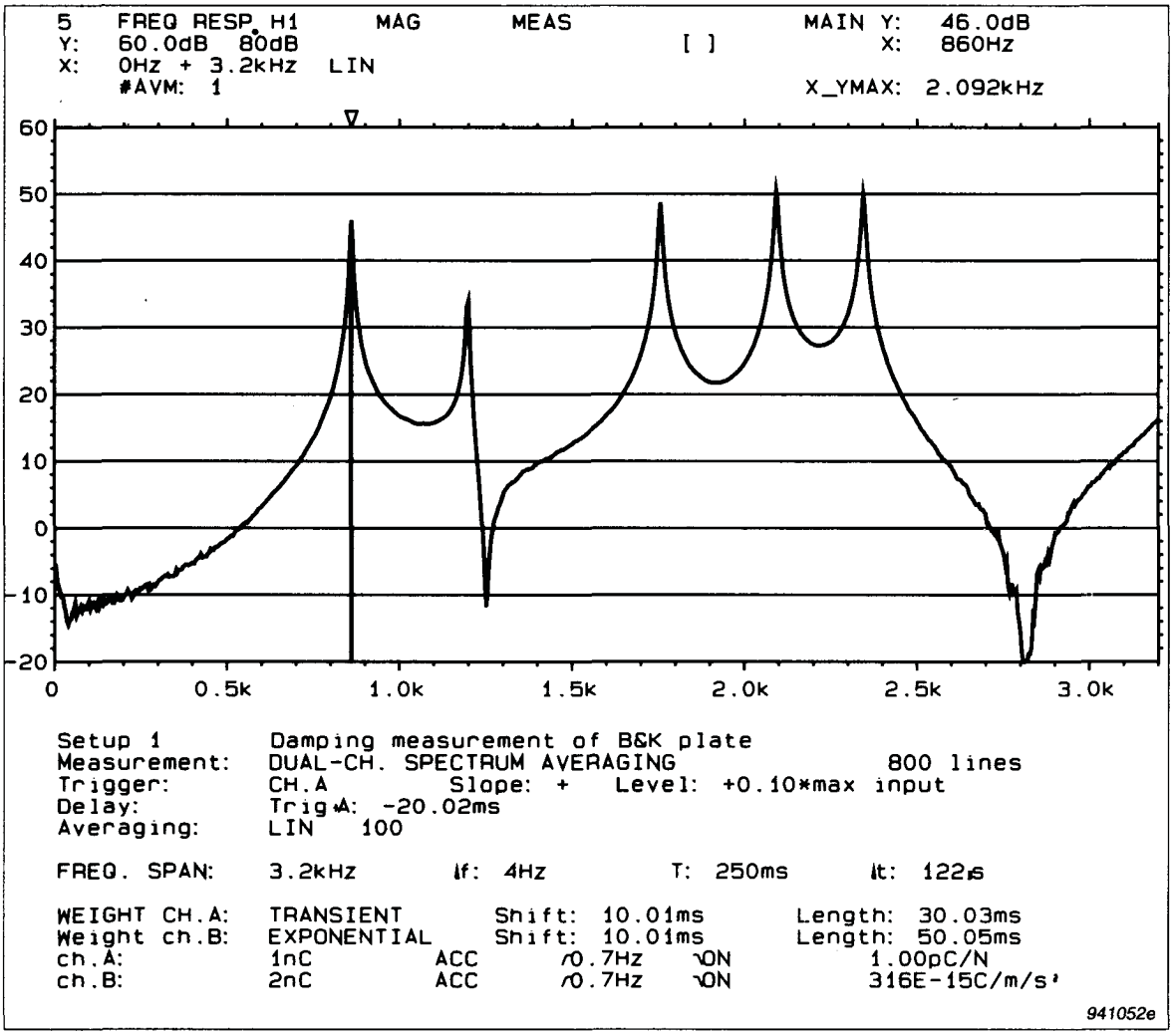

Fig. 10. Measurement setup for frequency response function measurement using impact hammer excitation and an estimated frequency response function (accelerance)

From the modal parameters, frequency, damping and residue, obtained from the curve fitting for the five modes, the frequency response function is synthesized and shown on top of the measured function in Fig. 12. Excellent agreement is observed indicating proper curve fitting. Such synthesis and comparison is also possible inside Multichannel Analysis System Type 3550 using User Definable Functions and superimposed format.

The estimated damping values are too high due to the exponential weighting. The influence of the weighting function is however well defined and can be corrected for as follows (see Ref. [10]).

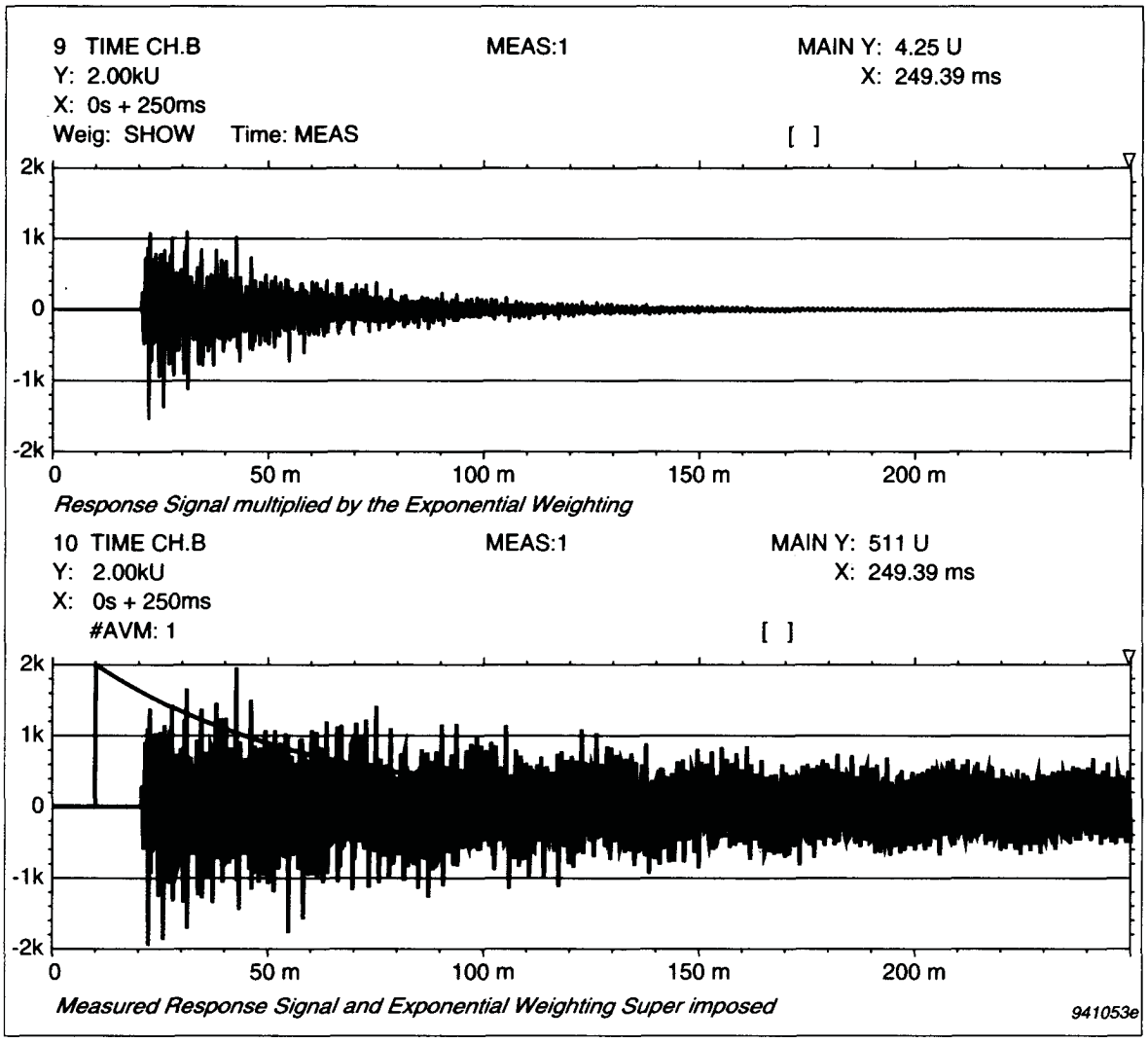

Fig. 11. Response signal (acceleration) with (a) and without (b) multiplication of the exponential weighting function

$$\zeta_{corr} = \zeta - \zeta_w$$
$$= \zeta - \frac{1}{2\pi f_o \tau_w} \tag{7}$$

where ζ is the estimated damping, ζ_w, is the damping from the exponential weighting, τ_w is the time constant (length) of the exponential weighting and f_o is the natural frequency of the mode. Such correction is provided in the modal software and the results are given in Table 2. Excellent agreement with the previous results are obtained.

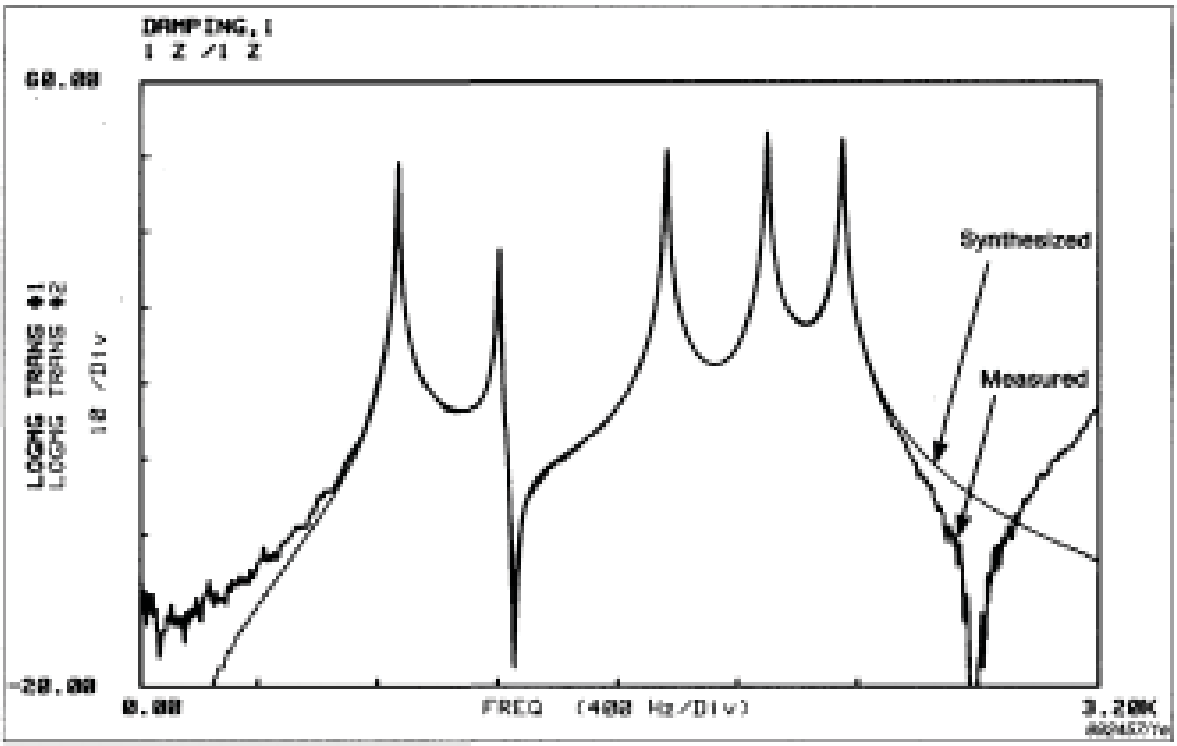

Fig. 12. Measured and synthesized frequency response function. The five modes were curve fitted using SDOF polynomial curve fitter

The advantage of this method, compared to the free decay methods (DF or FFT), is that very damped systems (vibration decay within the record length T) and systems with high coupling between the modes can be analysed. In situations with heavy coupling between the modes a MDOF curve fitter would have to be applied.

c) Curve Fit of FRFs measured using Random Excitation

The frequency response function (accelerance) is here estimated using a shaker and a random force signal as excitation. First a baseband measurement with a frequency span of 3.2kHz and resolution of ΔF = 4 Hz was used as for the impact hammer test b). The measurement setup and an estimated frequency response function is shown in Fig. 13. The levels of the resonances and the location of the anti-resonances is different from the impact test (Fig. 10) because the excitation is in a different point. This will however only affect the residues (which are local parameters) and not the frequency and damping values (which are global parameters for the structure).

Using only 4 Hz resolution the resonance peaks are however heavily affected by leakage as indicated by the low coherence at the resonance frequencies

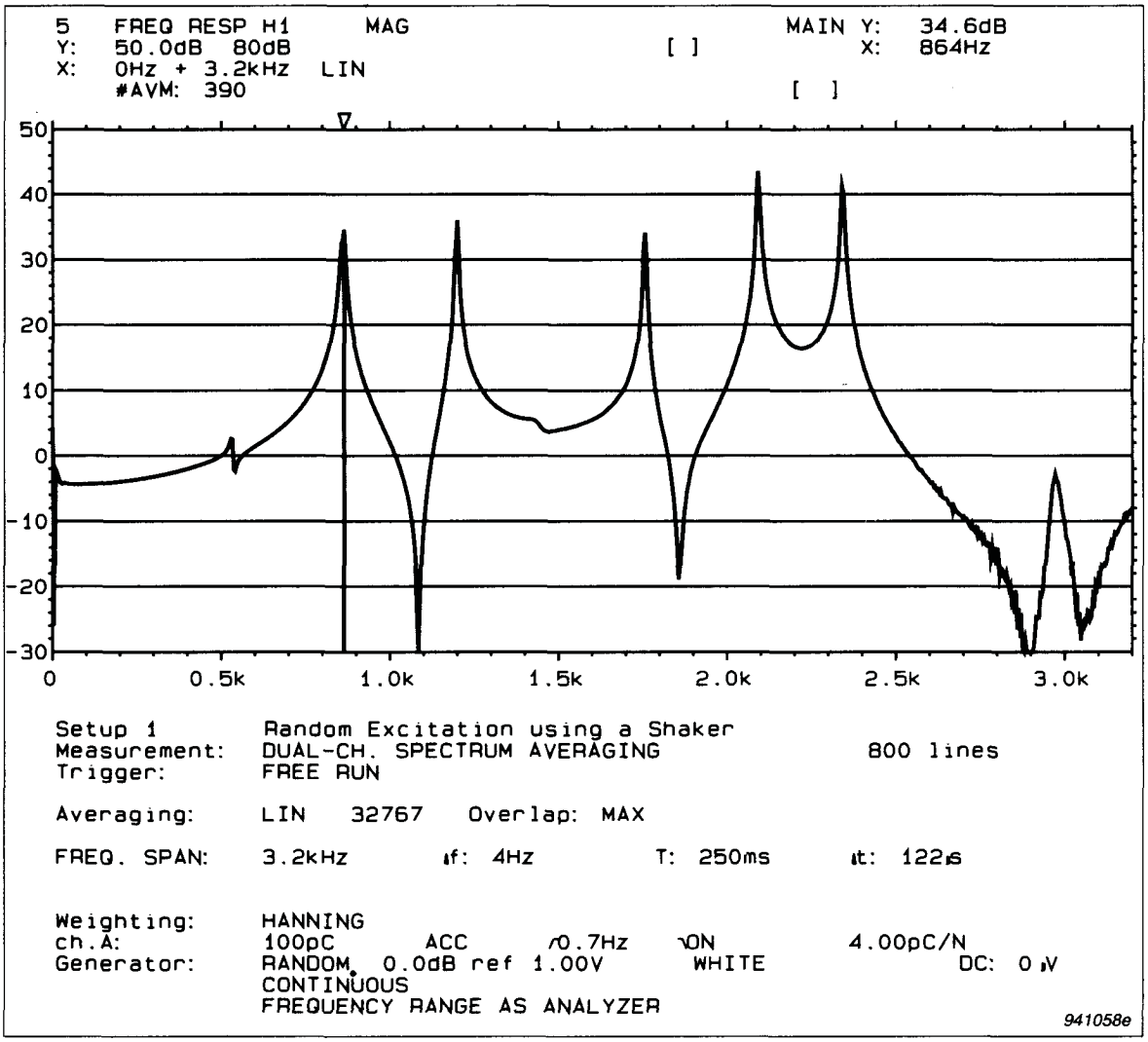

Fig. 13. Measurement setup and estimated frequency response function using random excitation with a shaker

(Ref. [10]) as shown in Fig. 14. The too low values of the frequency response function at the resonances is also called resolution bias due to the insufficient resolution in analysis.

Again the frequency response function was transferred to the modal software and the individual resonances were curve fitted using SDOF polynomial curve fitter.

The resulting damping values are found in Table 2. As expected the damping values are severely overestimated due to the leakage in the analysis. In order to avoid the influence of leakage (or resolution bias errors) 5 zoom measure-

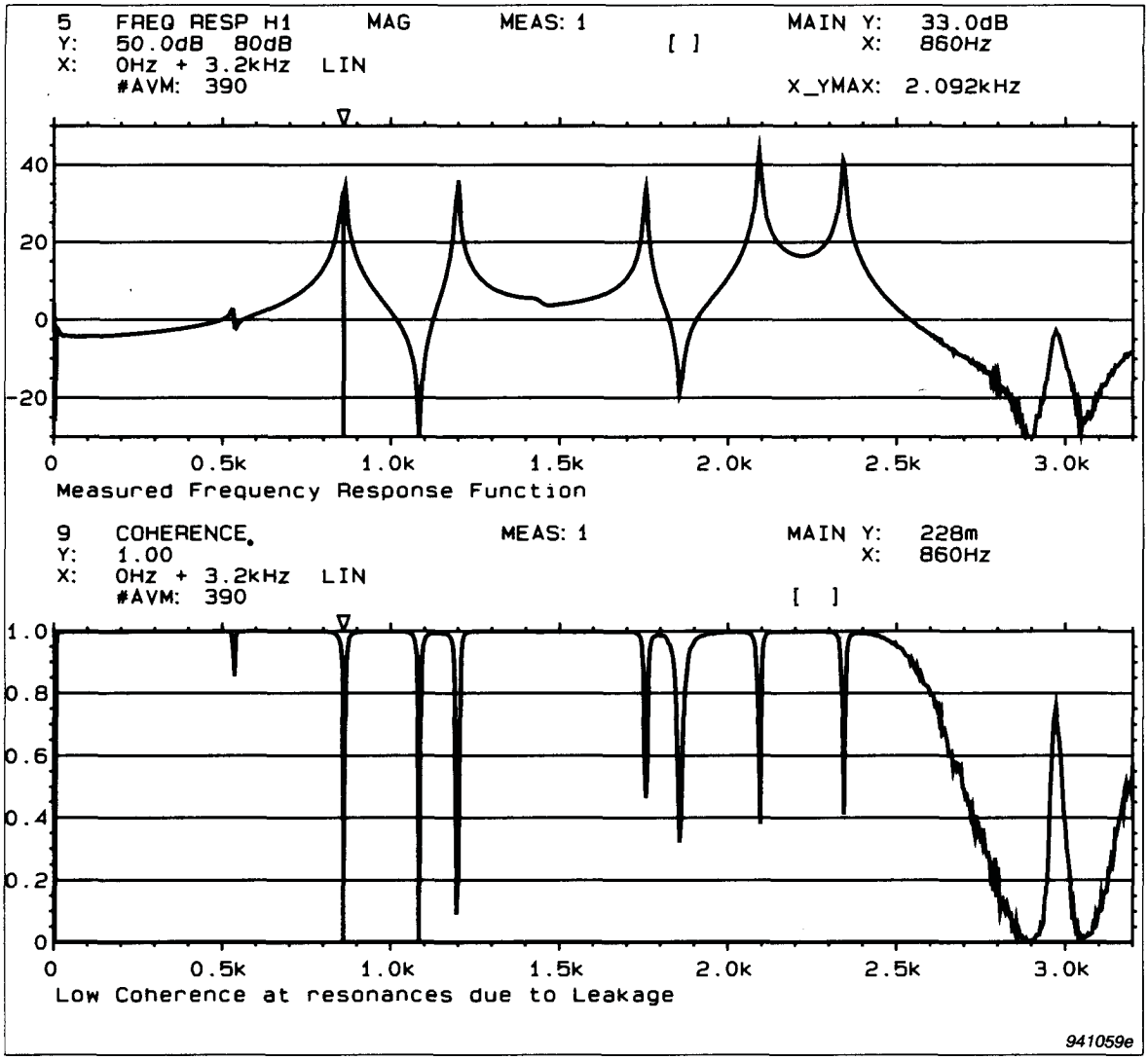

Fig. 14. Frequency response function and coherence in the baseband measurement using random force excitation. Notice the low coherence at the resonances due to leakage (resolution bias error)

ments were performed around each resonance with sufficient resolution so effect of leakage were eliminated.

The following resolutions were required:

ΔF = 7.8125 mHz for mode 1 at 860 Hz

ΔF = 62.5 mHz for mode 2 at 1198 Hz

ΔF = 125 mHz for mode 3 at 1756 Hz

ΔF = 125 mHz for mode 4 at 2091 Hz

ΔF = 125 mHz for mode 5 at 2341 Hz

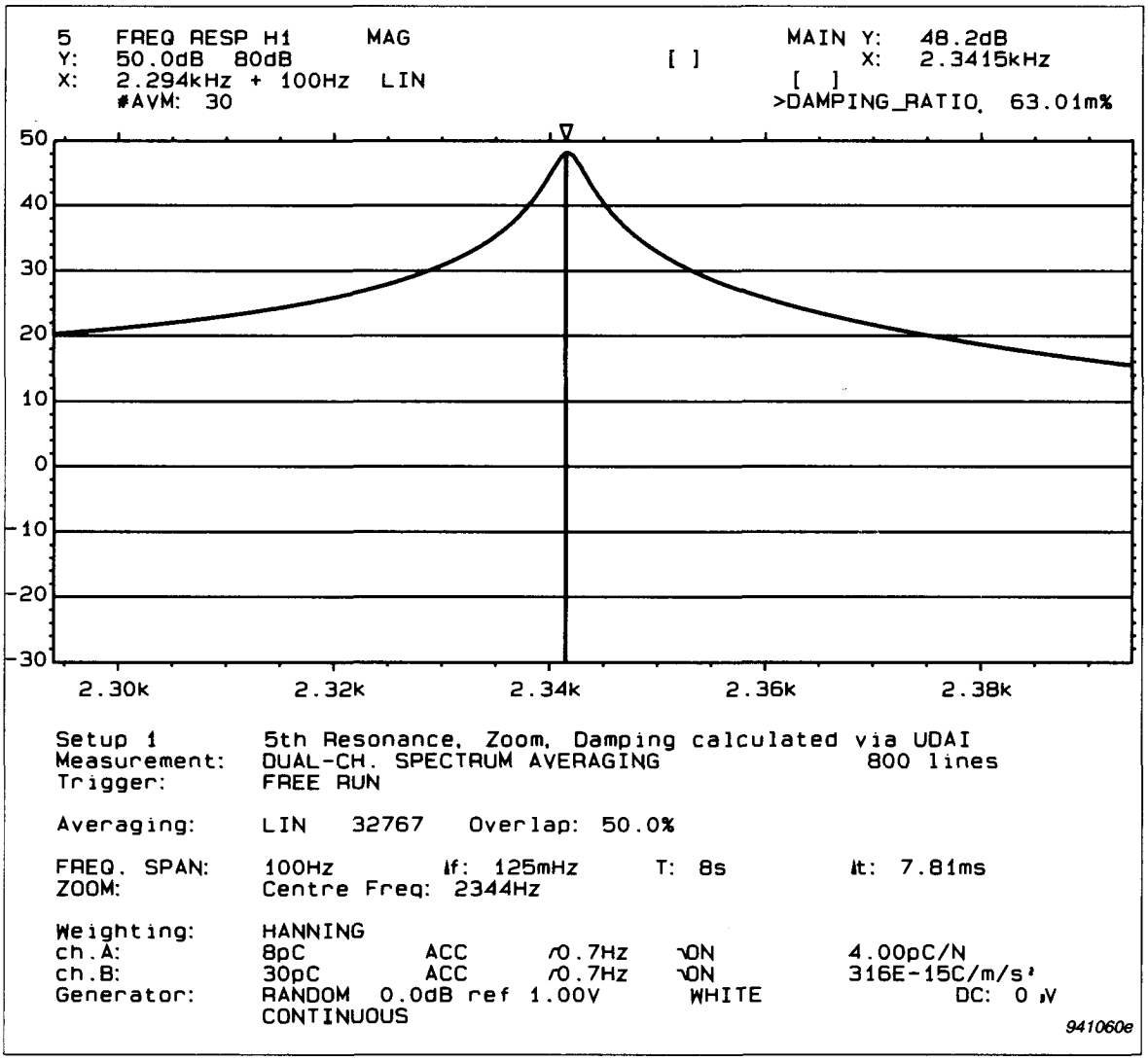

Fig. 15. Zoom measurement around the 5th resonance, Damping Calculated via a User Definable Auxiliary Information

This resolution ensured more than 10 frequency lines in the analysis within the 3 dB bandwidth Δf of the resonances. The force spectrum was very low at the resonance frequencies and thus contaminated with noise at these frequencies. $H_2(f)$ was used as the estimate of the frequency response function since $H_2(f)$ is immune against uncorrelated noise at the input (Ref. [10]).

For each Zoomed Frequency Response Function, damping could be calculated directly inside the analyzer using a User Definable Auxiliary Information see Fig.15. The results are given in Table 2. Except for the first two modes these damping values agree very well with those obtained from the decay

methods and the corrected values from method b). The higher value of the damping for mode 1 and 2 is probably caused by the influence of the force transducer attached to the structure at the excitation point.

The disadvantage of the zoom technique is the extremely long analysis time required, specially for the first mode. The record length was here $T = 1/\Delta F = 1/7.8125$ mHz = 128 sec, which means that e.g. 20 statistical independent averages performed with 50% overlap took (128+19 · 128/2)sec = 1344sec = 22min 24 sec.Ref.[12].

d) Decay of Impulse Response Function Calculated from Weighted Frequency Response Function

The frequency response function (accelerance) is estimated using shaker excitation as in c) here however, with a pseudo random force signal. The pseudo random signal is a periodic signal with a period length T equal to the record length T in the analyzer. The sinusoidal components in the spectrum thus coincides with the analysis lines in the analyzer and leakage is avoided using rectangular weighting (Ref.[101). The calculated lines in the frequency response function are thus samples of the "true" frequency response function and can be used for calculation of unbiased (with respect to damping) impulse response function or leakage-free curve fitting.

A baseband measurement with a frequency span of 3.2kHz (as previously) is performed. The measurement setup and an estimated frequency response function is shown in Fig. 16. A frequency weighting function consisting of a short rectangular weighting with 50% cosine taper were then used to isolate the different resonances in the frequency response function. Fig. 17 and 18 shows the weighted frequency response function and the corresponding impulse response function (magnitude) for mode 1 and 5 respectively. The decay appears on a logarithmic amplitude axis as a straight line. The damping is now extracted from the measured slope of the decay exactly as was done in the free decay method. A User Definable Auxiliary Information is used for the damping calculation. The resonance frequency is defined as a User Definable Variable. The reference cursor was used to define the two cursor points as seen in Fig. 17 and 18. The resulting damping values calculated by the User Definable Auxiliary Information are given in Table 2 and excellent agreement with the values from the zoom measurements in the random test c) is obtained except for the 1st mode where $\zeta_1 = 0.0134\%$ instead of $\zeta_1 = 0.011\%$. This could be caused by problems with uncorrelated noise in the input (force) at the resonances. The impulse response function was calculated from $H_1(f)$ which, as opposed to the $H_1(f)$ estimator, is biased (too low amplitude values) in case of

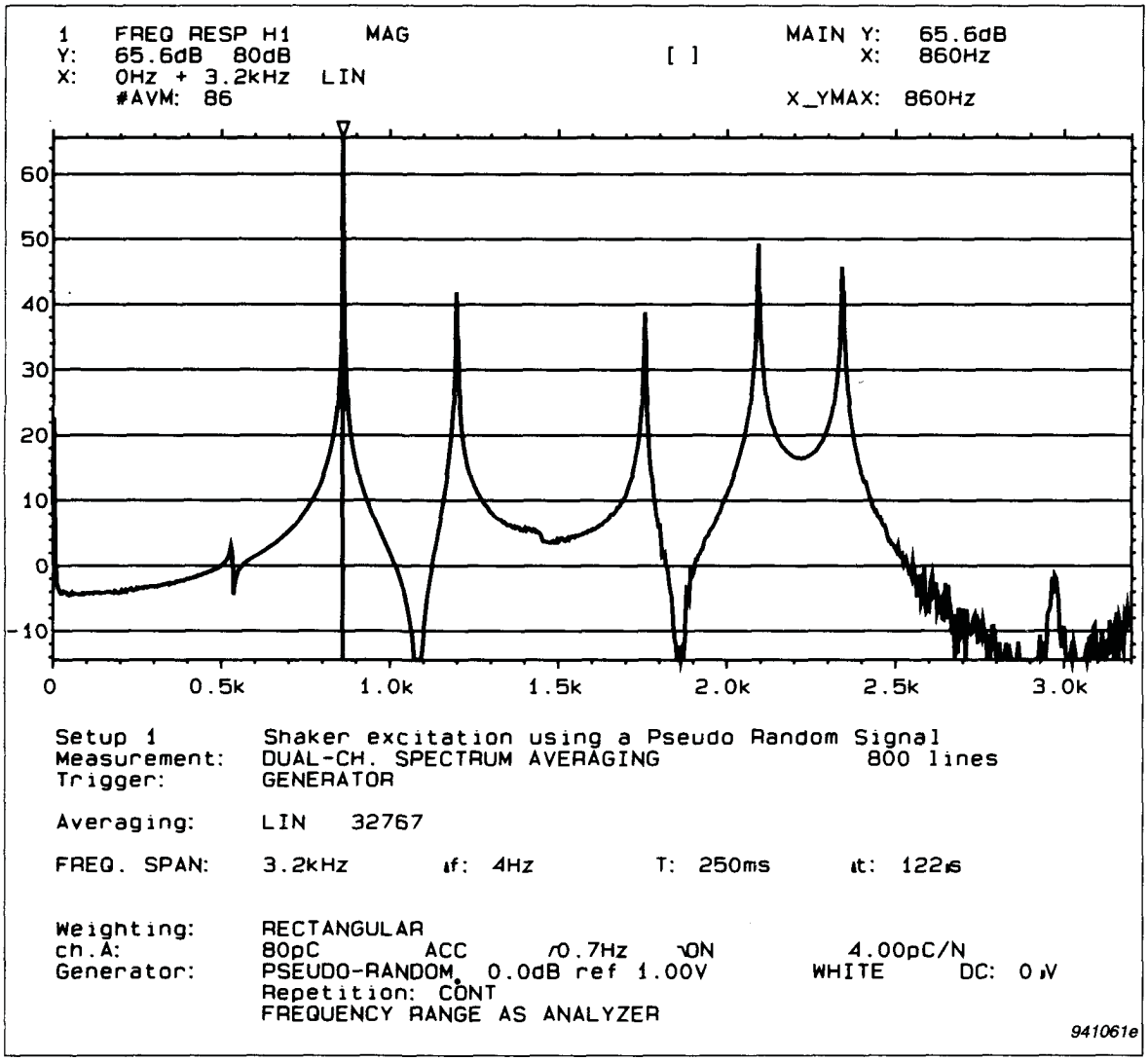

Fig. 16. Measurement setup and estimated frequency response function using pseudo random excitation with a shaker

noise at the input. The estimated damping values will thus be biased as well (too high).

The baseband frequency response function ($H_1(f)$) was also transferred to the modal software and SDOF polynominal curve fitting was performed on each resonance. The damping results are given in Table 2 and they are seen to be identical to the values estimated from the impulse responses.

Finally 100 Hz wide zoom measurements with ΔF = 125 mHz were performed around each resonance in order to investigate whether there was any influence of input noise as mentioned earlier. With ΔF = 125 mHz the signal/

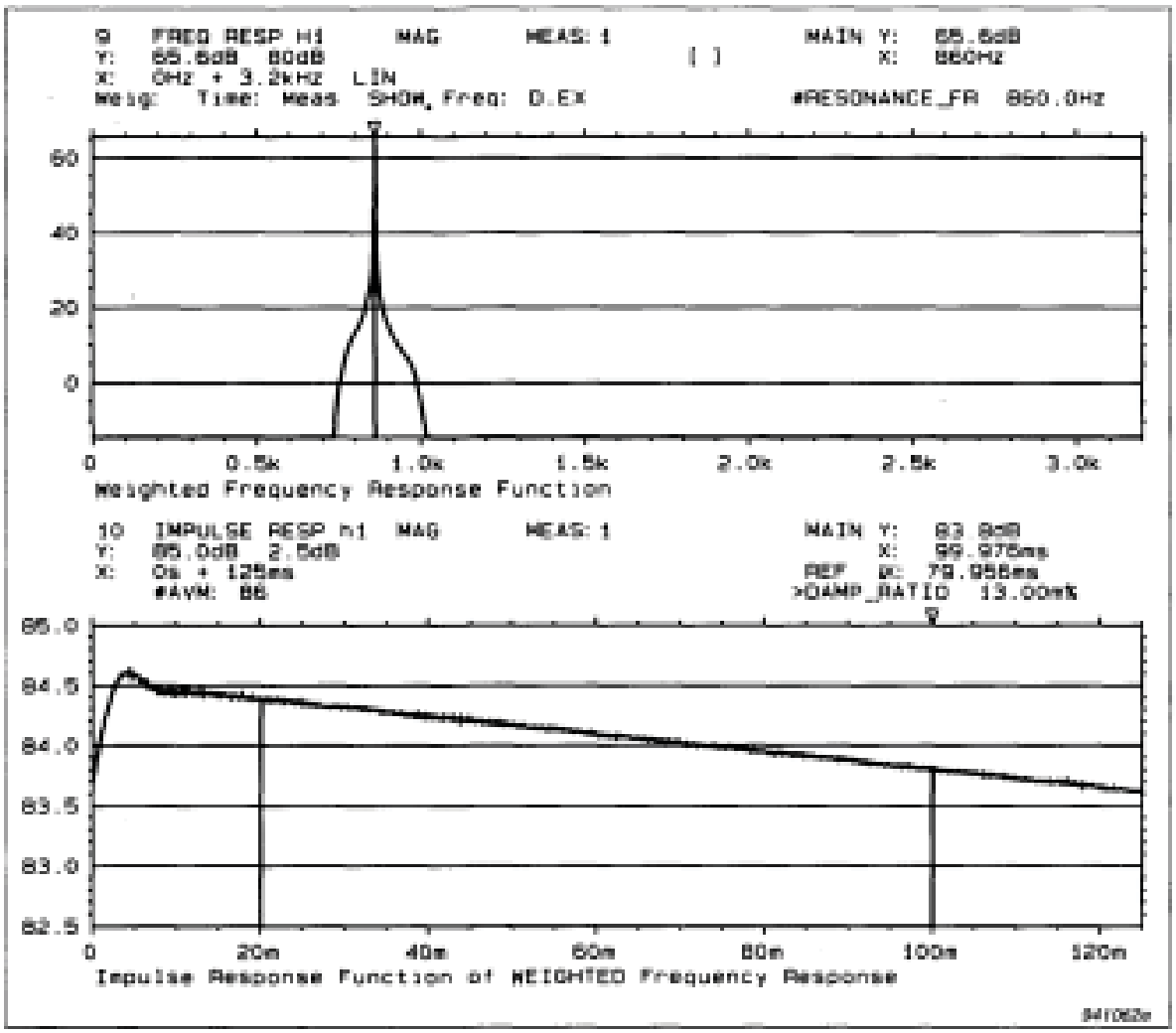

Fig. 17. Weighted frequency response function isolating the 1st resonance and corresponding impulse response function (magnitude). The weighting function is a transient window 40 frequency lines wide with 20 lines cosines taper on each side (50% cosine taper)

noise ratio is improved by a factor of 32 (15dB). The record length T is here 8 sec. The damping values calculated from the impulse responses of the zoom measurements are given in Table 2. For the 1st mode the damping is now estimated to be ζ_1= 0.0121% which is closer to the value from the random test with zoom. The damping values of the 3rd 4th and 5th mode gave, however, slightly higher values compared to the baseband test. The estimated damping values thus seems to be more influenced by small random errors than by systematic errors from the noise problem. This method, using pseudo random excitation, is thus much faster than the one using random excitation, since a

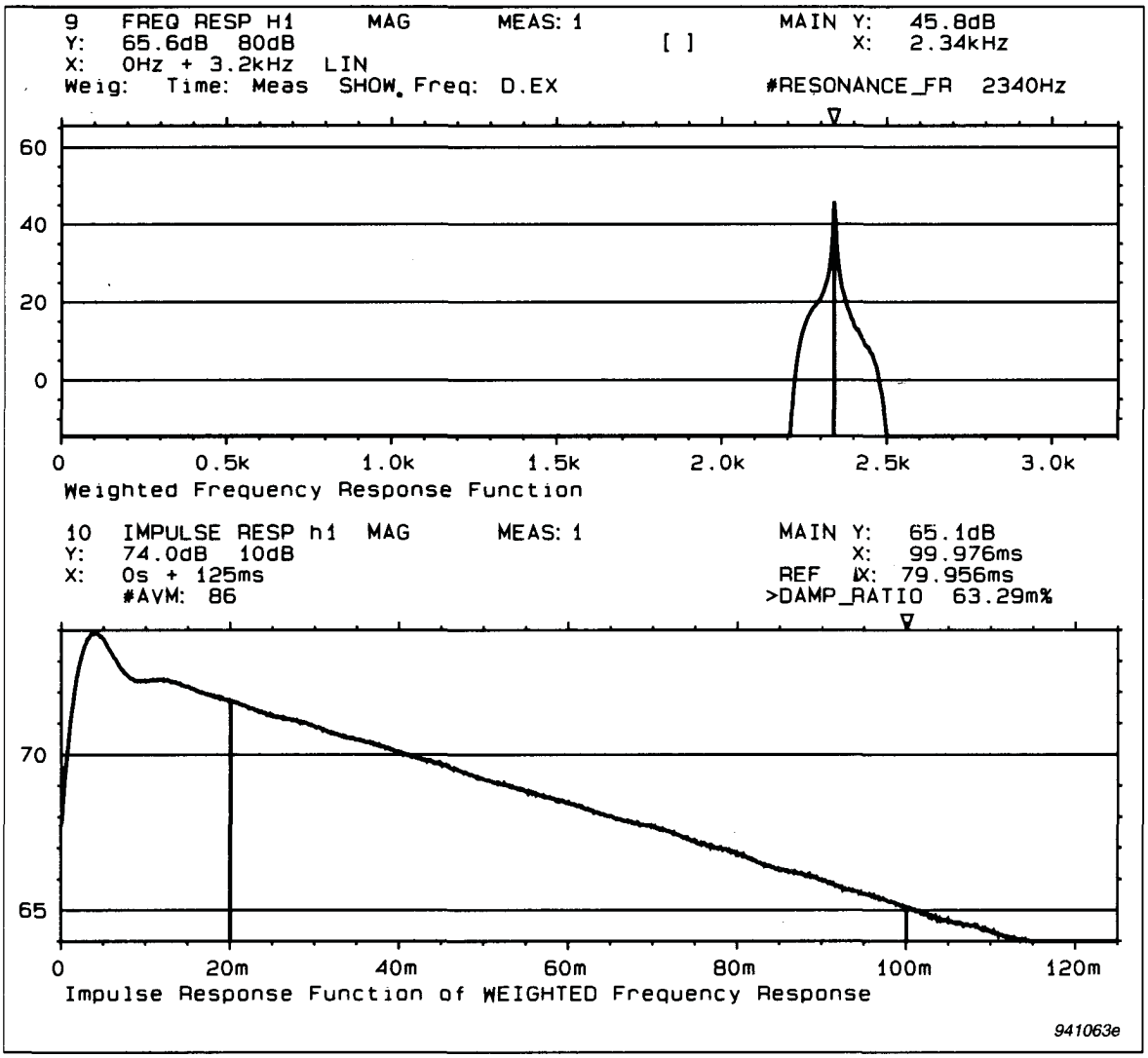

Fig. 18. Weighted frequency response function isolating the 5th resonance and the corresponding impulse response function (magnitude). The weighting function is a transient window 40 frequency lines wide with 20 lines of cosine taper on each side (50% cosine taper)

(baseband) measurement where $\Delta F \approx 50 \cdot \Delta f$ gives damping results within the overall accuracy determined by the setup. Ref. [16].

As for the decay methods, damping of single modes can only be determined if the modes are well separated in the spectrum (say by 10 analysis lines in this case). Otherwise an average damping of the modes in the bandwidth (determined by the frequency weighting function) is obtained and averaging over several excitation and response points would have to be performed in order to get consistent results.

Experimental Results Using Time-frequency Analysis Techniques

The Brüel&Kjær Non-stationary Signal Analysis Software, WT9362 offers three advanced Time-frequency analysis techniques, namely the Short-time Fourier Transform (STFT), the Wavelet Transform (WT) and the Wigner-Ville Distribution (WVD). Refs. [13,14,15].

Since signals from vibration decay measurements are highly non-stationary, these techniques are well suited for damping calculations using the free decay method.

STFT provides constant absolute bandwidth analysis, which is often preferred with vibration signals in order to identify harmonic components. STFT offers a constant resolution in time as well as in frequency domain irrespective of the actual frequency. The STFT is denned as the Fourier Transform of a Gaussian windowed time signal for various positions, b, of the window. This can be stated in terms of inner products between the signal and the window:

$$\begin{aligned} \mathrm{Sb} &= \int s\,(t)\, g^{*}\,(t-b)\, e^{-j2\pi f\,(t-b)}\mathrm{d}t \\ &= \langle s,\, g_{b,f} \rangle \end{aligned}$$

$$\text{with } g_{b,f}(t) = g\,(t-b)\, e^{j2\pi f\,(t-b)} \tag{8}$$

where s is the signal, g is the window, b is the time parameter and fis the frequency parameter. See Fig. 19.

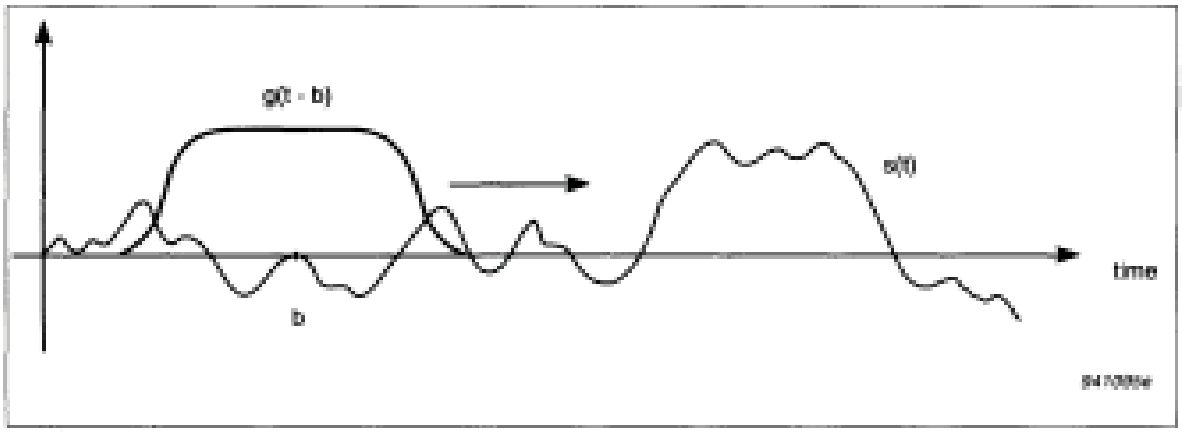

Fig. 19. The Short-time Fourier Transform (STFT). The Window, g(t - b) extracts spectral information from the signal around time b by means of the Fourier Transform

The Wavelet Transform (WT) is especially relevant for acoustic applications since it provides constant percentage bandwidth analysis (e.g. 1/3 octaves). Thus WT offers excellent frequency resolution at low frequencies and excellent time resolution at high frequencies. The WT is denned from a basic wavelet, ψ, which is an analyzing function located both in time and frequency. From the basic wavelet a set of analyzing functions is found by means of scalings (parameter a) and translations (parameter b):

$$S(b, a) = a^{-1/2} \int s(t)\, \psi^* \left(\frac{t-b}{a}\right) \mathrm{dt}$$
$$= \langle s, \psi_{b,a} \rangle$$
$$\text{with} \quad \psi_{b,a}(t) = a^{-1/2}\, \psi\left(\frac{t-b}{a}\right) \tag{9}$$

where s is the signal, ψ is the wavelet, b is the time parameter and a is the scale parameter. See Fig. 20.

The product between time (RMS duration) and frequency (RMS bandwidth) resolution cannot be smaller than 1/4 π for these two techniques, according to the Heisenbergs Uncertainty Principle.

The Wigner-Ville Distribution (WVD) is not limited by the uncertainty relationship, due to the fact that it is a more general transform, not using an analyzing function. Unfortunately this transform leads to the emergence of negative energy levels and cross terms, which are irrelevant from a physical point of view. Therefore the analysis results obtained with WVD can some-

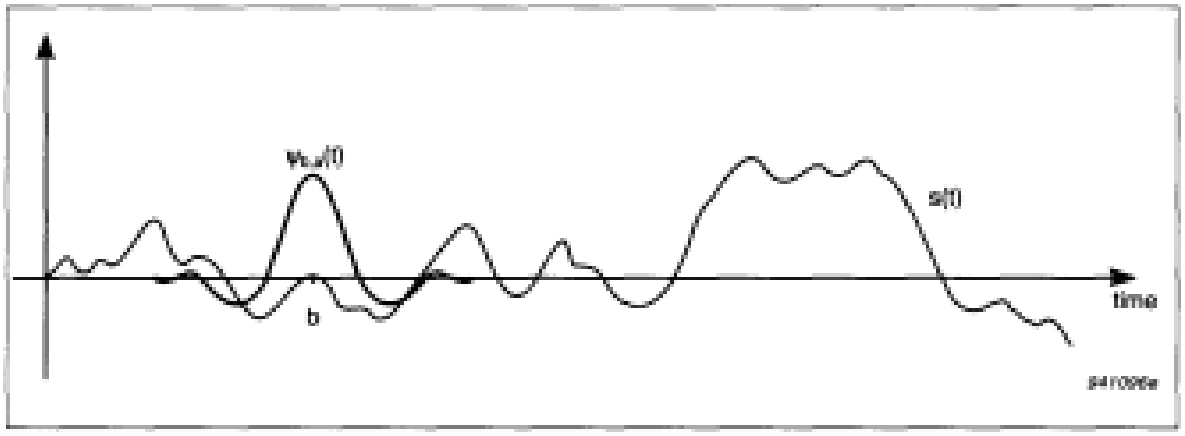

Fig. 20. The Wavelet Transform (WT). The Wavelet, ψ , extracts time scaled information from the signal around the time, b by means of inner products between the signal and scaled (parameter a) versions of the wavelet

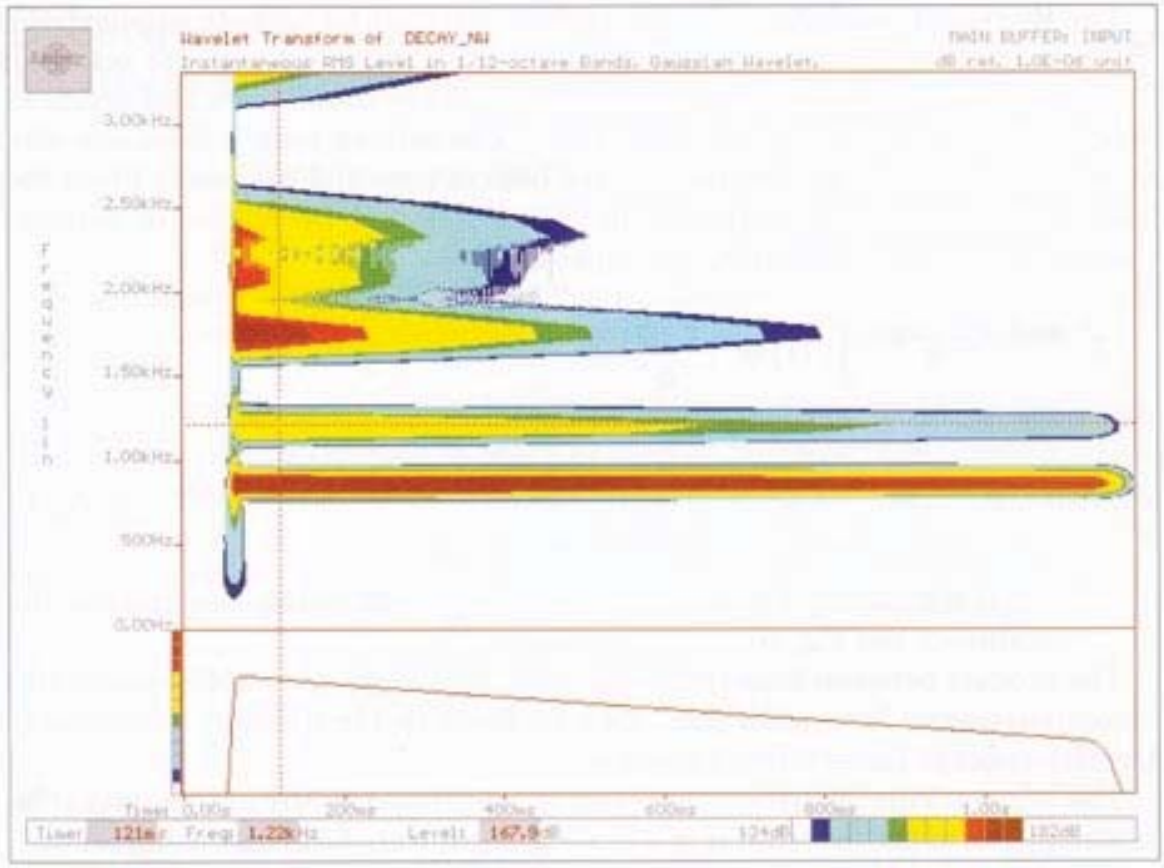

Fig. 21. 1/12th octave Wavelet Transform of a free vibration decay measurement. Notice a linear frequency axis has been selected for easy comparison with the results obtained by the STFT shown in Fig. 22. A slice cursor is used to extract the decay curve of one of the resonances for damping calculation

times be difficult to interpret. On the other hand the WVD, which is a global transformation, is regarded as being the most fundamental of all Time-frequency distributions and is defined as

$$W_s(\tau,f) = \int s\,(t + \tau/2)\; s^*\,(t - \tau/2) e^{-j2\pi ft} \mathrm{d}t \qquad (10)$$

where s is the time signal, τ is the time parameter and f is the frequency parameter. Note that WVD is a kind of combined Fourier Transform and auto-correlation calculation, i.e. autospectrum estimate as a function of time or autocorrelation estimate as a function of frequency. One other drawback of the WVD is that it requires large computational power.

As an example, a 1/12th octave WT was applied to the 32K Time Capture recording of the free vibration decay shown in Fig.9. The Time-frequency con-

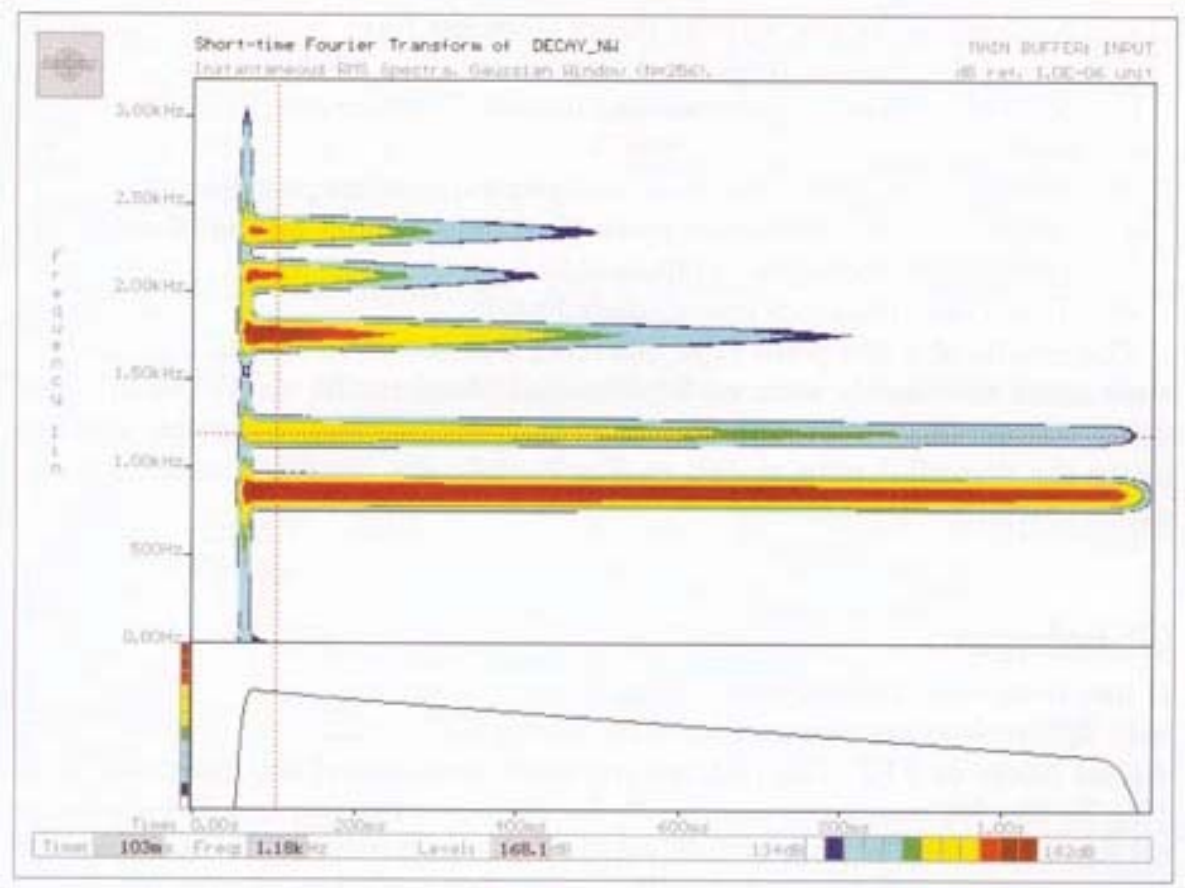

Fig. 22. A 256 point Short-time Fourier Transform of a free vibration decay measurement. A slice cursor is used to extract the decay curve of one of the resonances for damping calculation

tour map is shown in the upper trace of Fig. 21. As a postprocessing possibility the map can be integrated backwards (using the Schroeder method as mentioned earlier) if nescessary.

The 5 resonances are seen as 5 horizontal areas in the map, although the two highest resonances are only separated by two filter bandwidths as seen earlier in Figs. 3 and 5. A slice cursor can be used to extract the levels of a particular resonance frequency as a function of time. This is shown for the second resonance in the lower trace of Fig. 21. Cursor readings confirm the damping results as found earlier.

The main advantages of using fractional octaves Wavelet Transform compared to fractional octaves Digital Filtering for the analysis of non-stationary signals are as follows:

a) No "ringing" of the wavelet filters since the filter shapes and the envelope of the impulse response functions are Gaussian.
b) No RMS detector time-constant limitation, since envelope detection is used.
c) No frequency dependent time delay in the analysis process.
d) Optimum Time-frequency resolution, only limited by the Heisenbergs Uncertainty Principle, is obtainable.
e) True Time-frequency energy distribution.

The results of a 256 point (100 line) STFT is shown in Fig. 22. Again the 5 resonances are clearly seen as 5 horizontal areas in the map. The analysis using contour map shown in Fig. 22 is in practice identical to the analysis using the waterfall map shown in Fig. 9. Only the display format and the choice of window are different.

Conclusion

It has here been demonstrated how damping values of single resonances of very lightly damped structures can be determined by different methods using digital filters or FFT. The relative standard deviation of the estimates were 15% for the 1st resonance and 5-7% for the other resonances. The variation between the results were rather random than systematic. It was observed that extremely small changes in the setup and the environment influenced the damping values up to the observed variances. The use of Time-frequency analysis techniques was also demonstrated.

References

[1] JACOBSEN,F: *"Measurement of structural loss factors by the power input method".* Report No. 41,1986, Acoustics Laboratory of the Danish Technical University

[2] JACOBSEN.F., BAO.D.: *"Acoustic Decay Measurements with a Dual Channel Frequency Analyzer",* Journal of Sound and Vibration (1987) 115(3) pp. 521-537

[3] JACOBSEN.F.: *"A note on Acoustic Decay Measurements",* Journal of Sound and Vibration (1987) 115(1), pp.163-170

[4] JACOBSEN,F., RINDEL,J.H.: Letters to the editor: *"Time Reversed Decay Measurements",* Journal of Sound and Vibration (1987) 117(1), 187-190

[5] JACOBSEN,F.: *"Experimental Determination of Structural Damping",* Proceedings of Nordic Acoustical Meeting, Aalborg, Denmark, 1986, pp. 361-364

[6] CREMER.L., HECKL,M.: *"Structure-Borne Sound",* Berlin, Springer-Verlag, 1973

[7] ZAVERI,K.: *"Complex Modulus Measurements using Wide Band Random Excitation",* Proceedings of Internoise, Beijing, China, 1987, pp. 1383-1386

[8] BROCH,J.T.: *"Mechanical Vibration and Shock Measurements",* Brüel & Kjær, 1980

[9] SCHROEDER.M.R.: *"New Method of Measuring Reverberation Time"* J. Acou. Soc. Am. 37 (1965), pp. 409- 412

[10] HERLUFSEN.H.: *"Dual channel FFT analysis (Part I & II)"* Brüel &Kjaer Technical Review No. 1 & 2,1984

[11] CRAIK, R., NAYLOR, G.: Letters to the editor: *"Measurement of Reverberation Time via Probability Functions"* Journal of Sound and Vibration (1985) 102(3), pp.453-454

[12] GADE.S. & HERLUFSEN,H.: *"Use of Weighting Functions in DFTI FFT analysis",* Brüel & Kjær Technical Reviews Nos. 3 & 4,1987

[13] GRAM-HANSEN, K.: *"Simultaneous Time and Frequency Analysis"* Ph.D. Thesis 1990, The Electronics Institute, Technical University of Denmark

[14] RIOUL.O. & VETTERLI,M.: *"Wavelets and Signal Processing"* IEEE Signal Processing Magazine, October 1991

[15] Brüel&Kjær: *"Non-stationary Signal Analysis Software Type WT9362"* System Development, BU 0152, 1993

[16] HERLUFSEN, H. & GADE, S.: *"Errors Involved in Computing Impulse Response Function via Frequency Response Function".* Mechanical Systems and Signal Processing 6 (3), pp. 193-206,1992

Previously issued numbers of Brüel & Kjær Technical Review

(Continued from cover page 2)

1-1985 Local Thermal Discomfort

4—1984 Methods for the Calculation of Contrast
Proper Use of Weighting Functions for Impact Testing
Computer Data Acquisition from Brüel & Kjær Digital frequency Analyzers 2131/2134 Using their Memory as a Buffer

3-1984 The Hilbert Transform
Microphone System for Extremely Low Sound Levels
Averaging Times of Level Recorder 2317

2-1984 Dual Channel FFT Analysis (Part II)

1-1984 Dual Channel FFT Analysis (Part I)

4-1983 Sound Level Meters - The Atlantic Divide
Design Principles for Integrating Sound Level Meters

3-1983 Fourier Analysis of Surface Roughness

2-1983 System Analysis and Time Delay Spectrometry (Part II)

1-1983 System Analysis and Time Delay Spectrometry (Part I)

4-1982 Sound Intensity (Part II Instrumentation and Applications)
Flutter Compensation of Tape Recorded Signals for Narrow Band Analysis

3-1982 Sound Intensity (Part I Theory)

2-1982 Thermal Comfort

1-1982 Human Body Vibration Exposure and its measurement

4-1981 Low Frequency Calibration of Acoustical Measurement Systems
Calibration and Standards. Vibration and Shock Measurements

Special technical literature

Brüel & Kjær publishes a variety of technical literature which can be obtained from your local Brüel & Kjær representative.
The following literature is presently available:

- Modal Analysis of Large Structures-Multiple Exciter Systems (English)
- Acoustic Noise Measurements (English), 5th. Edition
- Noise Control (English, French)
- Frequency Analysis (English), 3rd. Edition
- Catalogues (several languages)
- Product Data Sheets (English, German, French, Russian)

Furthermore, back copies of the Technical Review can be supplied as shown in the list above. Older issues may be obtained provided they are still in stock.

Brüel & Kjær

WORLD HEADQUARTERS: DK-2850 Nærum · Denmark
Telephone: +45 42 80 05 00 · Telex: 37316 bruka dk · Fax: +45 42 80 14 05

Australia (02) 450-2066 · Austria 0222/816 74 00 · Belgium 016/44 92 25 · Brazil (011) 246-8149/246-8166
Canada (514) 695-8225 · Czech Republic 02-24 310 458 · Finland (0) 1481577 · France (1) 64 57 2010
Germany 04106/70 95-0 · Great Britain (081) 954-2366 · Holland 03402-39994 · Hong Kong 548 7486
Hungary (1) 215 83 05/215 89 29 · Italy (02) 57 60 41 41 · Japan 03-5420-7302 · Republic of Korea (02) 554-0605
Norway 66 90 44 10 · Poland (0-22) 40 93 92 · Portugal (1) 65 92 56/65 92 80 · Singapore 225 8533
Slovak Republic 07-55666 · Spain (91) 368 10 00 · Sweden (08) 711 27 30 · Switzerland (1) 862 19 60
Taiwan (02) 713 9303 · Tunisia (01) 232 478 · USA: MA (508) 481-7737 GA (404) 981-6225 MI (313) 522-860
IL (708) 358-7582 CA (714) 978-8066 WA (206) 883-2203/882-4359
Local representatives and service organisations world-wide

ISSN 007 – 2621
BV 0044 – 11

PRINTED IN DENMARK BY NÆRUM OFFSET

Technical Review

No. 2 – 1994

Damping Measurements – From Impulse Response Functions
– From Resonance and Non-resonance Excitation Techniques

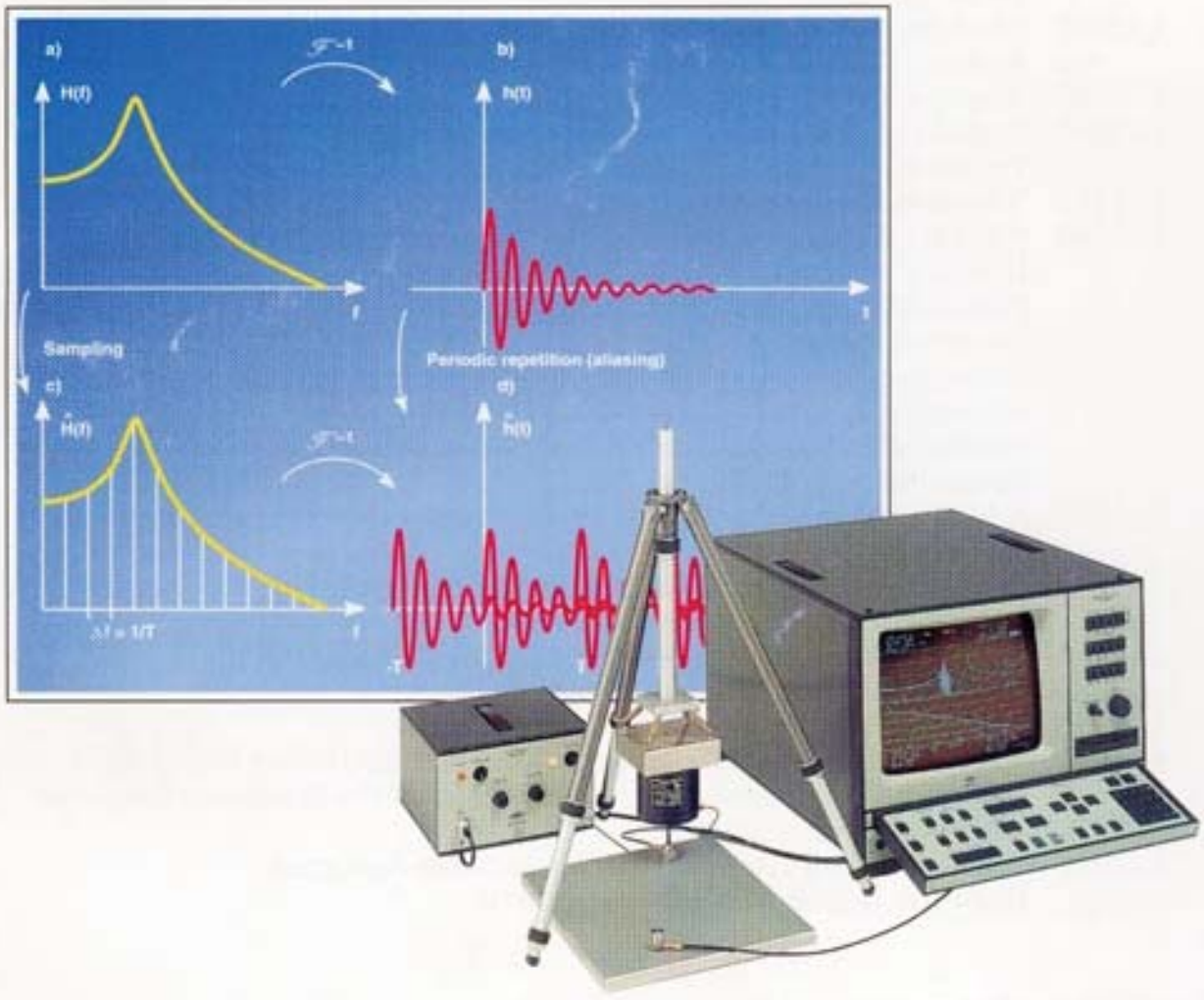

Brüel & Kjær

Previously issued numbers of Brüel & Kjær Technical Review

1 –1994	Digital Filter Techniques vs. FFT Techniques for Damping Measurements (Damping Part I)
2-1990	Optical Filters and their Use with the Type 1302 & Type 1306 Photoacoustic Gas Monitors
1 –1990	The Brüel & Kjær Photoacoustic Transducer System and its Physical Properties
2-1989	STSF — Practical instrumentation and application Digital Filter Analysis: Real-time and Non Real-time Performance
1 –1989	STSF — A Unique Technique for scan based Near-Field Acoustic Holography without restrictions on coherence
2-1988	Quantifying Draught Risk
1 –1988	Using Experimental Modal Analysis to Simulate Structural Dynamic Modifications Use of Operational Deflection Shapes for Noise Control of Discrete Tones
4-1987	Windows to FFT Analysis (Part II) Acoustic Calibrator for Intensity Measurement Systems
3-1987	Windows to FFT Analysis (Part I)
2 –1987	Recent Developments in Accelerometer Design Trends in Accelerometer Calibration
1 –1987	Vibration Monitoring of Machines
4-1986	Field Measurements of Sound Insulation with a Battery-Operated Intensity Analyzer Pressure Microphones for Intensity Measurements with Significantly Improved Phase Properties Measurement of Acoustical Distance between Intensity Probe Microphones Wind and Turbulence Noise of Turbulence Screen, Nose Cone and Sound Intensity Probe with Wind Screen
3 –1986	A Method of Determining the Modal Frequencies of Structures with Coupled Modes Improvement to Monoreference Modal Data by Adding an Oblique Degree of Freedom for the Reference
2 –1986	Quality in Spectral Match of Photometric Transducers Guide to Lighting of Urban Areas
1 –1986	Environmental Noise Measurements
4 –1985	Validity of Intensity Measurements in Partially Diffuse Sound Field Influence of Tripods and Microphone Clips on the Frequency Response of Microphones
3 –1985	The Modulation Transfer Function in Room Acoustics RASTI: A Tool for Evaluating Auditoria

(Continued on cover page 3)

Technical Review

No.2 -1994

Contents

Damping Part II

Editor: K. Zaveri Photographer: Peder Dalmo
Layout: Judith Sarup Printed by Nærum Offset

The use of Impulse Response Function for Modal Parameter Estimation

by Svend Gade & Henrik Herlufsen

Abstract

This article discusses the errors that are introduced when calculating the impulse response function from the frequency response function using DFT/ FFT analysis technique.

The impulse response function is used in many applications of system analysis where a description of the system characteristics is preferred in the time domain rather than in the frequency domain. The case where the system is a single degree of freedom system (SDOF), with viscous damping, is analysed. It is shown that the estimated impulse response function is not described by a single exponentially decaying sine wave but rather as a sum of exponentially decaying sine waves. It is important to apply this slightly more complex model when the measurements are to be used for mathematical modelling of systems containing lightly damped resonances and where measurements free of the influence of leakage are performed.

This article represents an expansion of papers presented at the Modal Analysis Conference ISMA 15, held in Leuven, Belgium 1990 and included in the Proceedings of IMAC 9, Firenze, Italy 1991.

Resume

Cet article décrit les erreurs pouvant survenir lors du calcul de la réponse impulsionnelle à partir de la fonction de réponse en fréquence, dans le cadre d'une analyse DFT/FFT.

La fonction de réponse impulsionnelle intervient lorsque, pour décrire les caractéristiques d'un système, les techniques d'analyse en fréquence dans le domaine temporel sont préférées à celles du domaine fréquentiel. Le cas d'un système à un degré de liberté (SDOF) avec amortisseurs à fluide est ici exa-

miné. II est montré que la fonction de réponse impulsioimelle estimée n'est pas représentée par une seule onde sinusoïdale à décroissement exponentiel mais plutôt par une somme de ces ondes. II est important d'appliquer ce modèle un peu plus complexe lorsque les mesures doivent servir de base à des modèles mathématiques de systèmes présentant des resonances légèrement amorties, et dans le cas de mesures ou l'influence de fuites n'est pas prise en compte.

Cet article se place dans le prolongement des articles exposes lors de la conférence sur l'analyse modale ISMA 15, à Louvain en 1990 et inclus dans le compte rendu de la conférence IMAC qui s'est tenue à Florence en 1991.

Zusammenfassung

In diesem Artikel werden die Fehler diskutiert, die entstehen, wenn die Impulsantwortfunktion mit DFT/FFT-Analysetechnik aus der Frequenzgangfunktion berechnet wird.

Die Impulsantwortfunktion wird bei zahlreichen Systemanalyse-Applikationen verwendet, wenn für die Beschreibung der Systemcharakteristiken der Zeitbereich gegenüber dem Frequenzbereich bevorzugt wird. Es wird der Fall eines Systems mit einem einzigen Freiheitsgrad (SDOF) und viskoser Damprung untersucht. Es wird gezeigt, daß die geschätzte Impulsantwortfunktion nicht durch eine einzelne exponentiell abklingende Sinuswelle, sondem eher als die Summe exponentiell abklingender Sinuswellen beschrieben wird. Es ist wichtig, dieses etwas komplexere Modell für Messungen anzuwenden, die zur mathematischen Modellierung von Systemen mit leicht gedämpften Resonanzen dienen, sowie für Messungen, die unbeeinflußt von Leckagen durchgeführt werden.

Der Artikel stellt eine Erweiterung der Dokumentation dar, die auf der Modalanalyse-Konferenz ISMA 15 in Leuven, Belgien, 1990 präsentiert und auf der IMAC 9, Florenz, Italien, 1991 in die Berichterstattung aufgenommen wurde.

Nomenclature

dB	decibels, ten times the logarithm to a (power) ratio
e	base of natural logarithm, 2.72 ....
i	an integer ($-\infty < i \leq 0$ or $0 \leq i < \infty$)
j	imaginary number, $\sqrt{-1}$
k	spectrum line number (an integer)
m	milli. 10^{-3}

n	relative time constant
s	seconds
A_0	constant amplitude, Residue
C, C1, C2	amplitude (bias) error
B & K	Brüel & Kjær
DFT	Discrete Fourier Transform
FFT	Fast Fourier Transform, fast version of DFT
FRF	Frequency response function
$H(f)$	Frequency response function
Hz	Hertz [s^{-1}]
IDFT	Inverse Discrete Fourier Transform
IRF	Impulse response function
$h(t)$	Impulse response function
$L\varepsilon$	amplitude error in dB
MDOF	Multi Degree of Freedom
R	residue
$\angle R$	angle of residue
SDOF	Single Degree of Freedom
SMS	Structural Measurement System, Inc.
STAS	Structural Testing and Analysis System
T	FFT record length
^	estimated value
ε_b	amplitude (bias) error
ζ	fraction of critical damping, damping ratio
φ	phase error [Radians]
σ	decay constant [s^{-1}]
σ_m	measured decay constant [s^{-1}]
σ_w	decay constant for exponential weighting [s^{-1}]
t	time [s]
τ	time constant [s]
ω_d	damped natural frequency [Rad/s]
Δf_{3dB}	3 dB bandwidth [Hz]
Δf	FFT line spacing [Hz]
%	per cent, $10\sim^2$
F	Fourier Transform
F^{-1}	Inverse Fourier Transform

Introduction

When measuring system characteristics, an input and an output must be denned. This will be in terms of a certain physical parameter, point, position, direction, etc. Simultaneous measurement of the input signal to the system (the excitation) and the output signal from the system (the response) allows calculation of the system characteristics such as damping. The function describing the dynamic behaviour of the system in the time domain is the impulse response function *h(t).* The corresponding frequency domain function is the frequency response function *H(f).*

Fig. 1 shows a system with input signal *a(t)* and output signal *b(t).* The Fourier spectra *of a(t)* and *b(t)* are *A(f)* and *B(f)* respectively, *F* denotes the Fourier Transform.

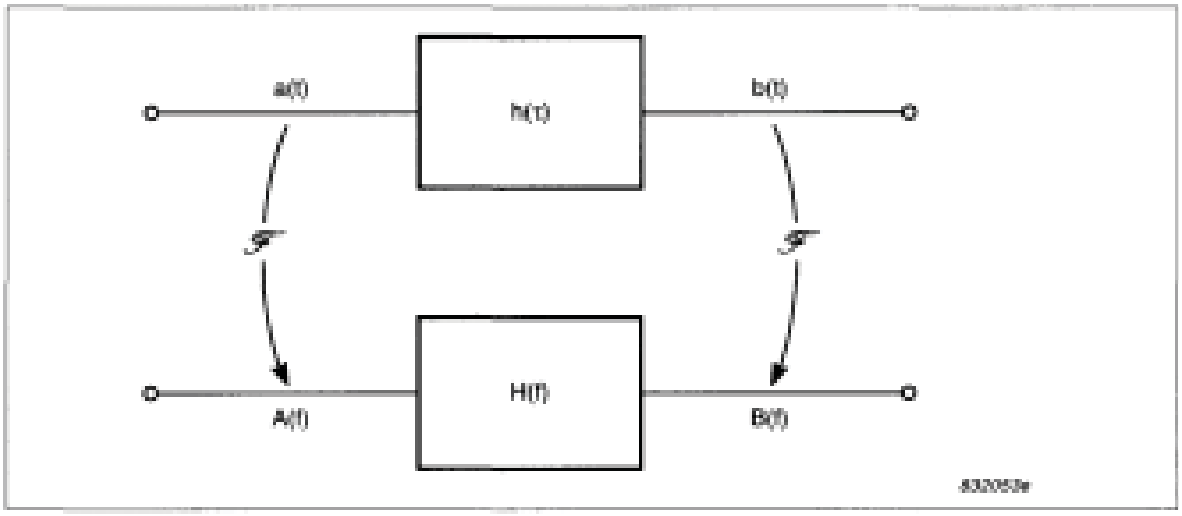

Fig. 1. System with input signal a(t) and output signal b(t). The Fourier Transforms of a(t) and b(t) are A(f) and B(f) respectively

For this description to be valid the system is assumed to be linear. This means that if $a_1(t)$ and $a_2(t)$ produce the outputs $b_1(t)$ and $b_2(t)$ respectively, then the input $a_1(t) + a_2(t)$ must produce the output $b_1(t) + b_2(t)$.

Physically the impulse response function *h(t)* is the response of the system to a unit impulse signal $\delta(t)$. $\delta(t)$, also called a Dirac delta function, is an infinitely short and infinitely high impulse at $t = 0$. Its time integral is unity and its Fourier spectrum is unity at all frequencies, i.e.

$$\int_{-\infty}^{\infty} \delta(t)\,dt = 1 \tag{1}$$

and

$$\mathcal{F}\{\delta(t)\} = 1 \quad -\infty < f < \infty \tag{2}$$

In order to find the relationship between the input signal and the output signal we can consider any input signal *a(t)* as a superposition of weighted and time-shifted delta functions, i.e.

$$a(t) = \int_{-\infty}^{\infty} a(t')\,\delta(t-t')\,dt' \tag{3}$$

Each of these weighted and time-shifted delta functions $a(t')\ \delta\ (t-t')$ at the input will produce a corresponding weighted and time-shifted impulse response $a\ (t')\ h\ (t - t')$ at the output. The output signal *b(t)* caused by the input signal *a(t)* will therefore be the superposition of these individual contributions and

$$b(t) = \int_{-\infty}^{\infty} a(t')\,h(t-t')\,dt' = a(t) * h(t) \tag{4}$$

where * denotes convolution.

The frequency response function *H(f)* is defined as the complex ratio *of B(f)* and *A(f),* i.e.

$$H(f) = \frac{B(f)}{A(f)} \tag{5}$$

or

$$B(f) = H(f)\, A(f) \tag{6}$$

h(t) and *H(f)* are related via the Fourier transform and therefore contain the same information about the dynamic behaviour of the system.

$$H(f) = \mathcal{F}\{h(t)\} \tag{7}$$

Since the multiplication involved in eq.(6) in most cases is a much simpler operation than the convolution in eq.(4), description and interpretation of phenomena is often done in the frequency domain.

In some applications, however, it is advantageous to present the information in the time (or delay) domain rather than in the frequency domain. Examples of such applications are:

- Determination of time delays in systems
- Identification of transmission paths
- Measurements of decays and determination of damping values
- Mathematical modelling and curvefitting for extraction of system parameters

In this article we will be dealing with the last two application examples. They represent situations where the impulse response function is prone to a bias error when calculated via an inverse Fourier transform from a leakage free measurement of the frequency response function using DFT/FFT technique.

When the system under investigation contains lightly damped resonances, the estimated impulse response function will be biased in both amplitude and phase.

Lightly damped resonances in a system causes the impulse response function to be long with decaying oscillations, which in the frequency domain corresponds to sharp, narrow peaks in the frequency response function.

If the record length in the FFT analysis is not sufficiently long compared to the time constant of the decay in the impulse response function, the bias error is observed. In the frequency domain this means that the above-mentioned bias error is observed if the resonance peak in the frequency response function is narrower than the resolution in the analysis even though the calculated samples of the frequency response function are free of the influence of leakage.

Using the impulse response function for system parameter identification (curvefitting) and modelling, such as in modal analysis, the bias error will be reflected in the residues for the resonances and thereby in the estimated mode shapes for the structure, while the natural frequency and damping will be correctly estimated.

Theory

Let us look at a simple single degree of freedom (SDOF) system. Fig. 2 shows a mechanical SDOF system with viscous damping. It consists of a mass *m* supported by a spring with a spring constant *k* and a viscous damper with damping coefficient *c*.

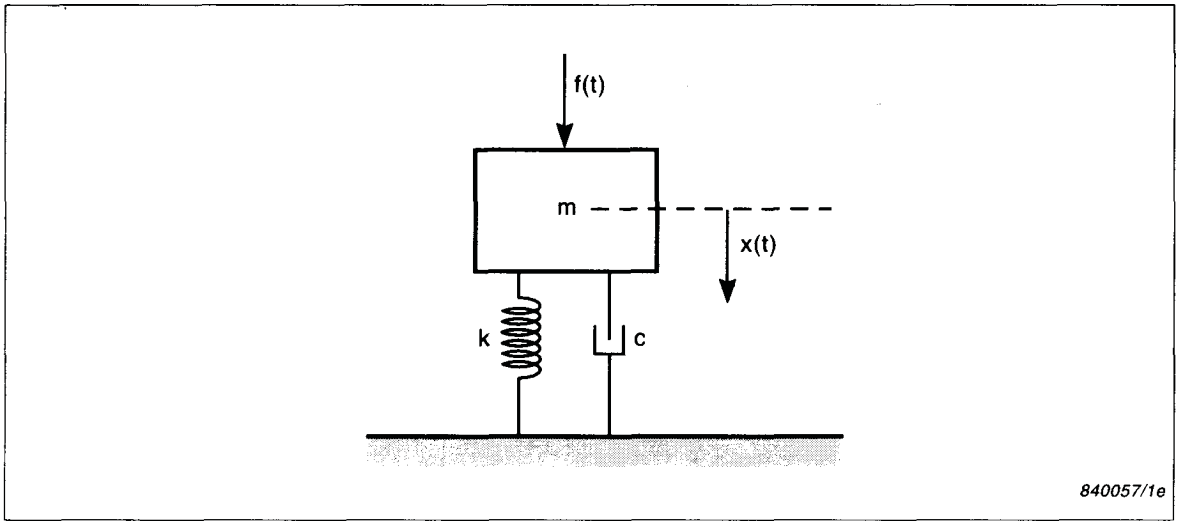

Fig. 2. Mechanical single degree of freedom system

The input is denned to be the force *f(t)* acting on the mass and the output is the displacement *x(t)* of the mass.

The frequency response function (FRF), in this case called the compliance of the system, is given by

$$H(f) = \frac{X(f)}{F(f)} = \frac{1/m}{-\omega^2 + j\omega\frac{c}{m} + \frac{k}{m}} = \frac{R}{j\omega - (j\omega_d - \sigma)} + \frac{R^*}{j\omega - (-j\omega_d - \sigma)} \quad (8)$$

where ω_d, the damped natural frequency, is given by

$$\omega_d = \sqrt{\frac{k}{m} - \frac{c^2}{4m^2}} \quad (9)$$

and σ, *the decay* constant, is given by

$$\sigma = \frac{c}{2m} \tag{10}$$

and *R* is a scaling constant, called the residue. (In the literature the residue is sometimes scaled differently by a factor of 2 and/or a 90 degree phase shift).

An example of the magnitude *of H(f)* is shown in Fig.3a). The corresponding impulse response function (IRF) is an exponentially decaying sine wave as shown in Fig. 3b).

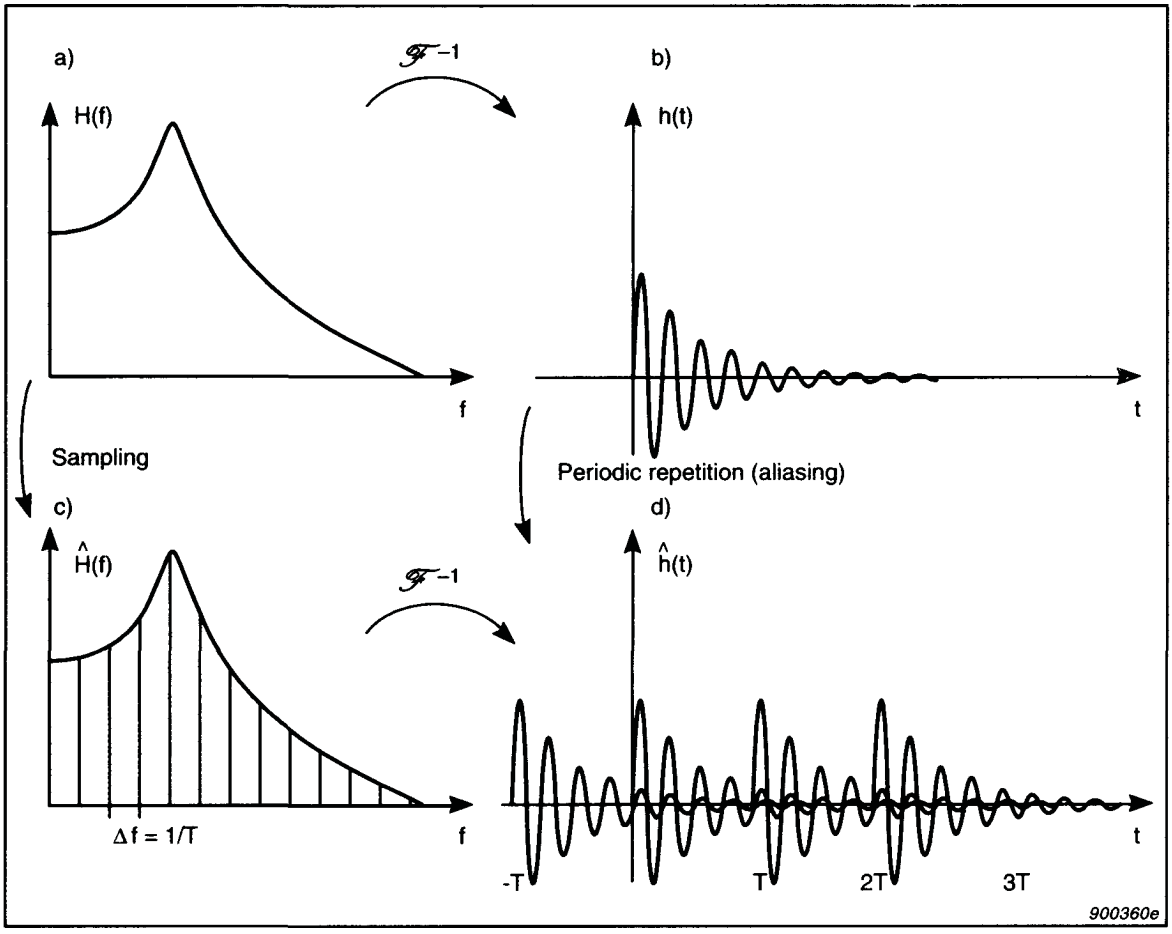

Fig. 3. a) Frequency Response Function (FRF) of a Single Degree of Freedom (SDOF) model, b) Impulse Response Function (IRF) of a SDOF model, c) Sampled FRF of a SDOF model, d) IRF of a sampled FRF SDOF model

Mathematically the IRF is given by

$$h(t) = A_o e^{-\sigma t} \sin(\omega_d t) \qquad 0 \le t \tag{11}$$

h(t) is thus a product of the three terms. $A_o = j2R$ is a (complex) scaling factor given by the residue *R,* except for a factor of 2 and a 90 degree phase shift. $e^{-\sigma t}$ is the exponentially decaying term, determined by the viscous damping and called the damping term. $\sin(\omega_d t)$ is the term that oscillates at a frequency which is the damped natural frequency.

If a leakage free measurement of the FRF is performed, the calculated lines in the estimated FRF are samples of the continuous ("true") FRF. The "sampling rate" is the line spacing Δf, given by the frequency span divided by the number of spectral lines in the FFT analysis. This is shown in Fig.3c).

Leakage free measurements can be obtained by using a periodic input signal (excitation waveform) with a period equal to the record length in the analysis. Pseudo-random, multisine and periodic random are examples of such excitation signals. See [1] for a discussion of this.

Another possibility is to apply a burst random signal whose burst length is sufficiently short to keep both the excitation as well as the response signals shorter than the record length.

Rectangular weighting should be used in the FFT analysis in all these cases.

Sampling in one domain corresponds to periodic repetition in the other domain, since multiplication by a periodic delta function (here with period $\Delta f = 1/T$) in one domain corresponds to a convolution with a periodic delta function (here with period $T = 1/\Delta f$) in the other domain.

This means that the IRF is repeated every T seconds, where $T = 1/\Delta f$ is the record length in the FFT as shown in Fig. 3d). The estimated IRF is thus given by

$$\hat{h}(t) = \sum_{i=-\infty}^{0} A_o e^{-\sigma(t - iT)} \sin(\omega_d (t - iT)) \qquad 0 \le t < T \tag{12}$$

where i is an integer. The estimated IRF, $\hat{h}(t)$ is said to be aliased, since *h(t)* is longer than the record length, T causing an interference by the periodic repetition.

Eq. (12) can also be written as

$$\hat{h}(t) = A_o e^{-\sigma t} \sum_{i=-\infty}^{0} e^{i\sigma T} \sin(\omega_d (t - iT)) \qquad 0 \le t < T$$

$$= A_o e^{-\sigma t} \sum_{i=-\infty}^{0} e^{iT/\tau} \sin(\omega_d t - i\omega_d / \Delta f) \qquad 0 \le t < T \tag{13}$$

which, in comparison with eq.(11), shows that the decay rate (i.e. the estimated damping) and the natural frequency are unaffected by the aliasing, while the magnitude and the phase of the IRF are dependent on record length, *T,* relative to time constant, τ (= $1/\sigma$), and on the location of damped natural frequency, ω_d, relative to the location of the frequency lines. As a simple interpretation we can conclude the following:

If ω_d coincides with a frequency line, all the decaying sine waves will be in phase and have an additive or constructive effect. If ω_d lies exactly between two lines, every second decaying sine wave will be in phase, while the rest will be in opposite phase giving a subtractive or destructive effect. In the first case the residue will be overestimated, while in the second case the residue will be underestimated.

In these two cases there is no phase error, while in the more general case, a phase error is also observed.

Case 1: Resonance Coinciding with a DFT Frequency Line

In the general case and only for $0 \le t < T$ and using complex notation, equation (13) becomes

$$\hat{h}(t) = A_o e^{-\sigma t} \frac{1}{2j} \sum_{i=-\infty}^{0} e^{i\sigma T} \cdot e^{j\omega_d t} \left(e^{-j\omega_d iT} - e^{-j\omega_d t} \cdot e^{j\omega_d iT} \right) \tag{14}$$

For a resonance coinciding with spectrum line number *k* we have

$\omega_d = 2\pi k \Delta f$ (and $T = 1/\Delta f$) (15)

Thus we have

$$\omega_d iT = 2\pi \cdot i \cdot k \tag{16}$$

which is a multiple of 2π.

Equation (14) can now be written as

$$\hat{h}(t) = A_o e^{-\sigma t} \sum_{i=-\infty}^{0} e^{i\sigma T} \left(\frac{e^{j\omega_d t} - e^{-j\omega_d t}}{2j} \right)$$

$$= A_o e^{-\sigma t} \sin(\omega_d t) \sum_{i=-\infty}^{0} e^{i\sigma T} \tag{17}$$

Comparing eq. (17) with eq. (11) it is seen that the (amplitude) error, ε_b, for the exponentially decaying sine wave can be written as:

$$\varepsilon_b = \sum_{i=-\infty}^{0} e^{i\sigma T} = \sum_{i=0}^{\infty} e^{-i\sigma T} = \frac{1}{1 - e^{-T\sigma}} = \frac{1}{1 - e^{-T/\tau}} \tag{18}$$

As a first order approximation we have

$$\varepsilon_b \approx \frac{\tau}{T} \qquad (\text{for } \tau > 3 \cdot T) \tag{19}$$

Equation (19) shows that the amplitude error is proportional to the time constant of the system if the time constant is considerably longer than the DFT/FFT record length, and that the amplitude is overestimated.

On a dB (logarithmic) scale the error can be expressed as:

$$L_\varepsilon = -20 \log (1 - e^{-\sigma T}) \quad \text{dB} \tag{20}$$

and as a first order approximation as:

$$L_\varepsilon \approx 20\log\ (\tau/T) \quad \text{dB} \quad (\text{for } \tau > 3 \cdot T) \tag{21}$$

which is shown in Fig. 4 as the upper curve.

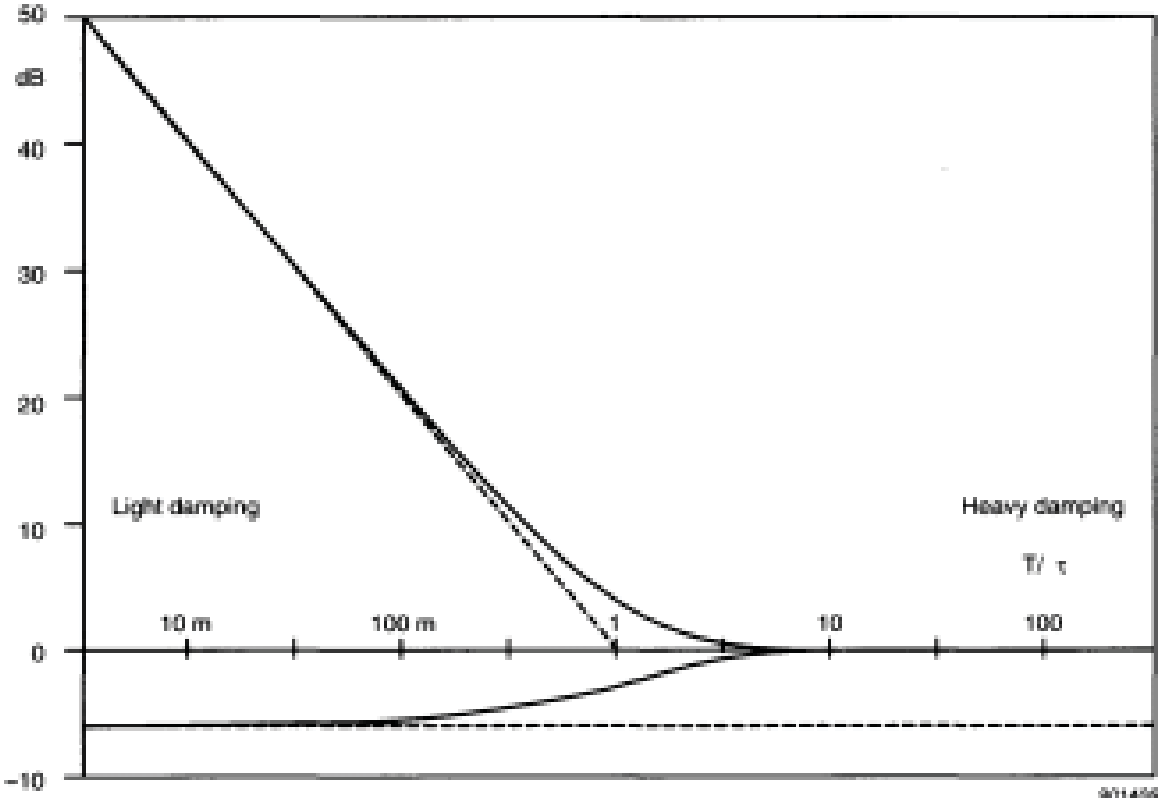

Fig. 4. Maximum amplitude error on Impulse Response Function as a function of relative damping

As seen, the amplitude error can be neglected if $T/\tau > 2.5$, in which case the impulse response is attenuated by approximately 20 dB at the end of the record. In the frequency domain this corresponds to a 3dB bandwidth of the system under test, which is larger than the DFT/FFT line spacing. As another example, if τ is 100 times longer than the record length, *T,* the amplitude error is 40dB.

Case 2: Resonance Exactly Between Two DFT Frequency Lines

In the case where the resonance is located exactly midway between line number k and k+1, equation (15) becomes

$$\omega_d = 2\pi \left(k + \frac{1}{2}\right) \cdot \Delta f \tag{22}$$

Thus equation (16) becomes

$$\omega_d iT = 2\pi \cdot i \cdot k + \pi \cdot i \tag{23}$$

For i even (0, -2, -4, etc.) we have

$$e^{-j\omega diT} = e^{j\omega diT} = 1 \tag{24}$$

and for i odd (-1, - 3, -5, etc.) we have

$$e^{-j\omega diT} = e^{j\omega diT} = -1 \tag{25}$$

So in this case we have an amplitude error of

$$\varepsilon_b = \sum_{i=0}^{\infty} e^{-i\sigma T}(-1)^i = \frac{1}{1+e^{-T\sigma}} = \frac{1}{1+e^{-T/\tau}} \tag{26}$$

As a first order approximation we have

$$\varepsilon_b \approx \frac{1}{2} \quad (\text{for } \tau > 3 \cdot T) \tag{27}$$

Equation (27) shows that the amplitude is underestimated by a factor of 2 if the time constant of the system is considerably longer than the DFT/FFT record length.

On a dB (logarithmic) scale the error can be expressed as

$$L_\varepsilon = -20 \log (1 + e^{-\sigma T}) \text{ dB} \quad (28)$$

and as a first order approximation

$$L_\varepsilon = -20 \log (2) \text{ dB} = -6 \text{ dB (for } \tau > 3 - T) \quad (29)$$

which is shown in Fig. 4 as the lower graph.

Time-Frequency Relationships

The amplitude error is seen to be given as a function of T/τ, i.e. the ratio between the record length (the analysis) and the time constant of the exponential decay (the damping descriptor). We could just as well use corresponding frequency domain descriptors, namely the line spacing Δf (the analysis) and the 3dB bandwidth Δf_{3dB} of the resonance peak (the damping descriptor).

The relationship between the different damping descriptors is shown in Table 1.

Natural frequency $\omega_o = 2\pi f_o$ ($\approx \omega_d$ for lightly damped resonances)					
Known \ Unknown	$\Delta\omega$=	Δf_{3dB} =	ζ =	σ =	τ =
3dB Bandwidth, $\Delta\omega$ (rad/s)	$\Delta\omega$	$\frac{\Delta\omega}{2\pi}$	$\frac{\Delta\omega}{2\omega_o}$	$\frac{\Delta\omega}{2}$	$\frac{2}{\Delta\omega}$
3dB Bandwidth, Δf_{3dB} (Hz)	$2\pi\Delta f_{3dB}$	Δf_{3dB}	$\frac{\Delta f_{3dB}}{2f_o}$	$\pi\Delta f_{3dB}$	$\frac{1}{\pi\Delta f_{3dB}}$
Fraction of critical damping, ζ,	$2\zeta\omega_o$	$2\zeta f_o$	ζ	$2\pi f_o\zeta$	$\frac{1}{2\pi f_o}$
Decay constant σ (s^{-1})	2σ	$\frac{\sigma}{\pi}$	$\frac{\sigma}{\omega_o}$	σ	$\frac{1}{\sigma}$
Time constant, τ (s)	$\frac{2}{\tau}$	$\frac{1}{\pi\tau}$	$\frac{1}{2\pi f_o\tau}$	$\frac{1}{\tau}$	τ

Table 1. Interrelationship between different "damping" descriptors

The basic relationship between time and frequency domain descriptors of the damping for a SDOF model is

$$\tau \cdot \sigma = 1 \tag{30}$$

i.e. time constant multiplied by one half the 3dB bandwidth (in radians per second) equals unity. This relationship is sometimes called the uncertainty principle. If we increase the resolution in one domain, we lose resolution in the other, or if the event becomes narrower in one domain it becomes broader in the other.

Eq. (30) can also be rewritten as

$$\tau \cdot \Delta f_{3dB} = 1/\pi \tag{31}$$

If we combine Eq. (31) with the general time-frequency relationship for DFT/ FFT analysis as indicated in Eq. (32),

$$T \cdot \Delta f = 1 \tag{32}$$

we get

$$\pi \cdot \frac{\Delta f 3dB}{\Delta f} = \frac{T}{\tau} \tag{33}$$

which shows that relative damping can be expressed both in the frequency and the time domain by easy to interpret numbers which only differ by a factor of π. Example: If the system 3dB bandwidth is equal to 10 times the line spacing, then the record length is 31.4 times longer than the system time constant.

General Case Error

The formula for the general case is shown in equation (13). Using the well-known relation

$$\sin(\alpha - \beta) = \sin\alpha \cdot \cos\beta - \cos\alpha \cdot \sin\beta \tag{34}$$

the impulse response can be written as

$$\hat{h}(t) = A_o e^{-\sigma t} \sum_{i=-\infty}^{0} e^{i\sigma T} [\sin(\omega_d t) \cdot \cos(\omega_d iT) - \cos(\omega_d t) \cdot \sin(\omega_d iT)]$$

$$= A_o e^{-\sigma t} \sin(\omega_d t) \sum_{i=-\infty}^{0} e^{\sigma iT} \cos(\omega_d iT)$$

$$-A_o e^{-\sigma t} \cos(\omega_d t) \sum_{i=-\infty}^{0} e^{\sigma iT} \sin(\omega_d iT) \qquad (35)$$

which in a simplified form is

$$\hat{h}(t) = A_o e^{-\sigma t} \sin(\omega_d t) \cdot C_1 - A_o e^{-\sigma t} \cos(\omega_d t) \cdot C_2 \qquad (36)$$

From eq. (36) it is clearly seen that the impulse response function can be expressed as a sum (difference) of two orthogonal exponentially decaying sinusoidal terms each weighted by a factor of C_1 and C_2 respectively, which are functions of σT and $\omega_d T$.

$$C_1 = \sum_{i=-\infty}^{0} e^{\sigma iT} \cdot \cos(\omega_d iT)$$

$$= \sum_{i=0}^{\infty} (e^{-\sigma T})^i \cdot \cos(\omega_d iT)$$

$$= \frac{1 - e^{-\sigma T} \cdot \cos(\omega_d T)}{1 - 2e^{-\sigma T} \cdot \cos(\omega_d T) + e^{-2\sigma T}} \qquad (37)$$

$$C_2 = \sum_{i=-\infty}^{0} e^{\sigma i T} \cdot \sin(\omega_d i T)$$

$$= -\sum_{i=0}^{\infty} (e^{-\sigma T})^{i} \cdot \sin(\omega_d i T)$$

$$= \frac{e^{-\sigma T} \cdot \sin(\omega_d T)}{1 - 2e^{-\sigma T} \cdot \cos(\omega_d T) + e^{-2\sigma T}} \tag{38}$$

Thus the impulse response function can be expressed as the sum of two orthogonal terms 90° out of phase with each other. The IRF can also be represented by one term including a phase shift, as shown in eq. (39), which is merely a conversion of eq. (36) from rectangular to polar coordinates:

$$\hat{h}(t) = A_o e^{-\sigma t} \cdot C \cdot \sin(\omega_d t - \varphi) \tag{39}$$

where

$$C = \sqrt{C_1^2 + C_2^2} = \sqrt{(1 - 2e^{-\sigma T}\cos(\omega_d T) + e^{-2\sigma T})^{-1}} \tag{40}$$

is the amplitude error and

$$\varphi = \arctan(C_2/C_1) = \arctan\left[\frac{e^{-\sigma T}\sin(\omega_d T)}{1 - e^{-\sigma T}\cos(\omega_d T)}\right] \tag{41}$$

is the phase error.

In the general case the amplitude error is found to have values between the limits shown in Fig. 4. Eight different cases including the curves from Fig. 4 are shown in Fig. 5. Please note that the x-axis is scaled differently from Fig. 4

according to equation (33). Thus Fig. 4 shows the error as a function of relative damping using the time domain damping descriptor τ, while Fig. 5 shows the error as a function of relative damping using the frequency domain damping descriptor, Δf_{3dB}.

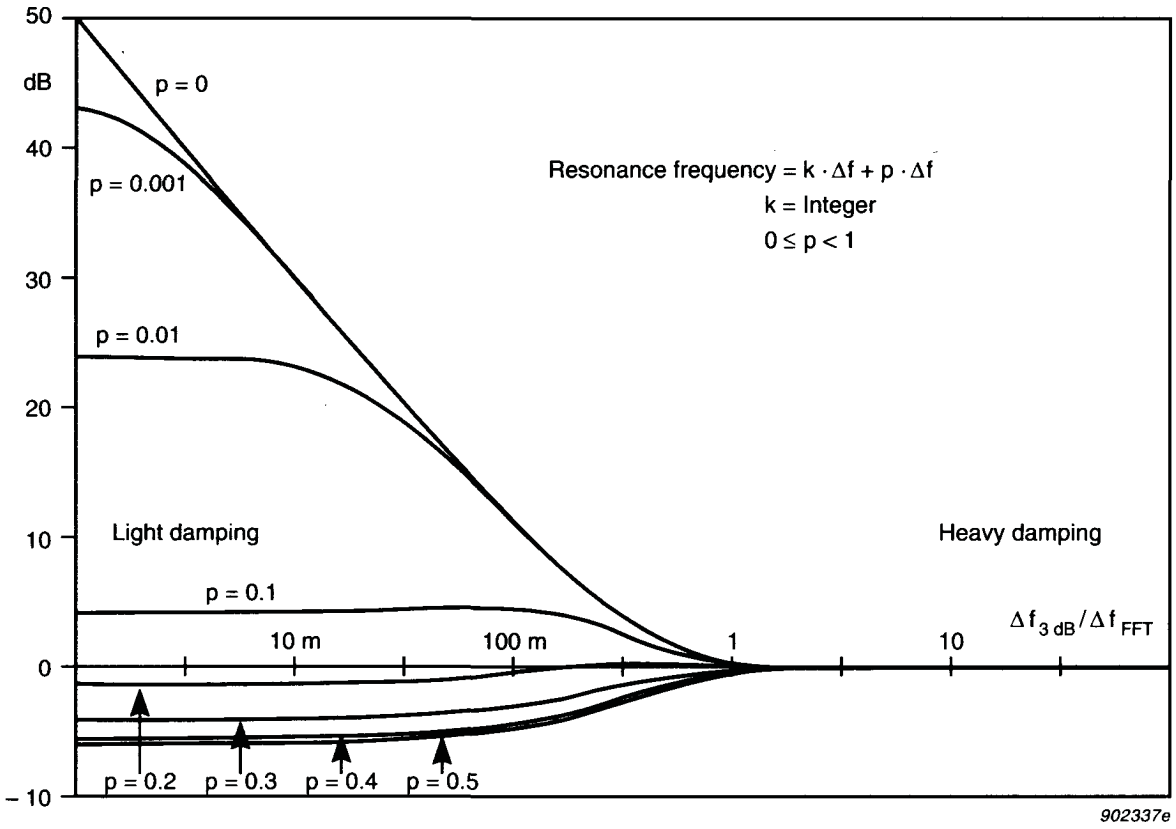

Fig. 5. Amplitude error of Impulse Response Function as a function of relative damping, for eight different cases of resonant frequencies

Fig. 6 shows the amplitude error as a function of resonance frequency in the interval between two DFT frequency lines. Four different damping cases are shown, namely where the system 3 dB bandwidth equals the line spacing and where the 3 dB bandwidth is 10, 100 and 1000 times narrower than the line spacing. It is clearly seen that overestimation only occurs when the natural frequency is in the vicinity of a DFT frequency line.

Fig. 7 shows the phase error as a function of frequency for the same four damping cases. There is no phase error in the two previous mentioned special

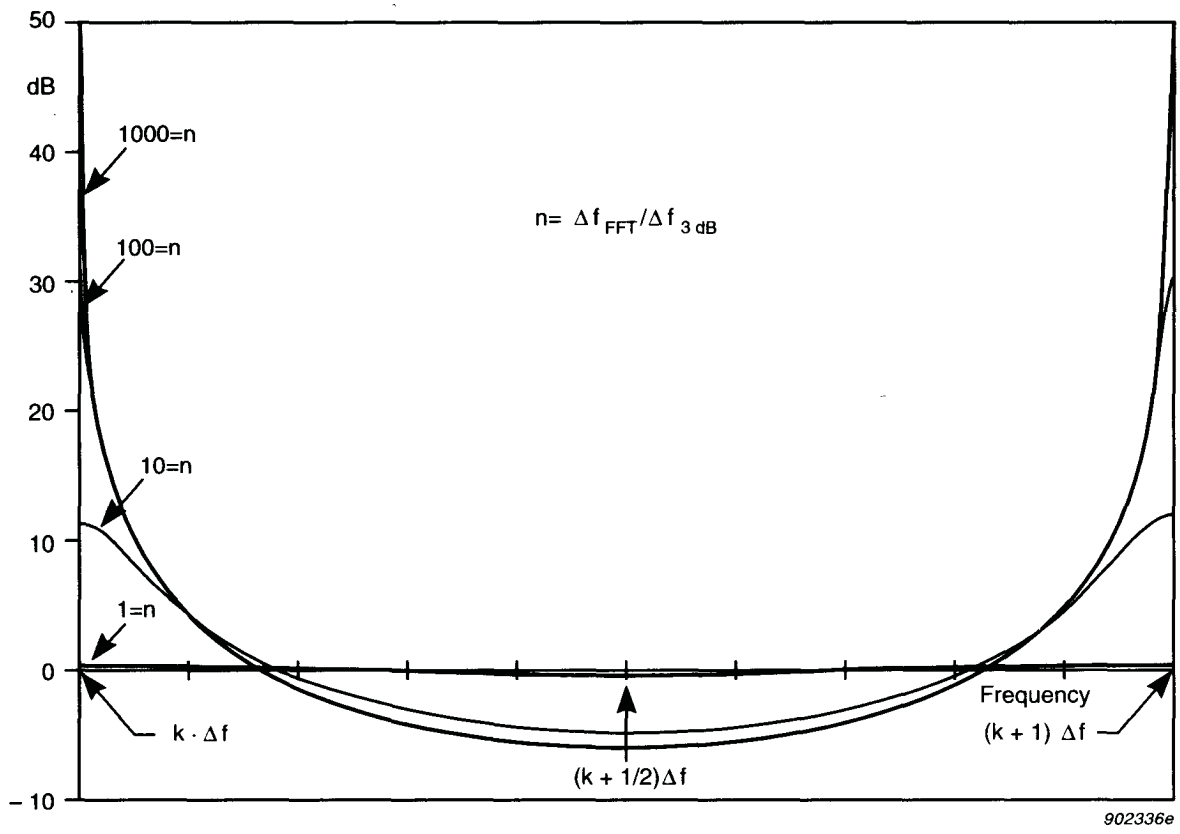

Fig. 6. Amplitude error of Impulse Response Function as a function of frequency, where k is DFT line no. k and (k + 1) is DFT line no. (k + 1). Four different damping cases are shown

cases, where the natural frequency either coincides with a spectral line or is exactly midway between two spectral lines. Furthermore, Figs. 6 and 7 show that the biggest amplitude and phase errors for very lightly damped system are found when the resonance frequency is close to a DFT spectral line.

As a final remark we can conclude that the errors can be neglected if the 3dB bandwidth of the system under test is broader than the DFT line spacing.

Computer Simulations

The theory and Figs. 4 to 7 have been verified by synthesizing FRFs with different damping and resonance frequencies. Both frequency domain and time domain curve fitters have been used to extract the system parameters (modal parameters). The modal software STAS SE v. 5.02 from SMS (Brüel&Kjær Type number WT 9100) has been used for these simulations.

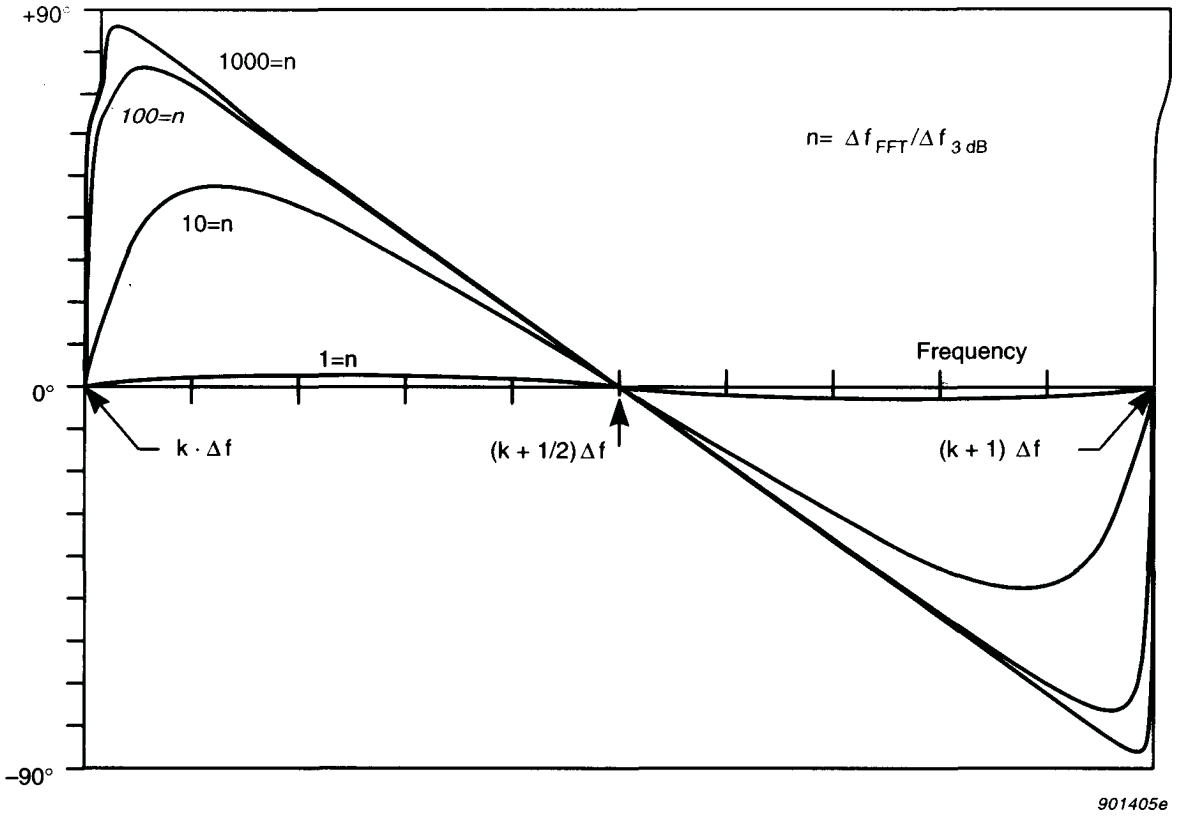

Fig. 7. Phase error on the Impulse Response Function as a function of frequency, where k is DFT line no. k and (k + 1) is DFT line no. (k + 1). Four different damping cases are shown

Measurement Conditions and Equipment Used

Some FRF measurements were performed on a freely suspended aluminium plate with the dimensions of 30cm x 25cm x 2cm. The structure was excited via a nylon stinger by a small Brüel & Kjær Vibration Exciter Type 4810 using a pseudo-random signal. The force signal was measured using a Brüel & Kjær Force Transducer Type 8200. The output vibration signal was measured using a small, lightweight (~2.4g) Brüel & Kjær Accelerometer Type 4375. The force and vibration signals were analysed using the Brüel & Kjær Multichannel Analysis System Type 3550 (DFT/FFT). A similar set-up is shown on the cover of this Technical Review.

Measurement Results

The modal parameters of the first resonance were determined using different resolutions, Δf, chosen in binary steps from 0.125 Hz to 16 Hz (see Table 2). The resonance of interest, located at 860.2 Hz, had a 3dB bandwidth of approximately 150 mHz corresponding to a time constant, τ of 2.1 s.

FFT Resolution		Relative Resolution		FRF Curve-fit			IRF Curve-fit		
Δf (Hz)	T (s)	$\Delta f_{3dB}/\Delta f$	T/τ	ζ (m%)	|R| (dB)	$\angle$R (°)	ζ (m%)	|R| (dB)	$\angle$R (°)
0.125	8	1.24	3.9	10	82.5	179	10	82.2	183
0.25	4	0.62	1.9	9	82.4	180	9	81.4	175
0.5	2	0.31	0.97	9	82.5	180	8	81.0	197
1	1	0.15	0.49	9	82.4	179	9	83.9	218
2	0.5	77m	0.24	9	82.4	179	9	86.9	232
4	0.25	39m	0.12	10	82.4	179	10	92.4	238
8	0.125	19m	61m	9	82.4	179	9	76.7	175
16	62.5m	10m	30m	11	82.4	179	10	79.9	134

Table 2. Resolution, record length, number of spectral lines per 3dB bandwidth, number of time constants per record length, damping estimate as function of critical damping from an FRF curve-fit, estimate of residue both magnitude and phase, estimate of damping and residue from an IRF curve-fit. In all cases the damped natural frequency was estimated within 6m% standard deviation

Both time as well as frequency domain curve fitters have been applied to the measurements. It can be seen when dealing with light damping that the time domain curve fitter extracts correct damping and resonance frequency (pole location) but incorrect residues.

In Fig. 8, plots of the impulse response function are shown for four cases. The magnitude of the analytical (complex) impulse response function is displayed. The analytical impulse response function is obtained by use of the Hilbert transform. The Hilbert transform of the real valued impulse response function *h(t)* (the real part) gives the imaginary part *j~h (t),* and the analytical impulse response function is defined as

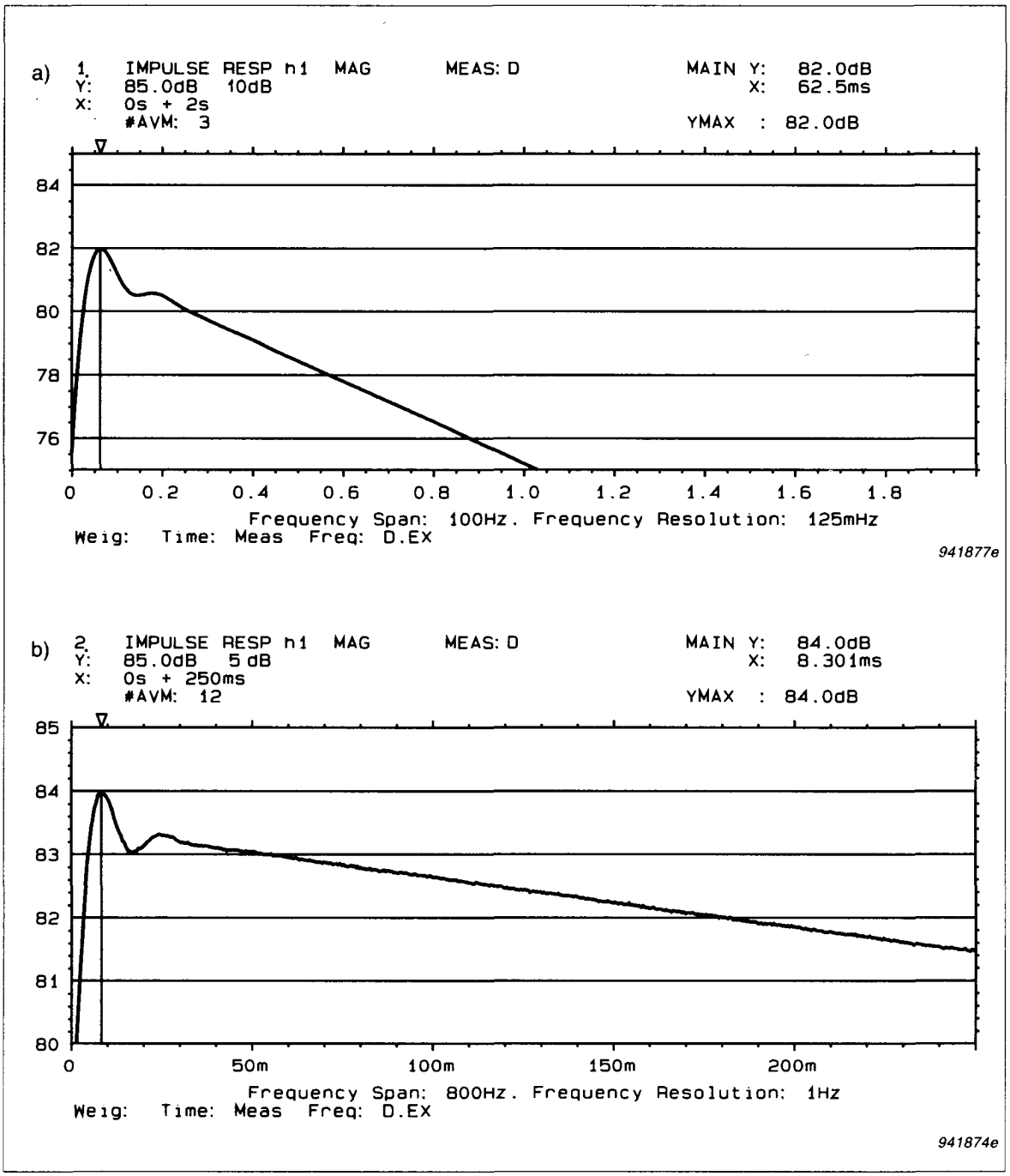

Fig. 8. Impulse response function for different resolutions, only the first half is shown. Note the difference in Y_{max} level near time zero for the four different cases
a) Δf = 125 mHz, b) Δf = 1Hz,

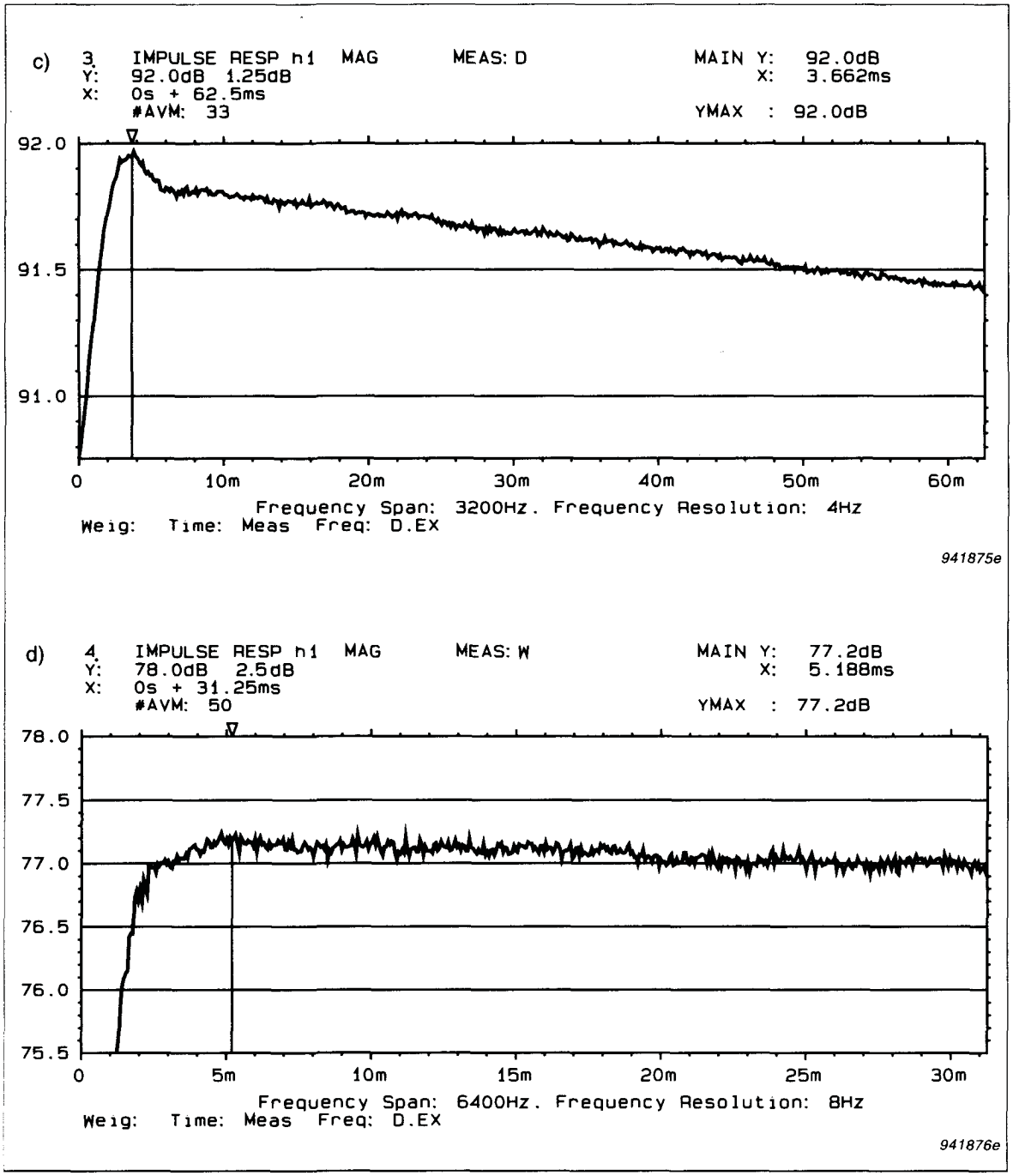

Fig.8 (cont.) Impulse response function for different resolutions,c) Δf= 4 Hz and resonance coinciding with a frequency line, d) Δf= 8 Hz and resonance exactly between two frequency lines

$$\overset{\nabla}{h}(t) = h(t) + j\tilde{h}(t) \tag{42}$$

The magnitude of the impulse response function is then given by

$$|\overset{\nabla}{h}(t)| = \sqrt{h^2(t) - \tilde{h}^2(t)} \tag{43}$$

The magnitude $|h(t)|$ can be considered as being the envelope of $h(t)$. For the SDOF system (eq.(11)), the magnitude of the impulse response function becomes

$$|\overset{\nabla}{h}(t)| = A_0 e^{-\sigma t} \tag{44}$$

The advantages of using the magnitude instead of the real part are that the magnitude does not feature the oscillations (given by the term sin ($\omega_d t$) and that the magnitude can be shown on a logarithmic (dB) amplitude scale. A logarithmic amplitude scale gives more "dynamic" range in the presentation and reveals the exponential decay (given by the term $e^{-\sigma t}$) as a straight line.

The magnitude of the estimated impulse response function $\hat{h}(t)$ is $A_o e \cdot C$ (eq. (39)) which on a logarithmic (dB) scale becomes $-\sigma t \cdot 10 \log e^2$ + constant = $-8.69 t/\tau$ + constant, i.e. a straight line with a slope of -8.69 dB per time constant τ. The magnitude at time $t=0$ is given by $A_o C$. The damping value is thus estimated from the slope and the residue is estimated from the magnitude at time $t=0$, found by extrapolation of the straight line of the decay back to time $t=0$.

The four cases in Fig.8 represent situations where the line spacing Δf is:

a) approximately equal to the 3 dB bandwidth of the resonance
b) 6 times the 3 dB bandwidth
c) 24 times the 3 dB bandwidth and the resonance frequency nearly coinciding with an analysis line
d) 48 times the 3 dB bandwidth and the resonance frequency nearly midway between two analysis lines.

In all four cases a correct decay constant, i.e. damping value, was found and the natural frequency was correct as well. For the magnitude, extrapolated back to time $t=0$, giving the residue, we have correct results only in case a), a slight overestimation in case b), high overestimation (10dB) in case c) and a moderate underestimation (5dB) in case d).

As seen from Table 2, the phase error, as expected, is very high, 58 degrees (238 - 180) in case c). In case d) the phase error is only 5 degrees, which also confirms the theory.

The authors experienced difficulties for both time and frequency domain curve fitters when the 3dB bandwidth was more than 200 times narrower than the line spacing. The problem is that we have too few frequency samples of the resonance. In this case an exponential weighting function with the identical time or decay constant, σ_w, could be applied to both excitation and response signal. This will widen the measured bandwidth of the resonances The residue and damped natural frequency will be correctly estimated, but the damping overestimated, as shown in Eq. (45):

$$\begin{aligned} \hat{h}(t) &= A_o e^{-\sigma t} \cdot e^{-\sigma w t} \cdot C \cdot \sin(\omega_d t - \varphi) \\ &= A_o e^{-(\sigma + \sigma w)t} \cdot C \cdot \sin(\omega_d t - \varphi) \\ &= A_o e^{-\sigma m \cdot t} \cdot C \cdot \sin(\omega_d t - \varphi) \end{aligned} \tag{45}$$

Thus the exponential weighting function behaves as an "antialiasing" filter This means that the correct damping can easily be calculated from the measured damping if the decay constant (the reciprocal of the time constant 01 length) of the exponential weighting is known:

$$\sigma = \sigma_m - \sigma_w \tag{46}$$

Applying the exponential weighting actually corresponds to not measuring the Transfer Function, *H(s),* along the $j\omega$ axis, $H(j\omega)$*,* but along a line parallel to the $j\omega$-axis crossing the real axis (σ or damping axis) at σ_w in the right hall plane. Thus the residue and the damped natural frequency will be correctly estimated.

Conclusion and Final Remarks

It has been shown that the impulse response function, when calculated from the frequency response function using DFT/FFT techniques, in some practical applications suffers a bias error. The bias error is caused by an aliasing effect

which appears during the inverse DFT/FFT from the frequency domain (FRF) to the time domain (IRF).

The error becomes significant when leakage free measurements of lightly damped systems are performed and the resolution in the analysis is not sufficiently high compared to the bandwidth of the resonance peaks. The error can be neglected if the 3dB bandwidth of the resonances is greater than the line spacing Δf.

The SDOF system with viscous damping has been investigated (eq.(39)). The error can in this case be expressed by an amplitude error (eq. (40)) and a phase error (eq. (41)). Both of these are given by the ratio of the record length T to the time constant τ (or the ratio of the 3dB bandwidth $\Delta f_{3\text{dB}}$ to the line spacing Δf) and the location of the damped natural frequency ω_d relative to the location of the frequency lines in the analysis.

The exponential decay, determined by the damping in the system, is not affected in the case of viscous damping. For other types of damping mechanisms, however, the aliasing effect could influence the damping value estimation.

When the impulse response function is used for mathematical modelling, such as in modal analysis, the error is directly reflected in the residues of the resonances and the given corrections have to be applied.

Special care should be taken when modal analysis is performed using single input/single output measurements with a shaker and one accelerometer. The accelerometer is in this case moved to a different position for each measurement. This can cause the damped natural frequency to be different in the different measurements due to the mass loading effect. The bias error will therefore be different for each individual measurement and, if the corrections are not applied on the estimated residues, the resulting mode shapes will be contaminated with what appears to be a random error.

Leakage free measurements can be obtained by using a proper excitation signal, such as pseudo-random, multisine, periodic random or burst random and applying rectangular weighting in the analysis.

If a random signal is used for excitation and Hanning weighting is applied in the analysis, at least 10 FFT lines per 3dB bandwidth are required to make the measurement appear leakage free [2, 3], and no effect of the bias error will be observed in the impulse response function. If the measurement is not performed with the required resolution, leakage will smear out the resonance peaks causing a so-called resolution bias error [1]. The resulting error in the estimated impulse response function can in this case not be compensated for.

For impulse excitation (hammer or impact excitation in structural analysis) an exponential weighting must be applied to the response signal to force this signal to be attenuated by approximately 40 dB at the end of the record. In this situation there will only be an influence of the exponential weighting which will appear as well-defined leakage. This can be compensated for as indicated in eq. (46) (see also [3]) and no effect of the aliasing is observed on the impulse response function.

References

[1] H. HERLUFSEN: *Dual Channel FFT Analysis (Parts I & II)* Brüel & Kjær Technical Review Nos. 1 & 2,1984

[2] S. GADE & H. HERLUFSEN: *Use of Weighting Functions in DFT/FFT Analysis,* Brüel & Kjær Technical Review Nos. 3 & 4,1987

[3] S. GADE & H. HERLUFSEN: *Digital Filter Techniques vs. FFT Techniques for Damping Measurements,* Brüel & Kjær Technical Review No.1, 1994

Complex Modulus and Damping Measurements using Resonant and Non-resonant Methods

by S. Gade, K. Zaveri, H. Konstantin-Hansen and H. Herlufsen

Abstract

Traditional methods of damping measurement involved the use of sinusoidal signals for the excitation at low frequencies for bending resonances of specimens and at high frequencies for longitudinal resonances. With the advent of the dual channel real-time analyzers, wide-band random excitation can be conveniently used to excite and measure the response of the specimens simultaneously, whereby considerable time savings can be achieved. Two methods, one non-resonant and the other resonant, are outlined, the former yielding the real and elastic modulus as a continuous function of frequency. The results of the two methods are also compared.

Resume

Les anciennes mesures d'amortissement faisaient intervenir des signaux d'excitation sinusoïdaux, à basse fréquence pour les résonances de flexion, et a haute fréquence pour les résonances longitudinales. Les analyseurs bicanaux temps réel autorisent aujourd'hui un considerable gain de temps en permettant l'utilisation de signaux aléatoires large bande pour l'excitation et la mesure de la réponse simultanées de l'objet teste. Deux methodes sont ici comparées, ainsi que leurs résultats respectifs, l'une faisant intervenir le phénomene de resonance, l'autre non. Cette demière méthode donne le module d'élasticité et le module réel comme une fonction de réponse en fréquence continue.

Zusammenfassung

Traditionelle Methoden für Dämpfungsmessungen pflegten sinusförmige Signale zur Anregung zu verwenden: tiefe Frequenzen für Biegungsresonanzen von Prüflingen und hohe Frequenzen für longitudinale Resonanzen. Mit Breitband-Rauschanregung durch Zweikanal-Echtzeitanalysatoren ist es

möglich geworden, auf bequeme Weise die Prüfstruktur gleichzeitig anzuregen und ihr Antwortverhalten zu messen, was eine beträchtliche Zeitersparnis bedeutet. Zwei Methoden, eine nichtresonante und eine resonante, werden skizziert, von denen die erstgenannte den reellen und Elastizitätsmodul als kontinuierliche Funktion der Frequenz liefert. Es erfolgt ein Vergleich der Ergebnisse beider Methoden.

Nomenclature

a	acceleration [m/s^2]
c	viscous damping coefficient [N · s/m]
d	deflection [m]
e	base of natural logarithm, 2.72...
f	force [N]
f_o	undamped natural frequency [Hz]
j	imaginary number, √-1
k	kilo, 10^3
k	stiffness [N/m]
I	length of isolator [m]
m	mass [kg]
t	time [s]
v	velocity [m/s]
x	displacement [ml
$\dot{x}$	velocity [m/s]
$\ddot{x}$	acceleration [m/s^2]
A	cross sectional area of isolator [m^2]
E^*	complex elastic modulus [N/m^2]
E'	modulus of elasticity. Young's modulus [N/m^2]
E''	loss modulus [N/m^2]
F	force spectrum [N · s]
H	compliance frequency response function [m/N]
X	displacement spectrum [m · s]
ε	sinusoidal strain [dimensionless]
$\hat{\varepsilon}$	strain, (relative elongation, $\Delta l/l$) [dimensionless]
η	loss factor [dimensionless]
π	pi, 3.14...
θ	angle of complex modulus [rad]
σ	sinusoidal stress [N/m^2]
$\hat{\sigma}$	stress [N/m^2]

ω	angular frequency [rad/s]
ω_o	undamped natural frequency [rad/s]
Δf	3 dB bandwidth [Hz]
Δl	elongation of isolator [m]

Introduction

The stress-strain relationship of visco-elastic materials, generally used in the damping treatment of structures, can be described by two properties, such as the perfectly elastic (in-phase) stress-strain modulus and the loss factor. The values of these properties need to be determined in tension or compression for materials used as unconstrained damping layers and as anti-vibration mountings under machinery and under foundation blocks.

Using a dual channel FFT analyzer, the specimen can be excited using wide-band random excitation, and the properties determined from the frequency response spectra, as a continuous function of frequency, as shown in the following.

Another possibility is to preload the specimen by a well-known mass, such that the preloaded damping material becomes a part of a resonant mass-spring-damper system. Damping, e.g. loss factor, is then determined from the 3 dB bandwidth of the resonance. The procedure is then repeated at different frequencies of the specimen using different mass-loadings.

The two methods are demonstrated and compared in this article.

Theory for the Non-resonant Method

As most elastomers are elastically imperfect, the strain lags the stress. An applied sinusoidal stress (force per area) usually results in a sinusoidal strain (relative elongation $\Delta l/l$), the phase angle θ between them remaining constant during a complete strain cycle, although it can vary with the strain amplitude and the frequency.

Let σ be a sinusoidal stress applied which, using complex notation, can be written as:

$$\sigma = \sigma \times e^{j\omega t} \tag{1}$$

The strain, e, resulting from this stress will be:

$$\varepsilon = \varepsilon \times e^{j(\omega t - \theta)} \tag{2}$$

Thus the complex elastic modulus, E^*, is:

$$E^* = \frac{\sigma}{\varepsilon} = \frac{\hat{\sigma}}{\hat{\varepsilon}} \times e^{j\theta} \tag{3}$$

The coincident (in phase) elastic modulus (modulus of elasticity or Young's Modulus), E', will be given by:

$$E'' = \left(\frac{\hat{\sigma}}{\hat{\varepsilon}}\right) \times \cos\theta \tag{4}$$

and the quadrature (90° out of phase) loss modulus, E'', will be given by:

$$E'' = \left(\frac{\hat{\sigma}}{\hat{\varepsilon}}\right) \times \sin\theta \tag{5}$$

The amount of imperfect elasticity possessed by the material is given by the ratio of these two moduli and is denned by the loss factor η as:

$$\eta = \frac{E''}{E'} = \tan\theta \tag{6}$$

Fig. 1 shows a vector diagram illustrating these quantities, where E^* represents the complex modulus. Thus only two properties need to be measured, either E^* and θ or E' and E'' (Magnitude/Phase or Real/Imaginary parts).

As stress is force F divided by area A and strain is deflection divided by original length l, eqs. (4) and (5) may be written as:

$$E' = \frac{|F|}{|d|} \times \frac{l}{A} \cos\theta = \text{Real}\,\frac{(F)}{(d)} \times \frac{l}{A} \tag{7}$$

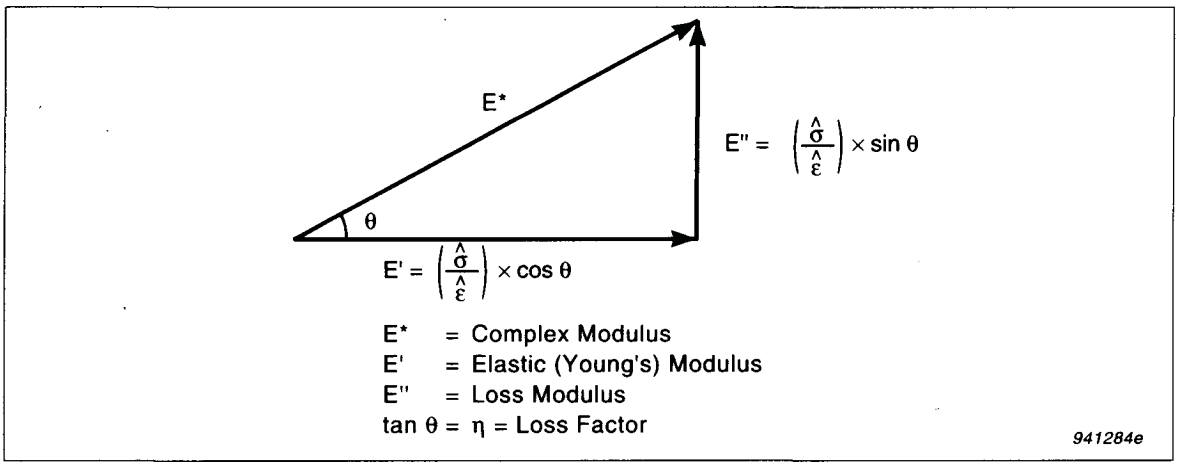

Fig. 1. Vector presentation of various moduli

$$E'' = \frac{|F|}{|d|} \times \frac{l}{A} \sin\theta = \text{Imaginary}\left(\frac{F}{d}\right) \times \frac{l}{A} \tag{8}$$

where A is the cross-sectional area of the isolator and *l* is the length of the isolator.

For random excitation, the ratio offeree to displacement, the dynamic stiffness, can be determined as the frequency response function between the force and displacement (acceleration integrated twice). The theory behind frequency response function measurements is found in Ref. [1].

The dynamic stiffness, being complex, can either be measured as magnitude and phase or as real and imaginary parts. By multiplying the dynamic stiffness by the length of the isolator and dividing by the cross-sectional area of the isolator, we obtain the complex elastic modulus *E**. The loss factor is given by the phase measurement.

A rigorous derivation of the theory can be found in Ref. [2].

Theory for the Resonant Method

By mounting a mass on top of the visco-elastic material, the combination behaves as a simple mass-spring-dashpot system, i.e., a single degree of freedom (SDOF) system, Fig.2.

Using Newton's second law and time domain formulation, we obtain:

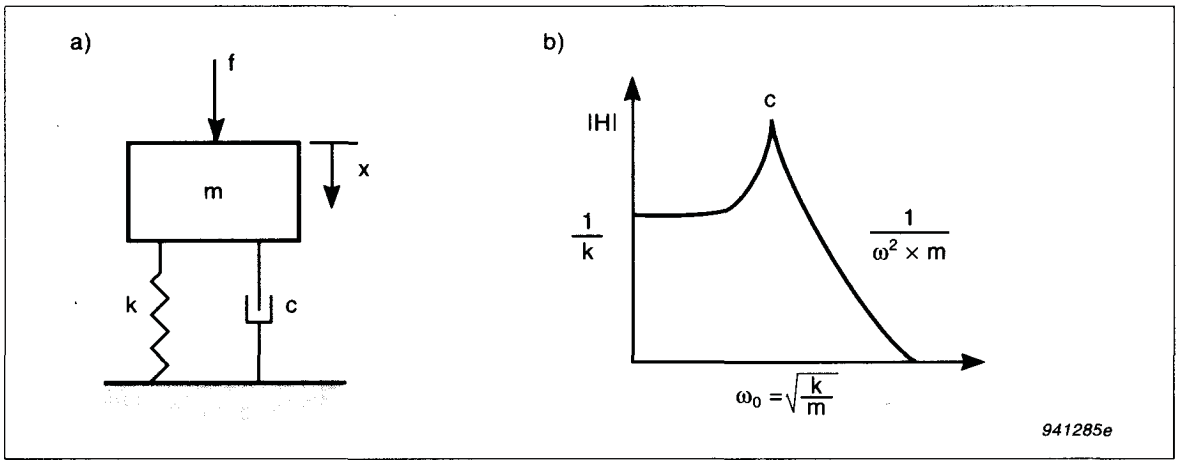

Fig. 2. a) A SDOF, Single Degree of Freedom Model, b) The magnitude of the frequency response functions |H| of a SDOF model

$$f(t) = m \times a(t) + c \times v(t) + k \times x(t)$$

$$= m \times \ddot{x}(t) + c \times \dot{x}(t) + k \times x(t) \tag{9}$$

Using the fact that differentiation corresponds to multiplication by $j\omega$ in the frequency domain, we obtain the following expression for the compliance Frequency Response Function, FRF:

$$H(\omega) = \frac{X(\omega)}{F(\omega)} = \frac{1}{-m\omega^2 + jc\omega + k} = \frac{1}{(k - m\omega^2) + jc\omega} \tag{10}$$

which shows that the compliance FRF equals the reciprocal of the stiffness, *k,* at low frequencies and that the accelerance FRF equals the reciprocal of the applied mass at high frequencies. See Fig. 2.

At the resonance frequency, ω_o the real part of eq.(10) becomes zero and the level is exclusively determined by the damping mechanism, c.

The resonance frequency is given by the square root of the ratio between stiffness and mass:

$$\omega_o = 2\pi f_o = \sqrt{\frac{k}{m}} \tag{11}$$

It can be shown that the loss factor, η, a measure for the damping, is given by the ratio between the 3 dB bandwidth, Δf, and the resonan ce frequency, f_o:

$$\eta = \frac{\Delta f}{f_o} \tag{12}$$

Different mass loadings yield damping at different frequencies. For random excitation the ratio of displacement to force (mobility type of calculation), the dynamic compliance, can be determined as the frequency response function between displacement (acceleration integrated twice) and force.

More detailed information about damping measurements using resonant methods is found in Ref.[3].

Experimental Procedure and Results for the Non-resonant Method

Fig.3 shows the instrumentation set-up used for the determination of the complex modulus and the loss factor of elastomers used for anti-vibration mountings. One isolator (machine-shoe) was placed on a seismic mass (concrete floor) and excited by a shaker via a nylon stinger. The excitation force was

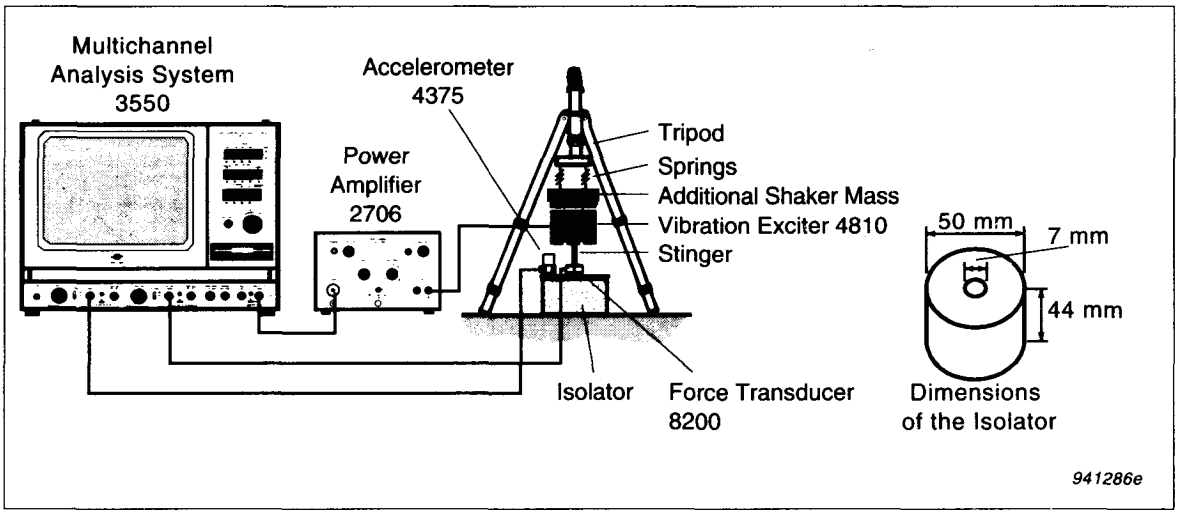

Fig. 3. Instrumentation set-up and dimensions of isolator

measured using a force transducer. An accelerometer was mounted beside the force transducer such that the force and the acceleration input to the isolator could be measured directly. The acceleration and force signals were fed to channels A and B of the analyzer, respectively. The shaker was fed a random noise signal from the generator section of the analyzer. The force and acceleration signals were both Harming weighted, and the acceleration signal double integrated in the analyzer for determining the displacement. See Fig.3.

Fig. 4 (lower) shows the measurement set-up giving the parameters chosen on the analyzer, while Fig.4 (upper) shows the magnitude of the stiffness Frequency Response Function. The cursor reading indicates a static stiffness of approximately k = 130 kN/m. The coherence function was unity at all frequencies (except below 10 Hz), illustrating a linear dependency between force and displacement signals. See also Fig. 11.

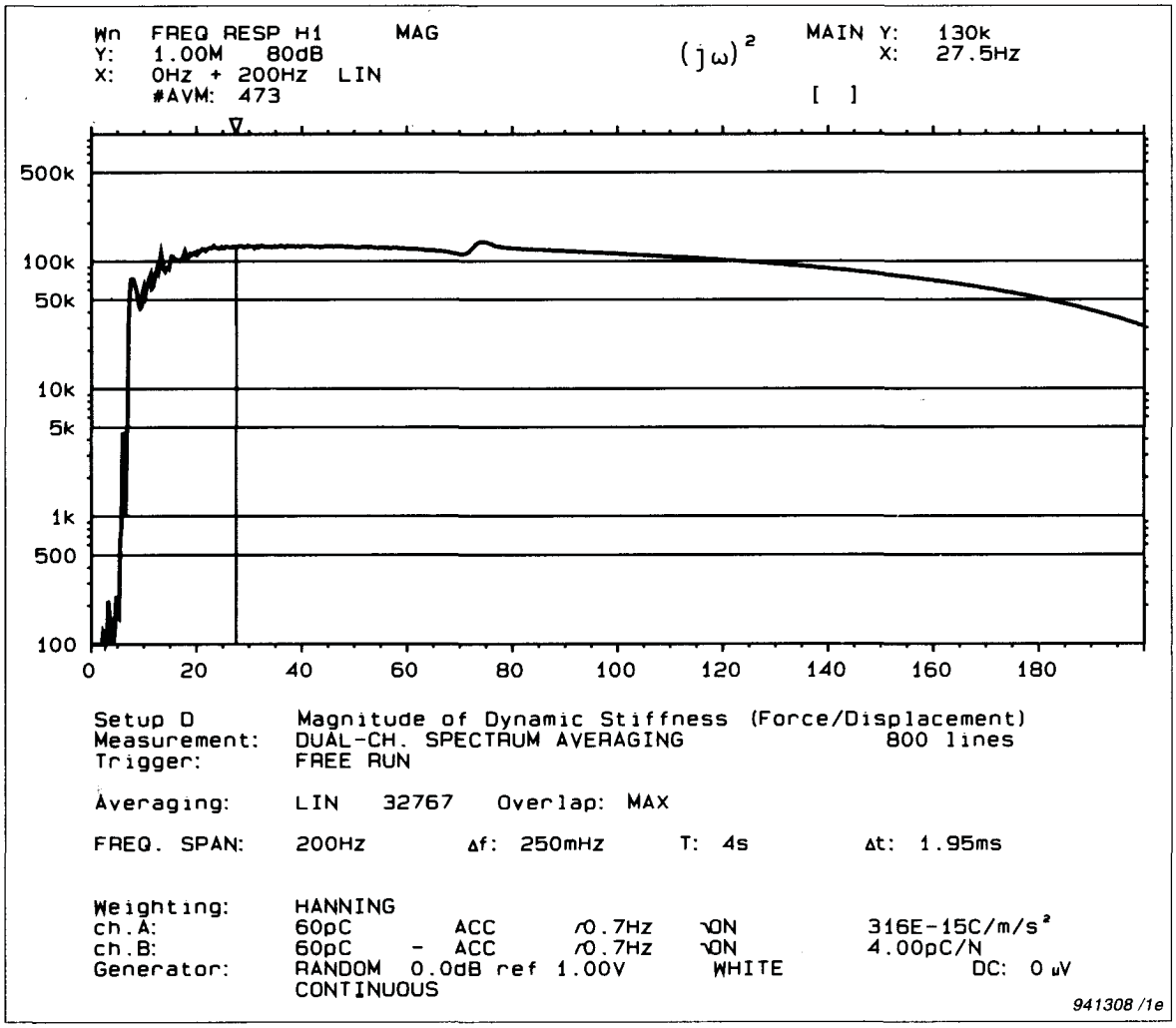

Fig. 4. The magnitude of the dynamic stiffness Frequency Response Function and Measurement set-up

Fig. 5 (upper and lower) shows the autospectra of the displacement and force signals respectively. The shapes of both these curves are similar, illustrating the spring-like behaviour of the isolator.

Fig. 6 shows the magnitude of the Complex Modulus, E^*. Thus the dynamic stiffness has been rescaled in the transducer set-up by a factor *of* $l/A = 22.41\text{m}^{-1}$, which is the ratio between the length, l and the cross-sectional area, A, of the isolator. (0.9941 is the transducer sensitivity "adjust".) The irregularity found at 75Hz is due to a stinger resonance. This was confirmed by using a stinger with different dimensions.

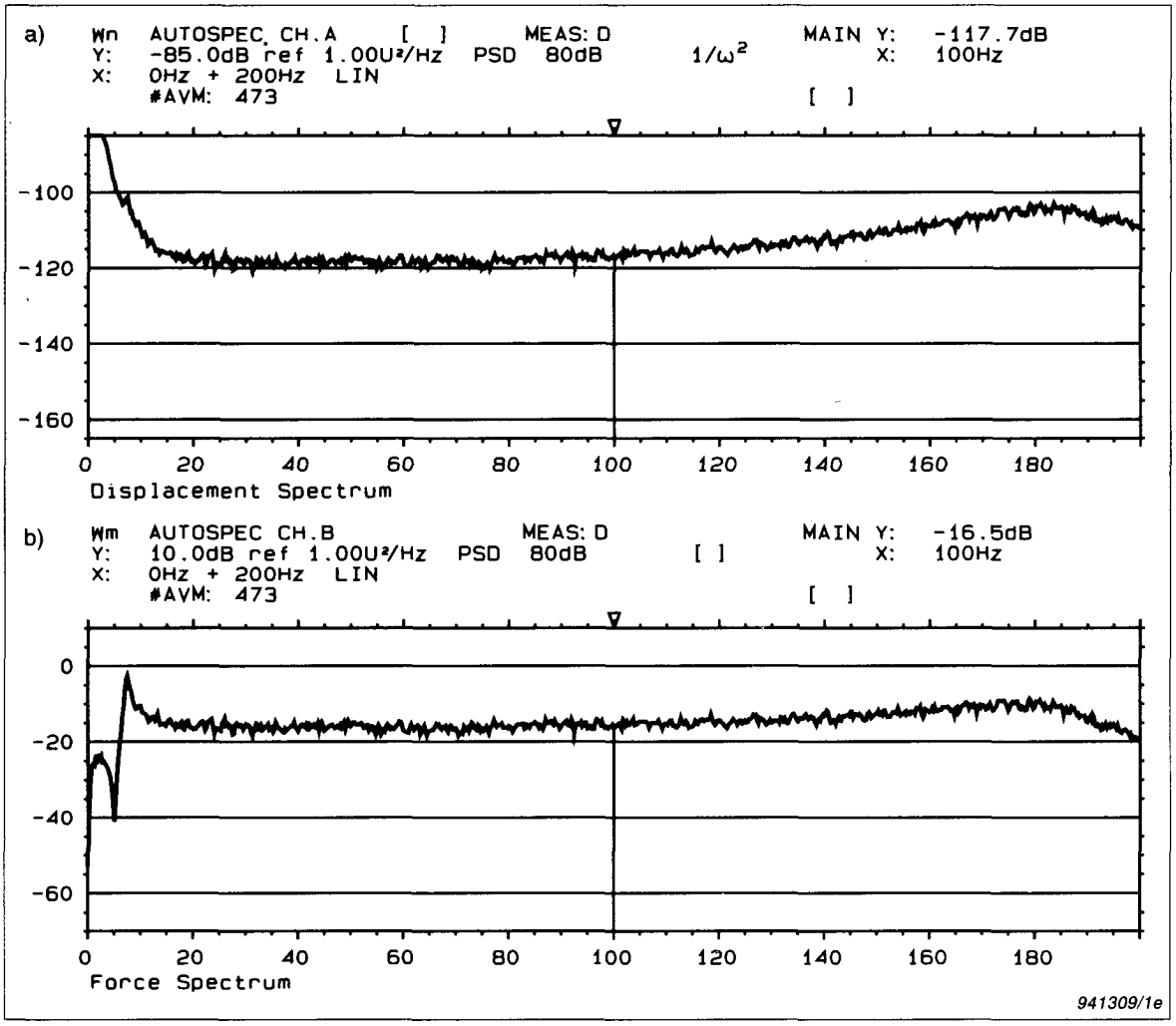

Fig. 5. Autospectra of displacement and force signals

Instead of plotting the magnitude and phase, the real and the imaginary parts of the dynamic complex modulus, i.e. the elastic (Young's) modulus and loss modulus can also be plotted as shown in Fig. 7 a) and b), respectively. It can be seen that for increasing frequency, the elastic modulus has a decreasing tendency whereas the loss modulus (i.e. the damping characteristics) seems to increase.

The loss factor, η (i.e. damping), can now be calculated as a continuous function of frequency simply by taking the tangent to the phase, tan (θ). This is implemented in the analyzer as a simple User Definable Display Function and shown in Fig. 8b).

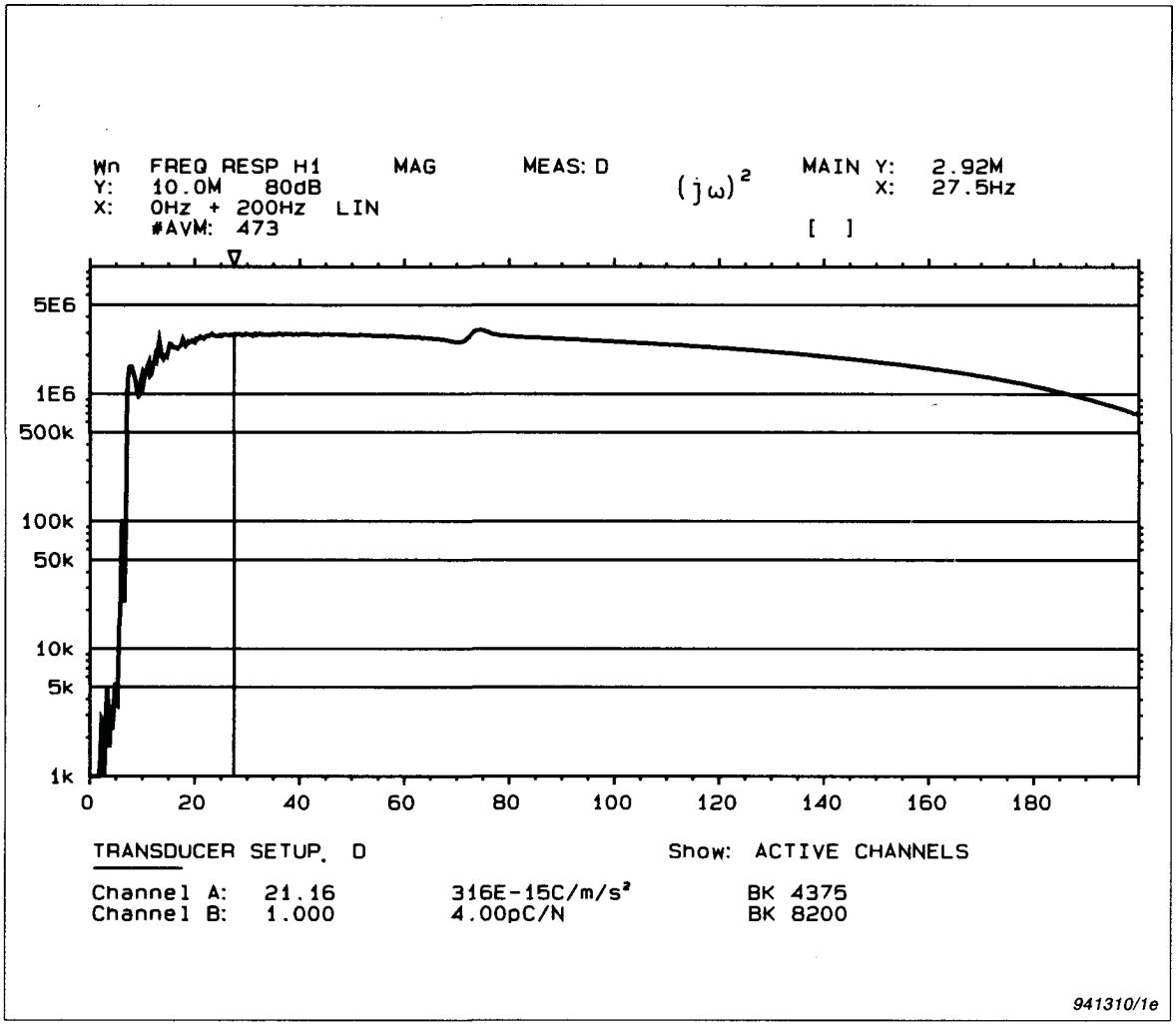

Fig. 6. Magnitude of Complex Modulus. Rescaling is done in the transducer set-up: 0.9941 x 22.41 = 21.16

The loss factor at 41 Hz is shown to be tan(4.5°) = 0.076 using the cursor readings. Some smoothing has been applied to the graph of the loss factor.

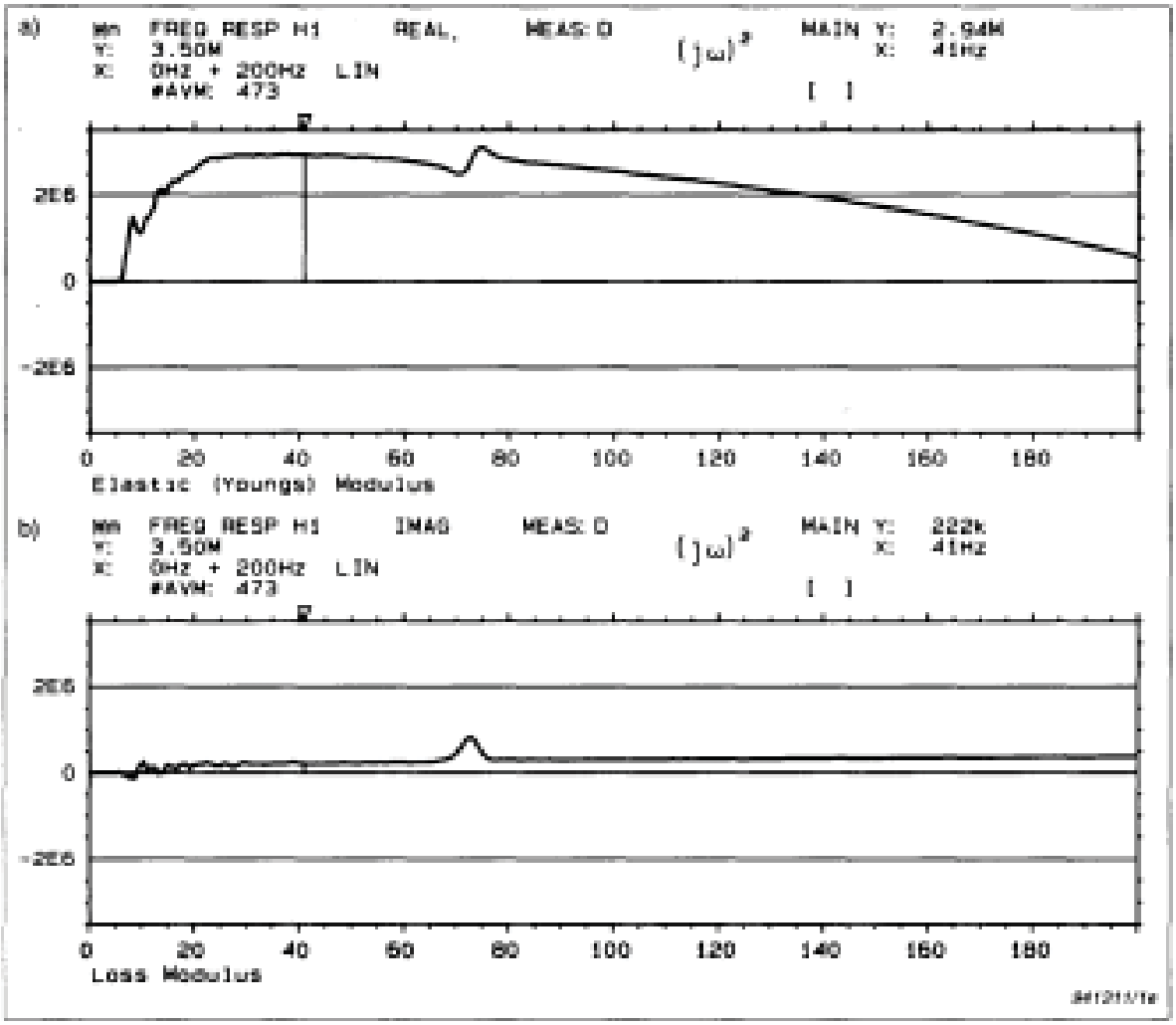

Fig. 7. a) Real part of complex modulus i.e. the elastic (Young's) modulus b) Imaginary part of complex modulus, i.e. the loss modulus

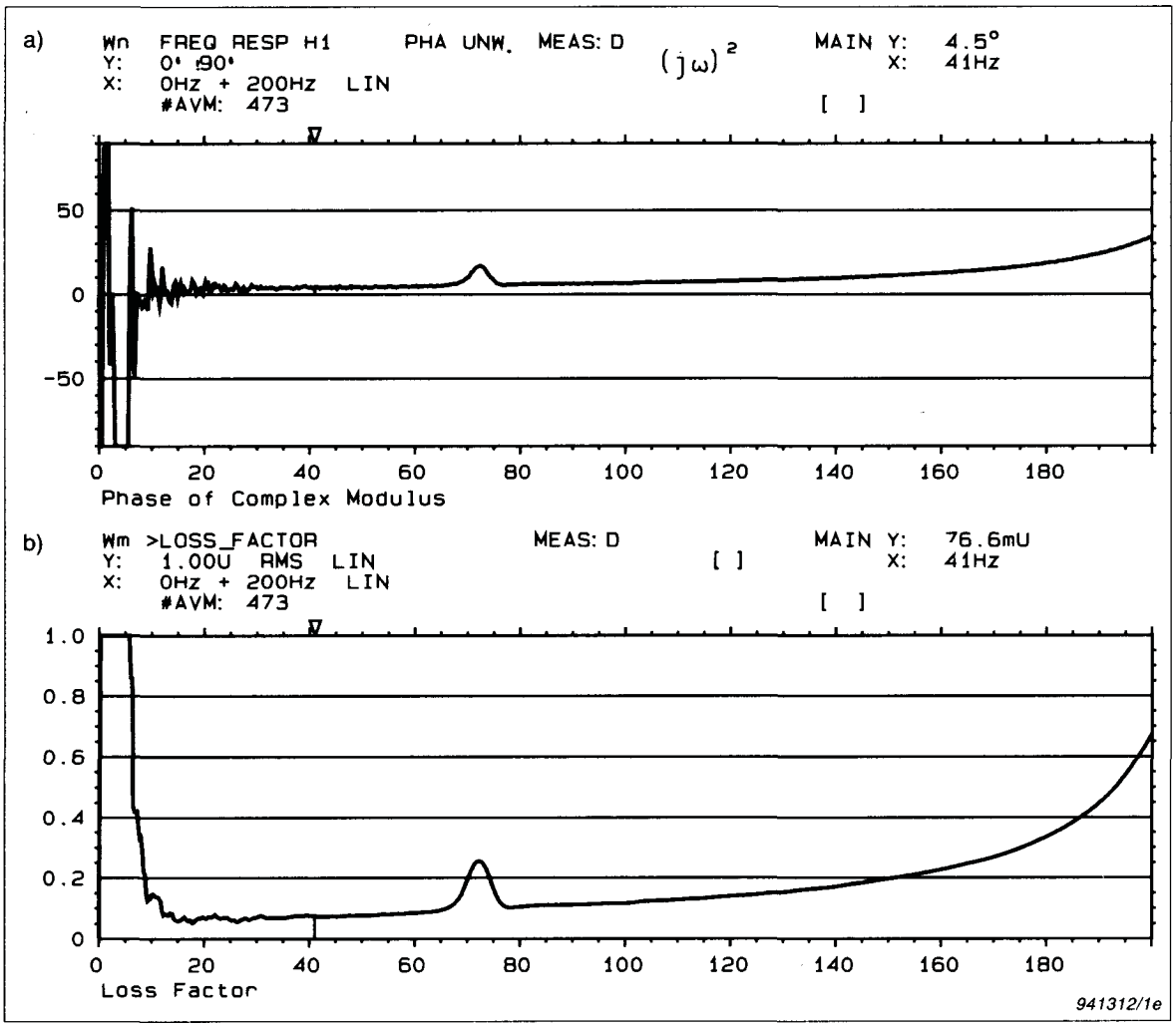

Fig. 8. a) Phase, θ of complex modulus b) Loss factor, η calculated as tan(θ) via a User Definable Display Function

Experimental Procedure and Results for the Resonant Method

The set-up is similar to the one shown in Fig.3 except that a rigid mass (a block of steel) of 2kg was placed on top of the isolator. See Fig.9.

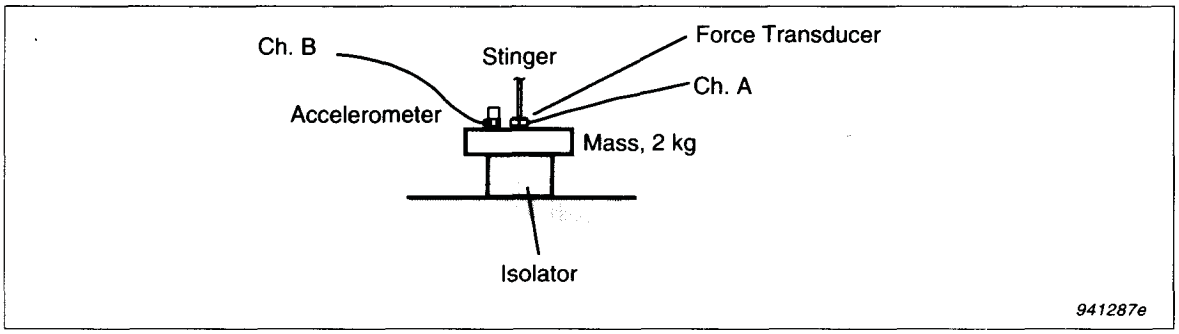

Fig. 9. A rigid mass of 2kg is mounted on top of the isolator

For convenience, the force transducer was connected to channel A and the accelerometer to channel B, in order to display mobility types of Frequency Response Functions directly, although the analyzer also includes the reciprocal of the measured frequency response function as a standard display function. Multisine excitation signal and rectangular weighting have been used in this case.

The result of this measurement is shown in Fig. 10 a). A resonance frequency is located at 42 Hz. A simple User Definable Auxiliary Information finds the 3dB bandwidth, Δf= 3.25 Hz, and thus the loss factor, η = 3.25/42 = 0.076, which is in agreement with the results obtained by the non-resonant method.

The static stiffness can be calculated from eq. (11): $k = (2\pi \times 42.625 \text{ Hz})^2 \times 2$ kg = 143 000 N/m which is within 10% of the results obtained with the non-resonant method.

Of course the static stiffness can be calculated by displaying the dynamic stiffness function, which is shown in the lower trace of Fig. 10b). The reciprocal of the accelerance function is multiplied by $(j\omega)^2$ in order to obtain the dynamic stiffness and cursor readings at lowest reliable frequency indicate a static stiffness of approximately 131kN/m.

In order to find damping at other frequencies, different mass loadings must be applied. In our case, measurement was repeated once with a 1kg mass.

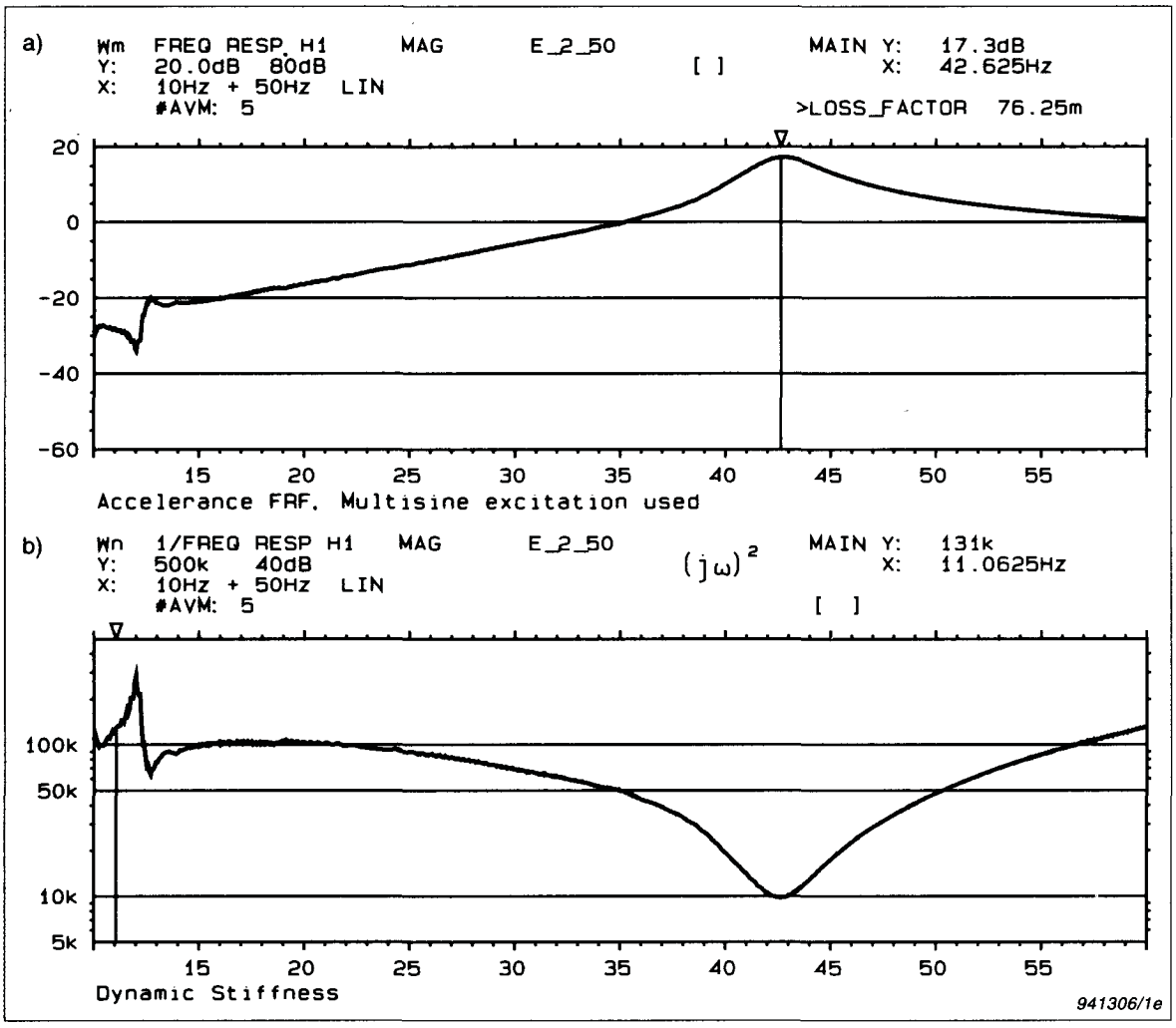

Fig. 10. a) Accelerance Frequency Response Function. Cursor readings indicate resonance frequency and loss factor, b) Dynamic Stiffness. Cursor reading indicates a static stiffness of approximately 131 kN/m

Examples of the results are shown in Fig. 11 a), which displays the dynamic stiffness. The resonance was located at 58.7 Hz (~ 42.6 Hz x $\sqrt{}$(2kg/1kg) = 60.2Hz).

The 3 dB bandwidth was 4.4 Hz yielding a loss factor of 0.075 and a static stiffness of k = 131kN/m. The lowest reliable frequency is found by viewing the coherence function, which is shown in the lower trace of Fig. 11 b). Again the results from the non-resonant methods were confirmed.

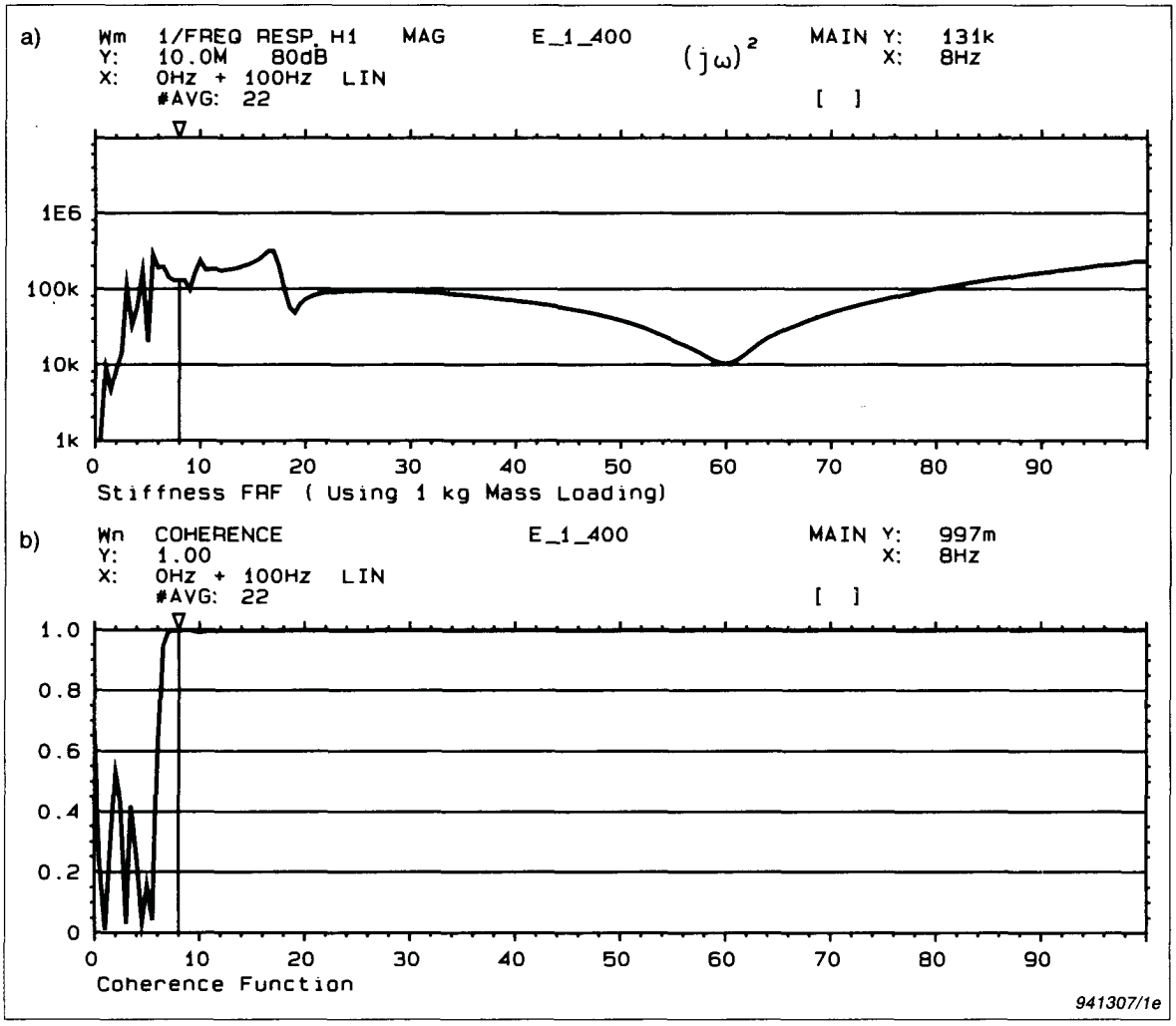

Fig. 11. a) Stiffness Frequency Response Function. Resonance found at 58.7 Hz. Cursor reading at 8 Hz indicates stiffness of 131 k.N/m. b) Coherence, lowest reliable frequency is found to be around 8 Hz

Conclusions

A relatively quick and easy method is described, whereby the elastic (Young's) and loss moduli as well as the loss factor of isolators and damping material can be obtained as continuous functions of frequency.

The results were verified at two frequencies using the well-known resonant method, where damping is calculated from a 3 dB bandwidth determination.

References

[1] HERLUFSEN, H.: *"Dual Channel FFT Analysis (Part I & II)",* Brüel & Kjær Technical Review No. 1 & 2,1984

[2] GANERIWALA, S.N.: *"Characterization of Dynamic Viscoelastic Properties of Elastomers using Digital Spectral Analysis",* Ph.D. Thesis. University of Texas at Austin 1982.

[3] GADE, S. & HERLUFSEN, H.: *"Digital Filter Techniques vs. FFT Techniques for Damping Measurements",* Brüel & Kjær Technical Review No. 1,1994

Previously issued numbers of Brüel & Kjær Technical Review

(Continued from cover page 2)

2-1985 Heat Stress
A New Thermal Anemometer Probe for Indoor Air Velocity Measurements
1 –1985 Local Thermal Discomfort
4 –1984 Methods for the Calculation of Contrast
Proper Use of Weighting Functions for Impact Testing
Computer Data Acquisition from Brüel & Kjær Digital Frequency Analyzers 2131/2134 Using their Memory as a Buffer
3 –1984 The Hilbert Transform
Microphone System for Extremely Low Sound Levels
Averaging Times of Level Recorder 2317
2 –1984 Dual Channel FFT Analysis (Part II)
1 –1984 Dual Channel FFT Analysis (Part I)
4 –1983 Sound Level Meters - The Atlantic Divide
Design Principles for Integrating Sound Level Meters
3 –1983 Fourier Analysis of Surface Roughness
2 –1983 System Analysis and Time Delay Spectrometry (Part II)
1 –1983 System Analysis and Time Delay Spectrometry (Part I)
4 –1982 Sound Intensity (Part II Instrumentation and Applications)
Flutter Compensation of Tape Recorded Signals for Narrow Band Analysis
3 –1982 Sound Intensity (Part I Theory)
2 –1982 Thermal Comfort

Special technical literature

Brüel & Kjær publishes a variety of technical literature which can be obtained from your local Brüel & Kjær representative.
The following literature is presently available:

○ Modal Analysis of Large Structures-Multiple Exciter Systems (English)
○ Acoustic Noise Measurements (English), 5th. Edition
○ Noise Control (English, French)
○ Frequency Analysis (English), 3rd. Edition
○ Catalogues (several languages)
○ Product Data Sheets (English, German, French, Russian)

Furthermore, back copies of the Technical Review can be supplied as shown in the list above. Older issues may be obtained provided they are still in stock.

Brüel & Kjær

WORLD HEADQUARTERS: DK-2850 Nærum · Denmark
Telephone: +45 42 80 05 00 · Telex: 37316 bruka dk · Fax: +45 42 80 14 05

Australia (02) 450-2066 · Austria 00 43-1-816 74 00 · Belgium 016/44 92 25 · Brazil (011) 246-8166
Canada: East (514) 695-8225 West (604) 591-9300 · China 1-84 19 625 · Czech Republic 02-67 02 1100
Finland (0) 1481577 · France (1) 64 57 20 10 · Germany 06151/8149-0 · Great Britain (081) 954-2366
Holland 03402-39994 · Hong Kong 548 7486 · Hungary (1) 215 83 05/215 89 29 · Italy (02) 57 60 41 41
Japan 03-5420-7302 · Republic of Korea (02) 554-0605 · Norway 66 90 44 10 · Poland (0-22) 40 93 92
Portugal (1) 38 59 256/38 59 280 · Singapore 735 8933 · Slovak Republic 07-55666 · Spain (91) 368 10 00
Sweden (08) 711 27 30 · Switzerland 01/940 09 09 · Taiwan (02) 713 9303 · Tunisia (01) 750 400 · USA (404) 981-9311
Local representatives and service organisations worldwide

ISSN 007 – 2621
BV 0045 – 11